

การสลายอะลาคลอร์ด้วยปฏิกิริยาไซโนโฟโตแคทาลิสต์โดย  
ไทเทเนียมไดออกไซด์ที่มีองค์ประกอบของซัลเฟอร์ภายใต้แสงขาว



นายคุณุวัช ทิพยารมณ

ศูนย์วิทยทรัพยากร  
จุฬาลงกรณ์มหาวิทยาลัย

วิทยานิพนธ์นี้เป็นส่วนหนึ่งของการศึกษาตามหลักสูตรปริญญาวิทยาศาสตรดุษฎีบัณฑิต

สาขาวิชาการจัดการสิ่งแวดล้อม (สหสาขาวิชา)

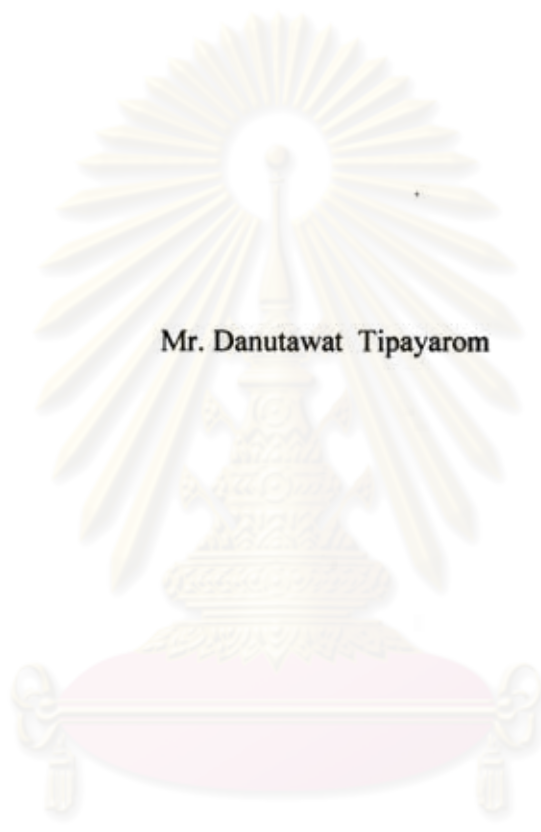
บัณฑิตวิทยาลัย จุฬาลงกรณ์มหาวิทยาลัย

ปีการศึกษา 2553

ลิขสิทธิ์ของจุฬาลงกรณ์มหาวิทยาลัย

530306

SONOPHOTOCATALYTIC DEGRADATION OF ALACHLOR USING  
CRYSTALLINE S-DOPED TiO<sub>2</sub> UNDER VISIBLE LIGHT



Mr. Danutawat Tipayarom

ศูนย์วิทยุโทรทัศน์  
จุฬาลงกรณ์มหาวิทยาลัย

A Dissertation Submitted in Partial Fulfillment of the Requirements  
for the Degree of Doctor of Philosophy Program in Environmental Management  
(Interdisciplinary Program)

Graduate School

Chulalongkorn University

Academic Year 2010

Copyright of Chulalongkorn University



5 0 8 7 8 0 6 3 2 0

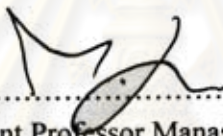
Thesis Title SONOPHOTOCATALYTIC DEGRADATION OF  
ALACHLOR USING CRYSTALLINE S-DOPED TiO<sub>2</sub>  
UNDER VISIBLE LIGHT  
By Mr. Danutawat Tipayarom  
Field of Study Environmental Management  
Thesis Advisor Associate Professor Nurak Grisdanurak, Ph.D.

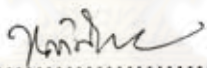
---

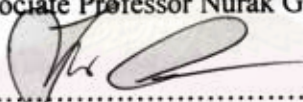
Accepted by the Graduate School, Chulalongkorn University in Partial  
Fulfillment of the Requirements for the Doctoral Degree

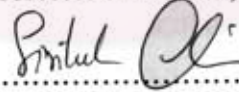
  
.....Dean of the Graduate School  
(Associate Professor Pornpote Piumsomboon, Ph.D.)

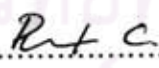
THESIS COMMITTEE

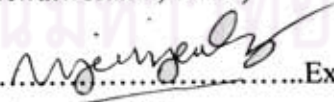
  
.....Chairman  
(Assistant Professor Manaskorn Rachakornkij, Ph.D.)

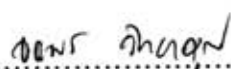
  
.....Thesis Advisor  
(Associate Professor Nurak Grisdanurak, Ph.D.)

  
.....Examiner  
(Associate Professor Jin Anotai, Ph.D.)

  
.....Examiner  
(Assistant Professor Siriluk Chiarakorn, Ph.D.)

  
.....Examiner  
(Pichet Chaiwiwatworakul, Ph.D.)

  
.....Examiner  
(Nyein Nyein Aung, Ph.D.)

  
.....External Examiner  
(Associate Professor Jatuporn Wittayakun, Ph.D.)

คณูวัช ทิพยามรณ: การสลายอะลาคลอร์ด้วยปฏิกิริยาโซโนโฟโตแคทาลิสต์โดยไทเทเนียมไดออกไซด์ที่มีองค์ประกอบของซัลเฟอร์ภายใต้แสงขาว (SONOPHOTOCATALYTIC DEGRADATION OF ALACHLOR USING CRYSTALLINE S-DOPED  $\text{TiO}_2$  UNDER VISIBLE LIGHT) อ.ที่ปริกษาวิทยานิพนธ์หลัก :รศ.ดร.นุรักษ์ กฤษดานุรักษ์, 110 หน้า.

อะลาคลอร์ [2-chloro-2', 6'-diethyl-N-(methoxymethyl) acetanilide] เป็นสารกำจัดวัชพืชที่ใช้กันอย่างแพร่หลาย มีความเป็นพิษสูงต่อระบบต่อมไร้ท่อและเป็นสารในกลุ่ม 2B ที่อาจทำให้เกิดมะเร็งในมนุษย์ สำหรับงานวิจัยนี้จะใช้กระบวนการปฏิกิริยาโซโนโฟโตแคทาลิสต์ (Sonophotocatalysis) สำหรับสลายอะลาคลอร์ในน้ำเสียนตัวเร่งปฏิกิริยาไทเทเนียมไดออกไซด์ที่มีองค์ประกอบของซัลเฟอร์ (S-doped  $\text{TiO}_2$ ) ที่มีคุณสมบัติ ดูดซับแสงขาว มีผลึกขนาดเล็ก (12 nm) และมีพื้นที่ผิวสูง (87 ตารางเมตรต่อกรัม) ปฏิกิริยาสลายอะลาคลอร์ภายใต้แสงขาว (ความยาวคลื่น > 450 นาโนเมตร) พบว่า S-doped  $\text{TiO}_2$  สามารถสลายอะลาคลอร์ได้ดีกว่า  $\text{TiO}_2$  โดยให้ค่าคงที่ปฏิกิริยาเท่ากับ 0.00138 ต่อนาที ที่สภาวะความเข้มข้นอะลาคลอร์ 10 มิลลิกรัมต่อลิตร ปริมาณ S-doped  $\text{TiO}_2$  1 กรัมต่อลิตร เมื่อนำไปทดสอบกับกระบวนการโซโนโฟโตแคทาลิสต์ศึกษาภายใต้ปัจจัย ความเข้มข้นเริ่มต้นของอะลาคลอร์ (5–30 มิลลิกรัมต่อลิตร) ปริมาณตัวเร่งปฏิกิริยา (0.5–2 กรัมต่อลิตร) แล้ว ความหนาแน่นของคลื่นอัลตราโซนิค (Ultrasonic sound) (0.163–0.538 วัตต์ต่อมิลลิเมตร) และผลของตัวออกซิไดซ์ ( $\text{K}_2\text{S}_2\text{O}_8$ : 0.0185–0.111 มิลลิโมลาร์ และ  $\text{H}_2\text{O}_2$ : 0.5–50.0 มิลลิโมลาร์) พบว่าปฏิกิริยาถูกเร่งเร็วขึ้น 11% เทียบกับปฏิกิริยาภายใต้แสงขาวอย่างเดียว ประสิทธิภาพของปฏิกิริยาโซโนโฟโตแคทาลิสต์ขึ้นกับปริมาณอนุมูล OH ที่ผลิตได้จากคลื่นอัลตราโซนิค (วัดโดย Fricke reaction) ตัวออกซิไดซ์  $\text{K}_2\text{S}_2\text{O}_8$  จะมีผลต่อปฏิกิริยามากกว่าตัวออกซิไดซ์  $\text{H}_2\text{O}_2$  โดยอะลาคลอร์สามารถถูกสลายได้ 65% ที่สภาวะ ความเข้มข้นเริ่มต้นของอะลาคลอร์ 10 มิลลิกรัม/ลิตร ปริมาณตัวเร่งปฏิกิริยา 1 กรัมต่อลิตร ความหนาแน่นของคลื่นอัลตราโซนิค 0.163 วัตต์ต่อมิลลิเมตร สำหรับศึกษาปัจจัยปฏิสัมพันธ์ระหว่าง 3 ปัจจัยที่ประกอบด้วย ปริมาณตัวเร่งปฏิกิริยา ความหนาแน่นของคลื่นอัลตราโซนิค และความเข้มข้นเริ่มต้นของอะลาคลอร์ โดยวิธีออกแบบการทดลองตามแบบจำลอง Box-Behnken พบว่าสภาวะที่เหมาะสมที่ทำให้การสลายอะลาคลอร์ได้ 85% ในเวลา 1 ชั่วโมงคือ ปริมาณความเข้มข้นของไทเทเนียมไดออกไซด์ที่มีองค์ประกอบของซัลเฟอร์เท่ากับ 1.785 กรัมต่อลิตร และ ปริมาณความหนาแน่นของคลื่นอัลตราโซนิค 0.55 วัตต์ต่อมิลลิเมตร ความเข้มข้นเริ่มต้นของอะลาคลอร์ 1 มิลลิกรัมต่อลิตร โดยผลการทดสอบแบบจำลองให้ค่าเบี่ยงเบน  $\pm 2\%$

สาขาวิชา การจัดการสิ่งแวดล้อม.....ลายมือชื่อนิสิต.....ศุภวัช.....กิมฑรมณ  
ปีการศึกษา 2553.....ลายมือชื่อ อ.ที่ปริกษาวิทยานิพนธ์หลัก.....

## 5087806320 : MAJOR ENVIRONMENTAL MANAGEMENT

KEYWORDS : VISIBLE LIGHT / SONOPHOTOCATALYSIS / S-DOPED TiO<sub>2</sub> / ALACHLOR / BOX-BEHNKEN DESIGN

DANUTAWAT TIPAYAROM: SONOPHOTOCATALYTIC

DEGRADATION OF ALACHLOR USING CRYSTALLINE S-DOPED TiO<sub>2</sub>

UNDER VISIBLE LIGHT. THESIS ADVISOR: ASSOC. PROF. NURAK

GRISDANURAK, Ph.D., 110 pp.

Alachlor [2-chloro-2', 6'-diethyl-N-(methoxymethyl) acetanilide], a widely used herbicide, has been known as a highly toxic endocrine disruptor and recognized as 2B chemical (possible to cause cancer to humans). In this study, a combination of photocatalysis with sonolysis generally called sonophotocatalysis has been used for treating alachlor in synthetic wastewater investigated under S-doped TiO<sub>2</sub> catalyst. The catalyst possesses a strong visible light absorption, small crystallite size (12 nm) and high relative surface area (87 m<sup>2</sup> g<sup>-1</sup>). S-doped TiO<sub>2</sub> showed the decomposition of alachlor higher than TiO<sub>2</sub> by given rate constant of pseudo-first order of 0.00138 min<sup>-1</sup>. It was tested under the condition: initial concentration and catalyst loading of 10 mg L<sup>-1</sup> and 1 g L<sup>-1</sup>, respectively. The degradation of alachlor on S-doped TiO<sub>2</sub> was also studied under sonophotocatalysis in visible light region. Parameters such as, alachlor initial concentration (5–30 mg L<sup>-1</sup>) catalyst loading (0.5–2 g L<sup>-1</sup>) ultrasonic density (0.163–0.538 W mL<sup>-1</sup>) and oxidizing agent effects (K<sub>2</sub>S<sub>2</sub>O<sub>8</sub> : 0.0185–0.111 mM and H<sub>2</sub>O<sub>2</sub> : 0.5–50.0 mM), were used for the investigation. Sonophotocatalysis enhanced the reaction rate 11% higher than photocatalysis. The reaction was influenced by OH radicals (through the Fricke reaction) generated from sonication. K<sub>2</sub>S<sub>2</sub>O<sub>8</sub> solution, an oxidizing agent, affected the degradation of alachlor, while H<sub>2</sub>O<sub>2</sub> did not affect. Mineralization of alachlor achieved 65% the optimal condition; alachlor initial concentration 10 mg L<sup>-1</sup> catalyst loading 1 g L<sup>-1</sup> and ultrasonic density 0.163 W mL<sup>-1</sup>. In the response surface methodology (Box Behnken model), three parameters were studied simultaneously. The optimum operating conditions were of alachlor concentration, 1.785 g L<sup>-1</sup> catalyst loading and 0.55 W mL<sup>-1</sup> to achieve 85% alachlor removal in 1 hr. The proposed model was deviated from the observed values by ±2%.

Field of Study : Environmental Management Student's Signature *Danutawat Tipayarom*

Academic Year : 2010 Advisor's Signature *Nurak Grisdanurak*

## ACKNOWLEDGEMENTS

This thesis would have not been possible without the extraordinary support of a number of people.

First of all, I would like to gratefully acknowledge my advisor, Assoc. Prof. Nurak Grisdanurak for his support, guidance and assistance throughout my study. I would also like to thank my respective committee members Assoc. Prof. Jatuporn Wittayakun, Assist. Prof. Manaskorn Rachakornkij, Assoc. Prof. Jin Anotai, and Asst. Prof. Siriluk Chiarakorn, Dr. Pichet Chaiwiwatworakul, Dr. Nyein Nyein Aung for their stimulating questions and valuable suggestions.

I would to express as well my gratitude to Prof. Teruhisa Ohno who supports me the catalyst (S-doped TiO<sub>2</sub>).

I particularly thank Dr. Kitirote Wantala, Dr. Pongtanawat Khemthong, Dr. Jitlada Chumee and Asst. Prof. Laksana Laokiat for useful comments, and invaluable suggestions.

I am very grateful to NCE-EHWM, Chulalongkorn University and Department of Chemical Engineering of Thammasat University. Additionally, I am grateful to Synchrotron Light Research Institute for their analytical laboratory and the Office of the Higher Education Commission (Targeted Research Initiatives), Thailand, for the financial support.

Finally and most importantly, I am extremely grateful for the support of my parents (Mr. Pichai and Mrs Mali Tipayaorm), my wife and family. This provides me with their emotional support throughout the thesis process. With each passing day, I understand more fully just how lucky I am to have Mrs. Aungsiri in my life, and can only hope that my boundless love for her offers some consolation for my constant preoccupations.

# CONTENTS

	PAGE
ABSTRACT (IN THAI).....	iv
ABSTRACT (IN ENGLISH).....	v
ACKNOWLEDGEMENTS.....	vi
CONTENTS .....	vii
LIST OF TABLES.....	xii
LIST OF FIGURES.....	xiii
NOMENCLATURES.....	xvii
CHAPTER I: INTRODUCTION.....	1
1.1 Motivations.....	1
1.2 Objectives.....	3
1.3 Hypotheses.....	4
1.4 Scopes of the study.....	4
CHAPTER II: LITERATURE REVIEW.....	5
2.1 General information of alachlor.....	5
2.1.1 Use.....	5
2.1.2 Properties.....	6
2.1.3 Source and environmental fate .....	7
2.1.4 Potential health effect and regulation.....	9
2.1.5 Situation of alachlor in Thailand.....	10
2.2 Conventional water treatment system.....	11

	PAGE
2.3	Advanced oxidation processes (AOPs)..... 13
2.4	Heterogeneous photocatalysis..... 15
2.4.1	Doping of TiO <sub>2</sub> ..... 18
2.4.2	S-Doped TiO <sub>2</sub> ..... 19
2.5	Sonochemistry..... 21
2.5.1	General principles of sonochemistry..... 21
2.5.2	Intensity and pressure amplitude..... 24
2.5.3	Aqueous sonochemistry ..... 25
2.6	Sonophotocatalysis ..... 27
2.6.1	Synergistic effect of sonophotocatalysis ..... 28
2.7	Influences of sonophotocatalytic activity..... 29
2.7.1	Effect of the catalyst loading ..... 29
2.7.2	Effect of pH..... 29
2.7.3	Effect of ultrasonic intensity..... 30
2.8	Design of Experiment (DoE)..... 30
2.7.1	Box–Behnken design (BBD)..... 33
CHAPTER III: MATERIAL AND METHODS..... 34	
3.1	Chemicals and instrumentation ..... 35
3.1.1	Chemicals..... 35
3.1.2	Instrumentation..... 35
3.2	Catalyst characterization..... 36
3.2.1	X-ray diffractometer (XRD)..... 36
3.2.2	UV-Vis diffuse reflectance spectrophotometer ..... 37

	PAGE
3.2.3 The Brunauer-Emmett-Teller (BET).....	37
3.2.4 Scanning Electron Microscopy/Energy dispersive Spectroscopy (SEM/EDS).....	38
3.2.5 Transmission Electron Microscopy (TEM).....	38
3.2.6 Zeta potential technique .....	38
3.3 Photocatalytic and sonophotocatalytic activities .....	39
3.3.1 Photocatalytic activities .....	39
3.3.2 Sonophotocatalytic activities .....	40
3.4 Analysis methods.....	42
3.4.1 Alachlor .....	42
3.4.2 Total organic carbon (TOC).....	42
3.4.3 Ion analysis.....	43
3.4.4 The quantitative determination of active radicals.....	43
3.5 Design of Experiment (DoE).....	44
<b>CHAPTER IV: RESULTS AND DISCUSSION.....</b>	<b>46</b>
4.1 Characterization results .....	46
4.1.1 X-ray diffraction spectra .....	46
4.1.2 UV-Visible diffuse reflectance spectra .....	46
4.1.3 Transmission Electron Microscopy.....	48
4.1.4 Point of zero charge (pzc) .....	50
4.2 Photocatalytic activities for alachlor degradation .....	51
4.2.1 Effect of catalyst concentration .....	53
4.2.2 Influence of initial concentration .....	54

	PAGE
4.2.3 Synergistic effect of sonophotocatalysis .....	55
4.3 Sonophotocatalytic activities for alachlor degradation .....	58
4.3.1 Effect of catalyst concentration.....	58
4.3.2 Effect of ultrasonic power .....	59
4.3.3 Kinetic model for sonophotocatalytic activity .....	61
4.3.4 Effect of $K_2S_2O_8$ addition.....	62
4.3.5 Effect of $H_2O_2$ addition.....	64
4.3.6 Mineralization study .....	65
4.3.7 Hydroxyl radical .....	67
4.3.8 Inorganic ion concentration.....	68
4.4 Design of experiments (DoE).....	69
4.4.1 Analysis of variance (ANOVA) and fitting model .....	72
4.4.2 Adequacy check of the model .....	74
4.4.3 Main and interaction effect and response surface analysis.....	76
4.4.4 Optimization.....	82
4.4.5 Verification of model .....	82
CHAPTER V: CONCLUSIONS AND RECOMMENDATIONS.....	84
5.1 Conclusions.....	84
5.2 Recommendations.....	85
REFERENCES.....	86



## LIST OF TABLES

TABLE	PAGE
2.1	8
2.2	11
2.3	13
2.4	14
2.5	17
2.6	31
2.7	32
4.1	47
4.2	58
4.3	70
4.4	71
4.5	73
4.6	73
4.7	83

## LIST OF FIGURES

FIGURE	PAGE
2.1 Potential for concentration of alachlor run off at the edge of the field to exceeded EPA's maximum contaminant level (2ppb) USDA .....	9
2.2 Crystal structure of TiO <sub>2</sub> : (a) anatase (b) rutile and (c) brookite .....	17
2.3 Mechanism of S-doped TiO <sub>2</sub> for the alachlor degradation .....	20
2.4 Cavitation, formation, growth and collapse bubbles adapted from He .....	26
3.1 The experimental framework of this study .....	34
3.2 A schematic diagram of the photocatalytic experimental setup.....	40
3.3 A schematic diagram of the sonophotocatalytic experimental setup.....	42
4.1 XRD patterns of S-doped TiO <sub>2</sub> and TiO <sub>2</sub> (P25) .....	47
4.2 Diffuse reflectance spectra of S-doped TiO <sub>2</sub> and TiO <sub>2</sub> (P25) .....	48
4.3 TEM images of (a) TiO <sub>2</sub> (P25) and (b) S-doped .....	49
4.4 Zeta potential of TiO <sub>2</sub> (P25) and S-doped TiO <sub>2</sub> .....	50
4.5 Concentration profiles and rate constants based on pseudo-first-order expression of photocatalytic degradation of alachlor over S-doped TiO <sub>2</sub> (gray color bar and dotted line) or TiO <sub>2</sub> (P25) (black color bar and black line) with different cutoff filters with 500 W xenon lamp (a) no cutoff $\lambda$ filter (b) 420 nm cutoff $\lambda$ filter (c) 450 nm cutoff $\lambda$ filter.....	52
4.6 Concentration profiles and the apparent rate constant of alachlor degradation for different catalyst loadings by S-doped TiO <sub>2</sub> = 1.0 g L <sup>-1</sup> (cutoff $\lambda$ filter at 450 nm).....	53
4.7 Linear plot of Langmuir–Hinshelwood (L–H) expression: alachlor 10 mg L <sup>-1</sup> , pH= 7, S-doped TiO <sub>2</sub> = 1.0 g L <sup>-1</sup> .....	55

FIGURE	PAGE
4.8 Pseudo-first-order profiles of alachlor degradation over TiO <sub>2</sub> (P25) (Round) and S-doped TiO <sub>2</sub> (Triangle); 1 g catalyst L <sup>-1</sup> at an initial pH of 7; sonocatalysis (US+S-doped TiO <sub>2</sub> ), sonophotocatalysis (US+light+S-doped TiO <sub>2</sub> ): catalyst (1 g L <sup>-1</sup> ), alachlor (10 mg L <sup>-1</sup> ), (black cross: TiO <sub>2</sub> (P25)) (black star: S-doped TiO <sub>2</sub> ) sonocatalysis (US+S-doped TiO <sub>2</sub> ) catalyst (1 g L <sup>-1</sup> ), alachlor (10 mg L <sup>-1</sup> ).....	56
4.9 Effect of catalyst loading of S-doped TiO <sub>2</sub> on 20 kHz in visible light; where C <sub>initial</sub> = 10 mg L <sup>-1</sup> , S-doped TiO <sub>2</sub> loading = 1 g L <sup>-1</sup> , 13 W ultrasonic power, light > 450 nm and pH = 7.....	59
4.10 Effect of ultrasound power (●, 13 W; ○, 23 W; ▼, 33 W; and Δ, 43 W) on sonophotocatalytic where C <sub>initial</sub> = 10 mg L <sup>-1</sup> , S-doped TiO <sub>2</sub> loading = 1 g L <sup>-1</sup> , light > 450 nm and pH = 7.....	60
4.11 Influence of C <sub>initial</sub> on the sonophotocatalytic degradation of alachlor by S-doped TiO <sub>2</sub> (● 5 mg L <sup>-1</sup> , ○ 10 mg L <sup>-1</sup> , ▼ 20 mg L <sup>-1</sup> , Δ 30 mg L <sup>-1</sup> ), where C <sub>initial</sub> = 10 mg L <sup>-1</sup> , S-doped TiO <sub>2</sub> loading = 1 g L <sup>-1</sup> , 13 W ultrasonic power, light > 450 nm and pH = 7.....	61
4.12 (a) Sonophotocatalytic degradation of alachlor under the irradiated S-doped TiO <sub>2</sub> with various concentrations of persulfate solutions (● without K <sub>2</sub> S <sub>2</sub> O <sub>8</sub> , ○ 0.1 mM, ▼ 0.25 mM, Δ 0.5 mM, ■ 1.0 mM, and ◆ 5.0 mM) where C <sub>initial</sub> = 10 mg L <sup>-1</sup> , 13 W ultrasonic power, light > 450 nm and pH = 7. (b) The rate constant of alachlor degradation with various concentrations of persulfate solutions.....	63

FIGURE	PAGE
4.13 Sonophotocatalytic degradation of alachlor under the irradiated S-doped TiO <sub>2</sub> with various concentrations of H <sub>2</sub> O <sub>2</sub> (● without H <sub>2</sub> O <sub>2</sub> , ○ 0.5 mM, ▼ 1.0 mM, Δ 10.0 mM, and ■ 50.0 mM) C <sub>initial</sub> = 10 mg L <sup>-1</sup> , S-doped TiO <sub>2</sub> loading = 1 g L <sup>-1</sup> , 13 W ultrasonic power, light > 450 nm and pH = 7.....	64
4.14 (a) alachlor degradation (● photocatalysis, ○ sonocatalysis, ▼ sonophotocatalysis, Δ sonophotocatalysis with adding 0.5 mM K <sub>2</sub> S <sub>2</sub> O <sub>8</sub> ) and (b) TOC reduction (● photocatalysis, ○ sonocatalysis, ▼ sonophotocatalysis, Δ sonophotocatalysis with adding 0.5 mM K <sub>2</sub> S <sub>2</sub> O <sub>8</sub> ) where C <sub>initial</sub> = 10 mg L <sup>-1</sup> , S-doped TiO <sub>2</sub> loading = 1 g L <sup>-1</sup> , 13 W ultrasonic power, light wavelength > 450 nm and pH = 7.....	66
4.15 Comparison of the photocatalytic and sonophotocatalytic oxidation of Fe <sup>2+</sup> over S-doped TiO <sub>2</sub> (○, photocatalysis; ●, sonocatalysis; ◀ sonophotocatalysis) where C <sub>initial</sub> = 10 mg L <sup>-1</sup> , S-doped TiO <sub>2</sub> loading = 1 g L <sup>-1</sup> , 13 W ultrasonic power, light wavelength > 450 nm and pH = 7.....	67
4.16 Inorganic ion concentration produced form the sonophotocatalytic oxidation of alachlor over S-doped TiO <sub>2</sub> (NO <sub>2</sub> <sup>-</sup> ; black bar, Cl <sup>-</sup> ; grey bar, NO <sub>3</sub> <sup>-</sup> ; dark grey bar) where C <sub>initial</sub> = 10 mg L <sup>-1</sup> , S-doped TiO <sub>2</sub> loading = 1 g L <sup>-1</sup> , 13 W ultrasonic power, light > 450 nm and pH = 7.....	69
4.17 An normal probability plot of the experimental data for alachlor Removal.....	75

FIGURE	PAGE
4.18 Histogram internally studentized residuals and normal % probability plot for alachlor removal.....	75
4.19 Main effect of matrix plots of experimental factors for percentage removal of alachlor in a three factors, three levels Box-Benkhen design....	77
4.20 Two-factor interaction of matrix plots of experimental factors for percentage removal of alachlor in a three factors, three levels Box-Benkhen design.....	78
4.21 Contour plot and surface plot of response for catalyst loading and initial concentration.....	79
4.22 Contour plot and surface plot of response for ultrasonic power intensity and initial concentration .....	80
4.23 Contour plot and surface plot of response for ultrasonic power intensity and catalyst loading.....	81
4.24 Optimality plot to locate optimum factor levels for maximized response...	82
4.25 Comparison of experimental and predicted values (predicted model and adjusted model) of four responses: observed value (●), predicted value (▼) adjusted value (◆).....	83

## NOMENCLATURES

SYMBOL / ABBREVIATION	NAME
$k_{app}$	Apparent rate constant
$K_{ad}$	Adsorption equilibrium constant
$k_{vis+US+TiO_2}$	Pseudo-first order rate constant under a combination system of sonolysis and photocatalysis
$k_{vis+TiO_2}$	Pseudo-first-order rate constant under photocatalysis
$k_{US+TiO_2}$	Pseudo-first-order rate constant of sonolysis
$CO_2$	Carbon dioxide
$C_{initial}, C_0$	Initial concentration
hr	Hour
M	Molar
min	Minute
mL	Milliliter
$mL\ min^{-1}$	Milliliter per minute
L-H	Langmuir–Hinshelwood expression
$r_0$	Initial rate
Ti	Titanium
$TiO_2$	Titanium dioxide
$TiO_2$ (P25)	Titanium dioxide Degussa P25 from Evonik Degussa Industry

# CHAPTER I

## INTRODUCTION

### 1.1 Motivations

Agricultural products are one of Thailand's primary exports. Production has steadily increased over the past decade due to the expansion of cultivated land, technological innovations, and heavy applications of fertilizers as well as pesticides and herbicides. Hundred million tons of herbicides, such as alachlor, atrazine and paraquat, are broadly utilized in agricultural areas around the world. In 2004, alachlor was ranked 14<sup>th</sup> (1,100 tons) among the growing herbicide imports to Thailand (Department of Agriculture Thailand, 2010).

Alachlor [2-chloro-2', 6'-diethyl-N-(methoxymethyl) acetanilide] has been known as a highly toxic endocrine disruptor and can cause cancer to humans (Orme and Kegley, 2005). It is classified as the human carcinogenic potential of agents of B2 group water (probable human carcinogen) from a six-category alphanumeric classification system (A, B1, B2, C, D and E) by the US EPA. Its maximum contaminant level established for drinking water is 2  $\mu\text{g L}^{-1}$  (WHO/FAO, 1996).

Evidently, this herbicide is a non-point source pollutant as it is found in agricultural runoff, rivers, soil and groundwater. In addition to this, accidental leakage and spills from the production and transfer process in both the industry and farmer's household possibly occurs. Due to alachlor's growing prevalence, alachlor leaching has to be dealt with immediately.

Several factories located in Suphanburi, Saraburi and Nakornrachasima has used alachlor as a mixing ingredient for its products, herbicides and pesticides. Alachlor also is used as one of ingredients for coating material in crop grain. It has been reported that the runoff from these industrials could cause the death of fish in the river, and consequently generate many problems to environment.

The treatment of this type of herbicide is quite challenges because its typically includes several benzene rings that cannot be degraded easily in conventional treatment methods (e.g., chemical, physical and biological methods). Therefore, advanced oxidation processes (AOPs) such as sonolysis, sonocatalysis, and photocatalysis probably are useful techniques for decomposing these organic pollutants in wastewater. In photocatalysis,  $\text{TiO}_2$  is widely used as a photocatalyst for the complete mineralization of toxic and non-biodegradable compounds to carbon dioxide and inorganic constituents in water and gas phases (Chen *et al.*, 2005). Simply put, photocatalysis occurs when a photocatalyst is activated by photons with energy equal or greater than its band gap energy thereby producing electron/hole pairs ( $e^-/h^+$ ).

However the wide band gap (3.2 eV) of  $\text{TiO}_2$  is effective only within UV range which accounts for about 4-6% of solar light. To utilize a wide range of incident light such as solar light, doping of  $\text{TiO}_2$  has been applied to reduce the required energy band gap and to increase electron acceptors resulting in reducing recombination effect. To develop the performance of  $\text{TiO}_2$ , doping of  $\text{TiO}_2$  relating to the addition of impurities such as metals and nonmetals into the photocatalyst is generally applied. However, metal doping can result in thermal instability and increasing carrier trapping (Chen, 2005). Thus, doping of the photocatalyst with metal showed lower activity under visible light and within the UV region compared to the non-doped photocatalyst.

Various nonmetal elements, such as B, C, N, F, S, Cl, and Br, have been successfully doped into  $\text{TiO}_2$  (Chen *et al.* 2005). A variety of mechanisms have been postulated to explain the shift of absorption threshold and the photocatalytic activity of nonmetal doped  $\text{TiO}_2$  photocatalysts.

The adsorption of light in visible region onto nonmetal of N and C doped  $\text{TiO}_2$  has been reported to be relatively low (Ohno *et al.*, 2004). Prof. Ohno and co-workers reported a good reaction to synthesize nonmetal substitutes of S on some lattice  $\text{TiO}_2$  (Ohno *et al.*, 2004). They also showed the efficiency of the propanol degradation over visible light. Moreover, the study of S-doped  $\text{TiO}_2$  is attractive by several researchers (Liu *et al.*, 2008; Rengifo-Herrera *et al.*, 2010).

In addition, ultrasonic sound (sonolysis) has been increasingly applied to enhance the mass transfer of chemical oxidation of organic pollutants. In the same way, utilizing ultrasonic sound and catalyst, called sonocatalysis, should improve the generation of active sites of high temperature and pressure by acoustic cavitation. These cause by the collapse of bubble resulting in the change of high local temperature and pressure. The overall water splitting was proposed to proceed by a two-step reaction. The cleavage of dioxygen and water molecules generates active species, such as  $H^\bullet$  and  $HO^\bullet$  radicals. In previous study, sonochemical degradation of alachlor was revealed at different sonication frequencies and dissolved gases by Wayment *et al.* (2002).

A combination of photocatalysis and sonocatalysis is named as sonophotocatalysis. With both promising technologies, it has been presumed that the system should present more effective on the treatment of organic compounds in wastewater.

Focusing on alachlor degradation, the study under a photocatalysis and/or a sonophotocatalysis were limited to using UV irradiation (Penuela and Barcelo, 1996; Wong and Chu, 2003; Ryu *et al.*, 2003; Chu and Wong, 2004; Bahena *et al.*, 2008). It is interesting that this study focuses on the use of photocatalysis and sonophotocatalysis under visible light. The effects of catalyst concentration and initial concentration of alachlor, influence of different visible wavelengths of light source, and synergistic effects of sonophotocatalysis and characterization of S-doped  $TiO_2$  are studied.

## 1.2 Objectives

### **Main objective**

To investigate the performance of photocatalytic and sonophotocatalytic alachlor degradation using suspended crystalline S-doped  $TiO_2$  under visible light

### **Sub-objectives**

1.2.1 To understand the physicochemical properties of crystalline S-doped  $TiO_2$  catalysts

1.2.2 To evaluate the effects of the conditions on catalyst activities using relevant parameters: initial concentration of alachlor, ultrasonic power intensity, and catalyst loading

1.2.3 To evaluate the kinetic degradation rate expression

1.2.4 To study the sensitivity analysis of the reaction through the design of experiment (DoE).

### **1.3 Hypotheses**

Alachlor can be degraded using S-doped  $\text{TiO}_2$  under visible light sonophotocatalytic reaction. Ultrasonic power, catalyst loading, and initial concentration of alachlor can affect the degradation rate. The studied variables are independent affecting the rate of reaction.

### **1.4 Scopes of the study**

1.4.1 For the photocatalysis and sonophotocatalysis with S-doped  $\text{TiO}_2$  and  $\text{TiO}_2$  (P25), visible light generated by 500W Xenon lamp corresponding to wavelength range longer than 420 nm and 450 nm is utilized.

1.4.2 Ultrasonic probe at 20 kHz frequency ranged from 10 W- 50 W in 80 mL reactor volume is applied in this study.

1.4.3 The effect of electron acceptors is studied with two reagents including hydrogen peroxide and potassium persulfate.

1.4.4 Box-Behnken technique is selected to evaluate the experimental design matrix for the design of experiment (DoE) in this study.

## CHAPTER II

### LITERATURE REVIEWS

Although its industrial sector is increasing rapidly, Thailand is considered as both an agricultural and industrialized country. Agricultural products from Thailand have been known worldwide. The country supplies food, particularly, rice, sugarcane, cassava, corn, soybean and etc. to all over the world. In order to enhance agricultural production and efficiency, farmers have utilized a lot of chemicals in fertilizers and herbicides. The amount of imported herbicides increases dramatically form year to year. Consequently, Thailand is ranked fourth in annual pesticide and herbicide consumption of 15 Asian countries (FAO, 2005).

A lot of pesticides, herbicides and insecticides persist in rivers, soil and groundwater, even in air. In order to utilize treatment system operating in visible light, advanced oxidation processes (AOPs) are effective methods to decompose these organic pollutants released from several agricultural activities. For this reason, a conventional water treatment system, an advance oxidation process, a heterogeneous photocatalysis, sonochemistry, and sonophotocatalysis to alachlor degradation has been reviewed.

#### 2.1 General information on alachlor

##### 2.1.1 Use

Agricultural products are one of Thailand's primary exports. Production has steadily increased over the past decade, due to expansion of cultivated land, technological innovations, and heavy applications of fertilizers as well as pesticides and herbicides. With increasing amounts of chemical pesticides and herbicides, contamination in a water stream has become a persistent problem in Thailand.

The higher amount of herbicides usage, the more mixing facilities are built. More than 20 factories regarding to herbicide mixing processes are located in our country. One of the existing problems is to treat wastewater contaminated with herbicides below the regulation level in a short period of time, before releasing to the environment.

Among these pollutants, alachlor (2-chloro-2, 6-diethyl-N-methoxy methyl Acetanilide) is widely used as an acetanilide herbicide for control of annual grasses and broadleaf weeds for agricultural products, primarily on corn and sorghum and soybeans. It is used on soybean, brassica, maize, sugar-cane and cotton crops as a pre-planting application or as a post-emergence at the 1 - 2 leaf stage. It requires moisture for activation. Emulsifiable concentrates are frequently tank-mixed with other herbicides and fertilizers. It is a selective systemic herbicide, absorbed by germinating shoots and by roots. It works by interfering with a plant's ability to produce protein and by interfering with root elongation. The action mode is elongase inhibition, and inhibition of geranylgeranyl pyrophosphate (GGPP) cyclisation enzymes, part of the gibberellin pathway (WHO/FAO, 1996).

### **2.1.2 Properties**

Alachlor was first registered in 1969 as a selective herbicide and it was produced by the Monsanto Company in the US. The properties of alachlor are presented in Table 2.1. Physically, alachlor is a white or cream, combustible crystalline solid without odor having a melting point at 39.5 - 41.5 °C. It is corrosive to steel and black iron but not stainless steel or aluminum. The solubility of alachlor in water is around 240 mg L<sup>-1</sup> at 25 °C. It is only soluble in most organic solvents, such as acetone, benzene, chloroform, ethanol, ether and ethyl acetate and sparingly soluble in heptane. It can be hydrolyzed by strong acids and alkali. At 105°C, it decomposes. It is stable under ultra violet radiation.

### 2.1.3 Source and environmental fate

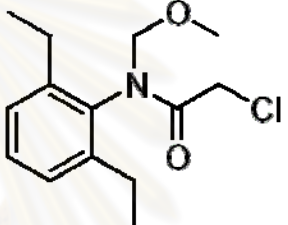
Alachlor is mainly released to the environment by its manufacture and utilization as herbicides in agricultural activities. In water, the degradation of alachlor is largely due to both biodegradation and photolysis while in shallow clean water, the part of photolysis becomes more significant, especially in the presence of sensitizers. Alachlor has a low affinity to soils and is expected to be highly mobile. Consequently, alachlor can be commonly found in groundwater. The mineralization of alachlor was less than 1% in 30 days in ground water aquifers. Alachlor in groundwater free of aquifer materials (e.g. sand) slowly disappear and has a long half-life, WHO/FAO (1996).

In soil, alachlor is changed to its metabolites primarily by biodegradation; however, its degradation rate is very slow due its toxicity to microorganisms. In addition, it is a persistent herbicide with a half-life in soil and water of over 70 and 30 days, respectively. The evaporation of alachlor from soil will increase as the moisture content and temperature of the soil is increased. Increase in alachlor sorption in soil will decrease evaporation as evidenced by slower evaporation with the increase in clay and organic matter content of soil. It has been concluded that the loss of alachlor from soil will be moderate and an estimated 3.5-6.5 kg ha<sup>-1</sup>yr<sup>-1</sup> or more alachlor will be lost from treated field. The estimated half-life of alachlor evaporation from soil is in the range 12 to > 200 days (US EPA, 2009).

In U.S., the Environmental Protection Agency proposed state management plans (SMPs) to provide insight on which watersheds have the greatest likelihood of needing technical assistance. SMPs consist of a national-level simulation conducted of the potential for pesticide loss from farm fields by using the National Resources Inventory (NRI). Maps (as presented in Figure 2.1) illustrate which watersheds have the greatest potential pesticide for runoff loss from farm fields to exceed water quality thresholds. The potential is much about 600,000-700,000 acres for alachlor in the U. S. (Kellogg *et al.*, 1998).

Alachlor runoff potential watershed-level risk is approximated in unit of Threshold Exceedence Units (TEUs) per watershed. Each NRI sample point was multiplied by the percent acres treated to represent acres in the map. Then, acres treated were multiplied by the concentration-threshold ratio for each pesticide at each NRI sample point, and the data were summed over all the sample points in the watershed. Thus, TEUs account for the amount the threshold was exceeded and the amount of acres treated in the watershed. TEUs were derived in this manner to compare risk among watersheds (Kellogg *et al.*, 1998).

Table 2.1 Chemical structure and chemical properties of alachlor

Structure	 <p>(2-chloro-20, 60-diethyl-N-methoxy methyl Acetanilide)</p>
Molecular weight	269.8
Solubility	240 mg/l
Molecular formula	C <sub>14</sub> H <sub>20</sub> ClNO <sub>2</sub>
CAS Number	15972-60-8
Melting Point	40°C
Density	1.133 at 25°C
Octanol/Water Partition (K <sub>ow</sub> )	Log K <sub>ow</sub> = 2.63 and 3.53
Soil sorption coefficient (K <sub>oc</sub> )	2.08 to 2.28; medium to high mobility in soil
Appearance	A colorless to yellow crystal compound
Form/Odor	Granular, emulsifiable concentrate and flowable formulations
Trade names	Alanex, Lasso, Lazo, Microtech, Pillarzo

Source: WHO/FAO (1996); US EPA (2009)

### 2.1.4 Potential health effect and regulation

In human health assessment, alachlor commonly has been classified as either category III (slightly toxic) or IV (practically non-toxic) toxicity categories of US EPA by using laboratory animals. Alachlor has been assessed for carcinogenic activity in rats and mice. Alachlor is classified as “likely” to be a human carcinogen at high doses, but “not likely” at low doses (US EPA, 1998). It is moderately toxic to fish and highly toxic to aquatic invertebrates: EC50 (48 h) water flea (*Daphnia magna*) 10 mg L<sup>-1</sup>; TL50 (72 hr) algae (*selenastrum capricornutum*) 0.012 mg L<sup>-1</sup> (Tomlin, 1997).

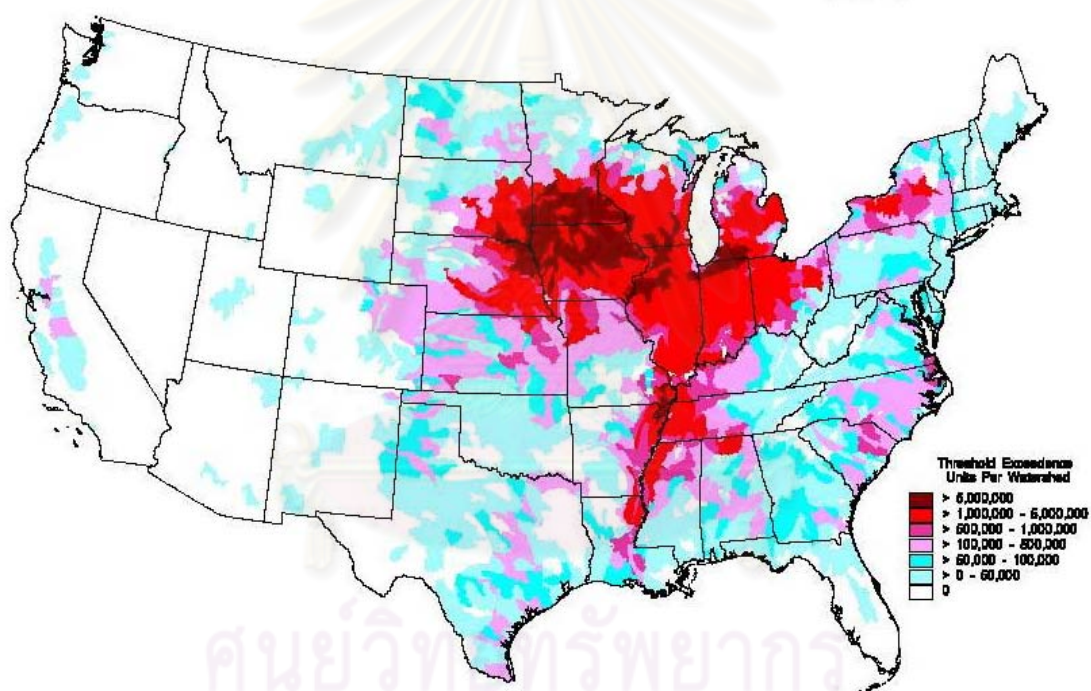


Figure 2.1 Potential for concentration of alachlor runoff at the edge of the field to exceed EPA's maximum contaminant level (2 ppb) USDA, US department of agriculture

The level of protection based on the best available science to prevent potential health problems has been set by US EPA. The maximum contaminant level goals (MCLG) for alachlor, which are any biological, physical, chemical, or radiological substances or matter in water, is zero. This regulation is close to the health goals as possible, considering cost, benefits and the ability of public water systems to detect and remove

contaminants using suitable treatment technologies. In 1992, the Phase II Rule, the regulation for alachlor, became effective. EPA required periodically reviewing the national primary drinking water regulation for each contaminant and revising the regulation by the Safe Drinking Water Act. EPA reviewed that the zero MCLG and 0.002 mg L<sup>-1</sup> or 2 ppb MCL for alachlor are still protective of human health (US EPA, 2010).

### **2.1.5 Situation of alachlor in Thailand**

In annual pesticide consumption, Thailand ranked fourth of 15 Asian countries. The average pesticide use per unit area is high enough to quickly place Thailand as the country with the third highest pesticide use rate, following only Korea and Malaysia (FAO Regional Office for Asia and the Pacific, 2005). With increasing amounts of chemical pesticides, 1,100 tons alachlor was the 14<sup>th</sup> imported pesticide in 2004, Thailand as shown in Table 2.2 (Department of Agriculture, Thailand, 2004).

In Thailand, alachlor was applied in the range 160-717 g per rai (0.16 Hectare) which is mixed with water and other herbicides to improve the herbicide efficiency. It is generally used in the corn field, cotton field, soybean field etc. It was also found that alachlor has moderate persistence in the soil because of the tension force between soil molecules and alachlor. This tension force depends on several factors such as texture of soil and amount of organic substance. It means that the higher amount of organic substances or clay soil occurs, the more alachlor persistence in the soil has been found. It is generally more than 3 months persistence (Himaman, 1998).

In 2005, government hospitals and health care centers reported over 1300 pesticide poisoning cases, which meant that there was over two incidents out of 100,000 of Thai residents being poisoned. Farmers were 61% of the poisoning incidents and the remaining incidents were farm labor workers. These acute poisoning incidents represent only the severest exposure cases that required medical attention (Ministry of Public Health, 2007).

Panuwet *et al.* (2008) reported that farmers from Inthakhin (a district of Chiangmai province, Thailand) had significantly higher concentrations of alachlor. Alachlor was the most predominantly detected metabolites with concentrations as high as 305 ng mL<sup>-1</sup> (221 µg g<sup>-1</sup> creatinine). In the southern part of Thailand, alachlor has been used in vegetable areas and was detected in all shallow and deep wells as well as in streams at Rattaphum catchment area in the Songkhla lake basin (Panapitukkul *et al.*, 2005)

Table 2.2 A summary report of imported agricultural hazardous substances in 2004

Rank	Chemical name	Amount (kg)
1	Glyphosate	27,783,266
2	Paraquat	9,543,341
3	2,4-D	5,219,349
4	Carbofuran	3,122,670
5	Mancozeb	2,311,584
6	Ametryn	2,290,215
7	Abamectin	2,135,833
8	Chlorpyrifos	2,038,977
9	Atrazine	1,997,800
10	Butachlor	1,668,002
11	Carbendazim	1,530,164
12	Propanil	1,420,847
13	Diuron	1,225,176
14	Alachlor	1,128,748

Source: Department of Agriculture, Thailand (2004)

## 2.2 Conventional water treatment system

For surface water, a typical system commonly consists of pre-settling, coagulation and flocculation, granular filtration, pH adjustment, and disinfection. They are placed sequentially together with an addition of a wide variety of chemicals (e.g., chlorine, ozone, ammonia, coagulants, etc.). The pre-settling process functions as a preliminary removal of materials from the raw water. The water is then treated with alum and polymers to encourage flocculation of the colloidal materials (including

suspended sediment) and then left to settle. After that the water is passed through a granular filter comprised of sand and possibly anthracite. After finishing filtration, the water is conditioned to prevent corrosion by pH adjustment and then disinfected using either chlorine or chloramines (US EPA, 2001).

Miltner *et al.* (1989) provided information on the possible removal of pesticides with conventional treatment. Two acetanilides (alachlor and metolachlor), linuron, and carbofuran were spiked into Ohio River. The test was carried out in jar tests. In coagulation and flocculation, the initial concentration of the pesticides was set at  $43.6 \mu\text{g L}^{-1}$ . In this study, alum was added with a loading of  $15\text{-}30 \text{ mg L}^{-1}$ . An initial turbidity of the raw water was of 6 - 42 NTU (Nephelometric Turbidity Units). It was found that the turbidity was dropped to less than 1 NTU in the settled water. The removal of alachlor was finally removed only 4 percent.

The process of softening or softening-clarification was evaluated for its ability to remove pesticides from water. Data collected from the full-scale treatment plants indicated that alachlor at initial concentrations in parts per billion level ( $\mu\text{g L}^{-1}$ ) were not removed by the softening-clarification process.

In laboratory studies conducted by Miltner *et al.* (1987), different oxidants were tested for their ability to remove alachlor in water. The oxidants were  $\text{O}_3$ ,  $\text{Cl}_2$ ,  $\text{ClO}_2$ ,  $\text{H}_2\text{O}_2$ , and  $\text{KMnO}_4$ . Table 2.3 shows the chemical oxidation results using different doses of oxidants, alachlor concentration, and contact time. Only ozone was found to be able to remove alachlor, with removal efficiencies ranging from 79 to 96% for surface water. Miltner *et al.* (1987 and 1989) studied the removal of alachlor using powdered activated carbon (PAC). Alachlor was adequately sorbed to activated carbon. The percent removal was 62% for alachlor. Granular activated carbon (GAC) was also known for adsorbing a wide variety of organic compounds as well as pesticides. The percent removal of alachlor was little higher 72% with GAC (Calgon Filtrasorb 300).

As seen, conventional water treatment (coagulation, sand filtration, and chlorination) is ineffective at removing herbicides such as alachlor and metolachlor.

Table 2.3 Removal of alachlor in different techniques of conventional treatment techniques for surface water

Treatment method	Initial concentration of alachlor ( $\mu\text{g L}^{-1}$ )	Removal (%)
<b>Coagulation</b>	43.6	4
<b>Softening-clarification</b>	3.62	0
<b>Disinfection/chemical oxidation</b>		
Ozone	0.39-5	79-96
Chlorine	31-61	0-5
$\text{ClO}_2$	61	9
$\text{H}_2\text{O}_2$	58 <sup>a</sup>	0
$\text{KMnO}_4$	58 <sup>a</sup>	0
<b>Carbon adsorption</b>		
Powdered activated carbon (Hydrodarco, ICI, America)	8.21	62
Granular activated carbon (Calgon Filtrasorb 300)	3.7	72

Source: Miltner *et al.* (1987); Miltner *et al.* (1989)

Remark: <sup>a</sup> distilled water

### 2.3 Advanced oxidation processes (AOPs)

Over the past fifteen years of the environmental regulation, the governments requires more and more stringent environmental law to protect the human health and environment from contaminants and toxic organic substances originating from human activities.

The development of newer technologies has been increased to destroy these contaminants. Among novel treatment technologies, advanced oxidation processes (AOPs) are effective methods that are useful to accelerate the non-selective oxidation and thus the destruction of a wide range of organic substances resistant to conventional technologies that are quite sufficient for the treatment of wastewater excluding toxic organics.

AOPs, based on physicochemical processes, generally, are the generation of in situ powerful species, predominantly hydroxyl radicals ( $\text{HO}^\bullet$ ) which are able to oxidize and mineralize almost any organic compounds to  $\text{CO}_2$ ,  $\text{H}_2\text{O}$  and inorganic ions (Augugliaro *et al.*, 2006). The reactivity of free hydroxyl radicals which is relatively unselective oxidizing agent, benefits to the treatment of diverse types of pollutants in both contaminated water and polluted air.

Table 2.4 Advantages and disadvantages of AOPs

Processes	Advantages	Disadvantages
UV/ $\text{H}_2\text{O}_2$	Relatively inexpensive, readily to form hydroxyl radicals	May not completely oxidize organics to $\text{CO}_2$ and $\text{H}_2\text{O}$
UV/ $\text{O}_3$	High degradation rate	Absorbs $\lambda < 300\text{nm}$ , a lesser component in solar radiation
Fenton system	High effective degradation rate for wastewater containing phenols, nitrobenzene, herbicides and COD	High volume of sludge Need an optimum pH
Sonolysis	High degradation rate (high mass transfer and free radicals)	High operating cost
Photocatalytic oxidation	Completely oxidize organics to $\text{CO}_2$ and $\text{H}_2\text{O}$	Requiring UV light to activate the catalyst

AOPs can be classified by many ways. By considering the system phase, AOPs are classified into homogenous and heterogeneous processes. There are chemical

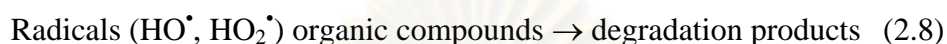
oxidation methods using various oxidants, such as ozone, hydrogen peroxide, potassium permanganate, sodium hypochlorite and Fenton's reagent. For this case, homogenous system is considered. A variety of techniques are also divided into non-photochemical and photochemical methods. The non-photochemical methods consist of ozonation, ozone/hydrogen peroxide, ozone/ultrasound, hydrogen peroxide/ultrasound, Fenton's reagent ( $\text{Fe}^{2+}$ / hydrogen peroxide), sonolysis, sonocatalysis and electro-Fenton. The photochemical methods are ultraviolet radiation/hydrogen peroxide, ultraviolet radiation/ozone, ultraviolet radiation/hydrogen peroxide/ozone, photo Fenton, photoelectro Fenton, photocatalytic ozonation, titanium dioxide/ultraviolet radiation (photocatalysis) and titanium dioxide/ultraviolet radiation/ultrasound (sonophotocatalysis). Based on including titanium dioxide, the process is considered heterogeneously. The advantages and disadvantages among AOPs are presented in Table 2.4.

#### 2.4 Heterogeneous photocatalysis

The heterogeneous photocatalytic process consists of utilizing the near UV radiation to photo-excite a semiconductor catalyst in the presence of oxygen. Under these circumstances oxidizing species, either bound hydroxyl radicals or free holes, are generated. Using photocatalysis, organic pollutants can be completely mineralized reacting with the oxidizers to form  $\text{CO}_2$  and water. The process is heterogeneous because there are two active phases, solid and liquid. This process can also be carried out utilizing the near part of solar spectrum which transforms it into a good option to be used (Malato *et al.*, 2002).

Heterogeneous photocatalysis has recently been attracting attention for treating water. In photocatalysis, electrons in conduction band ( $e_{cb}^-$ ) and holes in the valence band ( $h_{vb}^+$ ) are produced when the catalyst is irradiated with light energy higher than its band gap energy  $E_{bg}$  ( $h\nu > E_{bg}$ ) (Silva *et al.*, 2007), according to reactions (equation 2.1- 2.8):





For photocatalysis, semiconductor materials such as TiO<sub>2</sub>, WO<sub>3</sub>, ZnO, CdS, etc. present good properties such as stability (chemical inertness and photostability) and low cost.

In the applied photocatalysts, titanium dioxide (TiO<sub>2</sub>) is the most popular due to its peculiarities of chemical inertness, suitable band gap energy, non-photocorrosion and non-toxic influence on the microorganisms. TiO<sub>2</sub> is a transition metal oxide. There are three crystalline forms: anatase, rutile and brookite. The crystalline forms of both rutile and anatase form are in the tetragonal system, while brookite is in the orthorhombic system as shown in Figure 2.2.

However, the highly efficient use of TiO<sub>2</sub> is limited in the UV regime (3.0 eV for the rutile phase and 3.2 eV for the anatase phase) which is only a small fraction of the sun's energy (less than 10%) (Linsebigler, *et al.*, 1995). Therefore the TiO<sub>2</sub> should be developed to be active within the visible region.

In study of photocatalytic degradation of organic pollutant, several researchers presented their works focused on alachlor degradation as in Table 2.5. However no researcher emphasized on the photocatalytic degradation of alachlor under visible light.

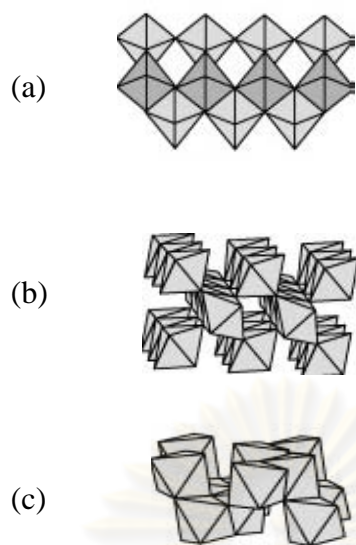


Figure 2.2 Crystal structure of  $\text{TiO}_2$ : (a) anatase (b) rutile and (c) brookite (Paola *et al.*, 2008)

Table 2.5 Examples of photocatalytic degradation of alachlor

Processes	Conditions	Results and discussion	References
Photocatalysis with addition of $\text{FeCl}_3$	A xenon arc lamp $\text{TiO}_2$ (P25) $\text{Fe}^{3+}$ ( $\text{FeCl}_3$ )	The degradation was extremely rapid with half lives varying from 10-17 minutes The degradation kinetics in photocatalysis followed first-order reaction.	Penuela and Barcelo (1996)
Direct photolysis and photocatalysis	UV lamps (254, 300 and 350nm) $\text{TiO}_2$ (P25) $\text{TiO}_2$ , anatase (BDH)	The photocatalytic degradation follows pseudo-first-order kinetics. The photocatalytic activity of $\text{TiO}_2$ -P25 was more effective than that of $\text{TiO}_2$ BDH (Anatase $\text{TiO}_2$ (particle size of 40–500 nm)	Wong and Chu (2003) <sup>a</sup>

Continued Table 2.5 Examples of photocatalytic degradation of alachlor

Processes	Conditions	Results and discussion	References
Photocatalysis with addition of H <sub>2</sub> O <sub>2</sub>	UV lamps (300 and 350 nm) TiO <sub>2</sub> (P25)	The addition of TiO <sub>2</sub> to photolysis of alachlor increased the reaction rates by 12 and 26 times using 300 and 350 nm UV irradiation, respectively. An overdose of H <sub>2</sub> O <sub>2</sub> hinders the degradation rate. The degradation mechanisms include dechlorination, dealkylation, hydroxylation, cyclization, scission of C-O bond, and N-dealkylation	Wong and Chu (2003) <sup>b</sup>
Photocatalysis	UV lamps (300 nm) TiO <sub>2</sub> (P25)	The addition of TiO <sub>2</sub> enhanced the reaction rates by about 12 times as compared with direct photolysis of alachlor. When the initial pH of alachlor solution increased, the degradation of alachlor and the total organic carbon (TOC) enhanced slightly. The TOC analysis presented the different degradation stages of the reaction and followed a pseudo-first-order TOC decay	Chu and Wong (2004)

Source: Sakkas *et al.* 2010

#### 2.4.1 Doping of TiO<sub>2</sub>

A lot of TiO<sub>2</sub> photocatalyst have been applied under UV region which generates energy higher than the band-gap energy of 3.0 or 3.2 eV in the rutile or anatase crystalline phase, respectively. In order to improve photocatalytic activity, TiO<sub>2</sub> is required to develop its photoactivating under sunlight or visible light irradiation. Doping relates to the addition of impurities into the photocatalysts. There are several

methods to overcome this objective. Initially, doping TiO<sub>2</sub> with some elements can narrow the electronic properties and improve the optical properties of TiO<sub>2</sub>. Secondly, sensitizing TiO<sub>2</sub> with other colorful inorganic or organic compounds can enhance its optical activity in the visible light region. Thirdly, coupling collective oscillations of the electrons in the conduction band of metal and non-metal nanoparticle surfaces to those in the conduction band of TiO<sub>2</sub> in metal-TiO<sub>2</sub> can improve the performance (Chen *et al.*, 2005).

To develop the performance of TiO<sub>2</sub>, doping of TiO<sub>2</sub> with metals and non-metals is generally applied. Doping of photocatalysts with metal ions (for example Cr<sup>3+</sup>, Fe<sup>3+</sup>), generates local energy levels within the band gap of the catalyst, with corresponding absorption in the visible region (Fujishima and Zhang, 2006). There are some cases that doping of photocatalysts with metal showed lower activity under visible light and in the UV region compared to the non-doped photocatalysts due to higher recombination. Moreover, metal doping can result in thermal instability and increased carrier trapping (Chen, 2005).

Doping of TiO<sub>2</sub> with non-metals obviously presents the improvement of photocatalytic reactions under visible light irradiation because of the shift of the absorption threshold of TiO<sub>2</sub> into the visible range. Various mechanisms have been postulated to explain the shift of absorption threshold and the photocatalytic activity of non-metal doped TiO<sub>2</sub> photocatalysts. In previous study, various nonmetal elements, such as B, C, N, F, S, Cl, and Br, have been successfully doped into TiO<sub>2</sub> (Chen *et al.*, 2005). Among these, S-doped TiO<sub>2</sub> have been developed by many studies which have been reported as having a reaction property active under visible light (Ohno *et al.*, 2004; Liu *et al.*, 2008; Rengifo-Herrera *et al.*, 2010).

#### **2.4.2 S-Doped TiO<sub>2</sub>**

In particular, S-doped TiO<sub>2</sub> showed strong absorption for visible light and high activities for degradation of methylene blue, 2-propanol in aqueous solution (Ohno *et*

*al.*, 2004). They also reveal that atom ( $S^{4+}$ ) could substitute on some of the lattice titanium atoms during the phase of preparation of S-doped  $TiO_2$  (Ohno *et al.*, 2004). This circumstance can generate an isolated narrow band above the valence band and narrow the band-gap and then form a second adsorption edge in the visible region as shown in Figure 2.3. However, with the increasing amount of the sulfur doped content, the position of the new-generated band-gap structure elevated and could act as recombination centers for electron-hole pairs (Liu *et al.*, 2008). Hydroxyl radicals with higher oxidation power generated by valence band holes under visible light could be the main active species able to degradealachlor and convertalachlor to  $CO_2$ ,  $H_2O$ ,  $NO_2^-$ ,  $NO_3^-$ ,  $Cl^-$  as presented in Figure 2.3.

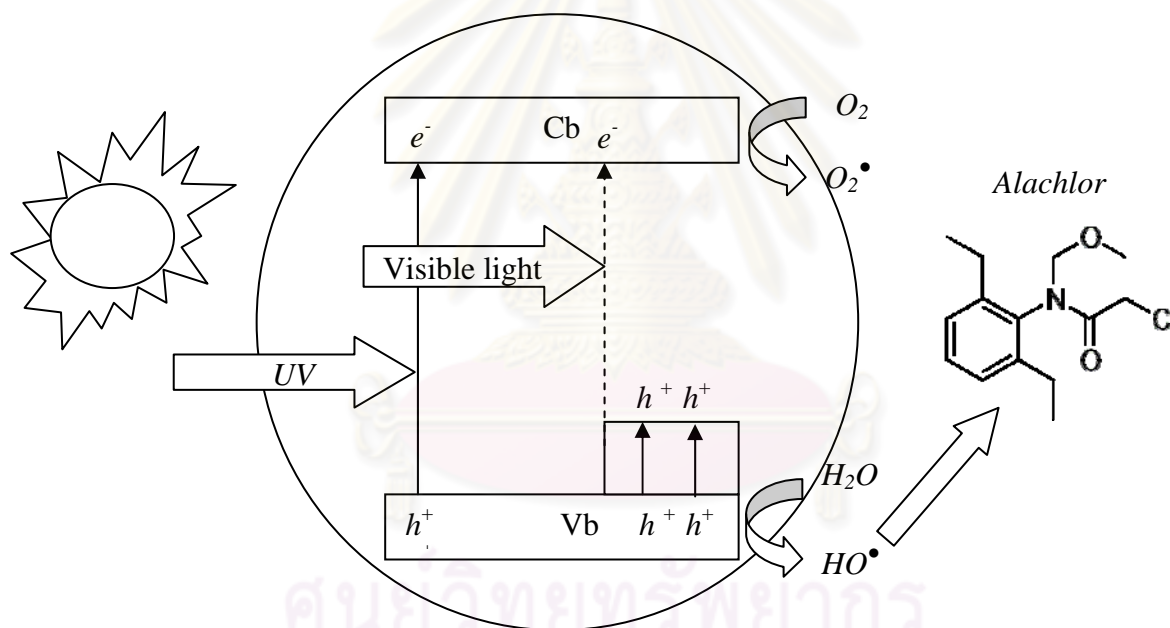


Figure 2.3 Mechanism of S-doped  $TiO_2$  for the alachlor degradation

Source: Rengifo-Herrera *et al.* (2010)

## 2.5 Sonochemistry

### 2.5.1 General principles of sonochemistry

In this part, an acoustic wave theory is discussed in terms of chemistry in applying ultrasound to their reaction system and the use of mathematical concepts to encourage qualitative arguments.

In applying a sound wave, ultrasound is transmitted through any phases including solid, liquid or gas, which have elastic properties. The movement of the vibrating body (i.e. sound source) is contacted to the molecules of the medium, each of which transmits the motion to an adjoining molecule before returning to approximately its original position. For liquid and gases, particle oscillation occurs in the direction of the wave and produces longitudinal wave. Conversely, solids having shear elasticity can also support tangential stresses giving rise to transverse wave and particle movement takes place perpendicular to the direction of the wave (Wayment, 1997, Mason and Lorimer, 2002).

In liquid phase, an example of longitudinal wave likes the coil of the spring. At anytime ( $t$ ) the displacement ( $x$ ) of an individual air molecule from its mean rest position is given by equation 2.9

$$x = x_A \sin(2\pi \cdot f \cdot t) \quad (2.9)$$

Where  $x_A$  is the displacement amplitude or maximum displacement of the particle,  $f$  is the frequency of the sound wave and  $t$  is considering time.

For the particle velocity ( $v$ ), differentiation of the above leads to an expression (equation 2.10)

$$v = \frac{dx}{dt} = v_A \cos(2\pi \cdot f \cdot t) \quad (2.10)$$

Where  $v_A$  is the maximum velocity of the particle (Wayment, 1997, Mason and Lorimer, 2002).

A sound wave is a periodic pressure wave passing through a medium with amplitude  $P$  at any point in time  $t$  as described by equation 2.11, where  $P_A$  is the maximum pressure amplitude.

$$P = P_A \sin(2\pi \cdot f \cdot t) \quad (2.11)$$

To overcome the surface tension of the liquid and form cavities within the liquid, the net negative pressure of the rarefaction cycle  $P_{rare}$  is equal to the difference between the negative maximum pressure amplitude  $P_A$  and the hydrostatic pressure  $P_0$  as shown in equation 2.12.

$$P_{rare} = P_A - P_0 \quad (2.12)$$

When  $P_{rare}$  is greater than or equal to the necessary amplitude for overcoming the surface tension of the liquid medium  $P_{thresh}$  cavitation can occur.  $P_{thresh}$  can be calculated by equation 2.13.

$$P_{thresh} = P_0 + \frac{\sigma}{9} \sqrt{\frac{3\sigma}{2(P_0 + 2\frac{\sigma}{R_B})R_B^3}} \quad (2.13)$$

Where  $\sigma$  is the surface tension and  $R_B$  is the critical radius of the cavity. The derivation of this equation neglects inertial and viscous effects and assumes that gas diffusion occurs slowly compared to mechanical bubble formation (Wayment, 1997).

There are two types of acoustic cavitation consisting of stable and transient cavitation (Flynn, 1964). Stable cavitation is a phenomenon in which gas bubbles oscillate many times around their equilibrium radius by low acoustic pressure. Transient cavities on the other hand, display much larger variations in their sizes from the equilibrium radius and undergo a violent collapse within a few acoustic cycles.

The collapse of the cavity performs work and concentrates enormous amounts of energy at a small volume. The hot spot theory (Suslick, 1988) predicts that the

collapse of the bubble will be resisted by the gas inside the bubble, consisting of the vapor of the solvent and whatever gas that may reside in the liquid medium. The gas inside the bubble will be compressed so rapidly that heat is not transferred out of the bubble and hence the collapse is adiabatic. The temperature and pressure inside the bubble during this collapse will increase tremendously.

Rayleigh was the first who described quantitatively the process of bubble collapse by assuming that a spherical bubble is suddenly annihilated from an infinite mass of incompressible and homogeneous fluid (Wayment, 1997).. In assumption, the formation of a vacuum occurs within the bubble and the radius of bubble will collapse down to zero, giving rise to a singularity. In fact, a near vacuum hardly exists for a relatively long time and the pressure inside the void is rapidly built up to several dozen torr in the process of the evaporation of fluid inside the bubble and from the diffusion of dissolved gasses. The presence of this residual pressure  $p_i$ , in the bubble at the maximum radius  $R_{max}$  eliminates the singularity in the Rayleigh's model. The model of collapse (Flynn, 1964) usually does not take into consideration the surface tension (a good approximation for bubbles with radius  $r$  of more than 1 micron because  $2\sigma/r$  is negligible) and assumes that the compression is adiabatic. The model gives the maximum pressure  $P_{max}$  and temperature  $T_f$  reached by the gas in the bubble when the radius rapidly drops from  $R_{max}$  to  $R_{min}$  in equation 2.14 and 2.15;

$$T_f = T_i \left( \frac{R_{max}}{R_{min}} \right)^{3(\gamma-1)} \quad (2.14)$$

$$P_{max} = p_i \left[ \frac{P(\gamma-1)}{p_i} \right]^{\gamma(\gamma-1)} \quad (2.15)$$

Here  $T_i$  is the temperature of the gas before collapse,  $P$  is the external pressure in the liquid (a sum of hydrostatic and acoustic pressures), and  $p_i$  is the initial pressure of the non-condensable gas (in the absence of dissolved gasses,  $p_i$  may be estimated as the equilibrium vapor pressure at  $T_i$ ) inside the bubble of radius  $R_{max}$ .

From equation 2.14, one can see that by changing the gas dissolved in the liquid medium, it is possible to affect the maximum temperature reached inside the collapsing bubble by choosing gases with different polytropic ratios (ratio of specific heats)  $\gamma = C_p/C_v$ . For a monatomic gas with a polytropic ratio of 1.67,  $T_i = 27^\circ\text{C}$  and  $P/p_i = 15$ , the final collapse temperature is calculated using equation 2.14 to be  $1077^\circ\text{C}$ . Suslick has measured this temperature to be  $4927^\circ\text{C}$  with pressures of hundreds of atmospheres (Wayment, 1997).

### 2.5.2 Intensity and pressure amplitude

Sound was a form of kinetic energy coming from vibratory motion of the particles of the medium. Therefore the kinetic energy (KE;  $mv^2/2$ ) of the layer is given by equation 2.16.

$$KE = \frac{1}{2}(\rho A dx)v^2 \quad (2.16)$$

Where  $A$  is the area of the movement of a layer of the medium and thickness under the action of the ultrasonic wave is  $dx$ .

The energy for the whole wave,  $E_t$ , may be obtained by summing all such elements by integrating equation 2.16 to provide equation 2.17.

$$E_t = \frac{1}{2}(\rho A x)v^2 \quad (2.17)$$

The energy per unit volume ( $Ax$ ) or energy density,  $E$ , given by equation 2.18

$$E = \frac{1}{2}\rho v^2 \quad (2.18)$$

If the sound energy passes through unit cross-sectional area ( $A = 1$ ) with a velocity of  $c$ , then the volume swept out in unit time is  $c$  (since  $A = 1$ ), and the energy flowing in unit time is given by  $Ec$ . Since intensity ( $I$ ) has been defined as the amount of energy flowing per unit area ( $A = 1$ ) per unit time (equation 2.19)

$$I = E c \quad (2.19)$$

and from equation 2.18

$$I = \frac{1}{2} \rho c v^2 \quad (2.20)$$

For maximum particle velocity,  $v_A$ , the amplitude of the oscillating acoustic pressure,  $P$ , is given by equation 2.21.

$$\frac{P}{v_A} = \rho c \quad (2.21)$$

Thus the intensity of the sound wave (from equation 2.20 and 2.21) may be expressed as equation 2.22

$$I = \frac{P^2}{2\rho c} \quad (2.22)$$

In order to evaluate the sound intensity at a particular point in a medium, either the maximum particle velocity,  $v_A$  (equation 2.10) or the maximum pressure amplitude,  $P$  (equation 2.22) must be measured (Wayment, 1997, Mason and Lorimer, 2002).

### 2.5.3 Aqueous sonochemistry

Since the early 20<sup>th</sup> century, ultrasound has been applied to chemical systems. Most of researchers carried out with ultrasound at frequencies of 20 kHz (using a horn sonicator) and 40-50 kHz (cleaning bath). As acoustic wave irradiates through a liquid medium, alternating compression and (rarefaction) cycles occur. When the amplitude of the sound wave is high enough, a void containing the liquid vapor, dissolved gases and volatile solutes is formed during the expansion cycle. For the period of the compression cycle, the cavity is compressed rapidly, resulting in high temperatures and pressures within the bubble. Micro voids grow up upon many acoustic cycles of time and lastly attain a critical size. This critical size is unstable and finally the critical bubble is exploded tremendously as presented in Figure 2.4.

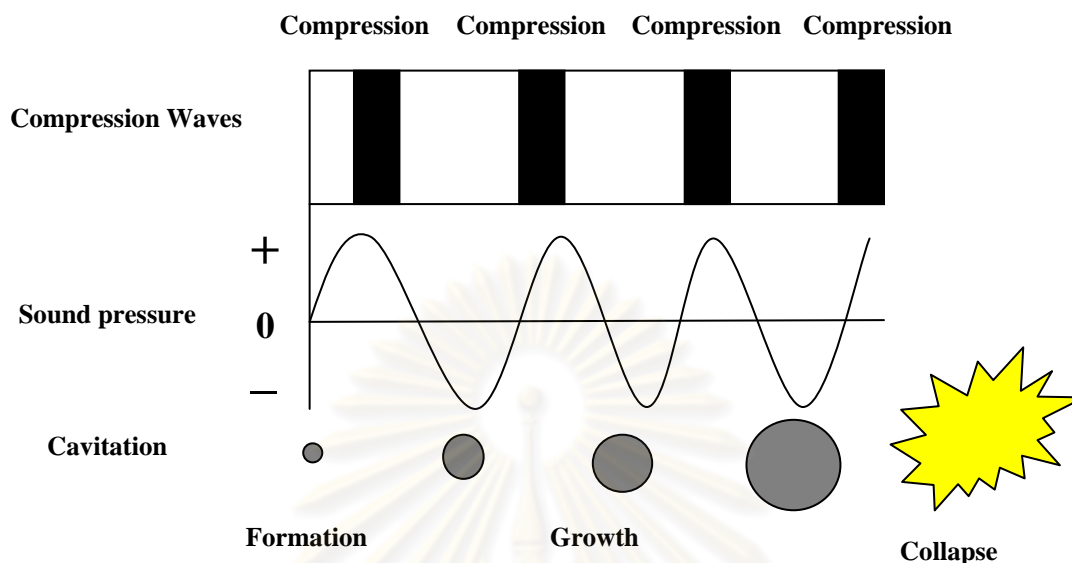


Figure 2.4 Cavitation, formation, growth and collapse bubbles adapted from He  
Source: He (2009)

In cavitation, there are three regions consisting of the gas phase, the interfacial region, a thin shell of superheated liquid surrounding the vapor phase, and the bulk liquid.

Aqueous sonochemistry results from two sources: (1) the degradation of the solute within the cavitation bubble by direct thermal action, and (2) the reaction of dissolved solute with hydrogen. Hydroxyl and other free radicals produced from the water vapor and dissolved gasses. The cleavage of dioxygen and water molecules produces active species, such as  $\text{H}^\bullet$  and  $\text{HO}^\bullet$  radicals in equation 2.23.



It is capable of attacking the organic compounds in water. Hydrogen radicals from the above reaction can also interact with the oxygen present in the system to form peroxide radicals,  $\text{HO}_2^\bullet$ , and hydrogen peroxide,  $\text{H}_2\text{O}_2$  (Augugliaro *et al.*, 2006).

Therefore heterogeneous photocatalysis and ultrasonic irradiation can cause degradation of organic pollutants in water by the same species, notably HO<sup>•</sup> radicals.

In previous study of alachlor degradation, the rate of sonodegradation was approximately 25 times faster at 300 kHz under argon saturation than at 20 kHz at the same input energy of ultrasound. Argon presented higher rate of alachlor degradation compared to oxygen or air under sonication at 300 kHz. In sonodegradation of alachlor in an argon-saturated solution, products of the degradation came from bond scission. Its products resulted from both bond scission and oxygen addition when the dissolved gas was oxygen (Wang *et al.*, 2007).

## 2.6 Sonophotocatalysis

The combination of photocatalytic activity and ultrasonic irradiation can enhance the degradation of organic pollutants for water by the species, notably HO<sup>•</sup> radicals, as was presented in equation 2.8 and 2.23. The assistance of ultrasound to photocatalysis may be related to an increase in the production of hydroxyl radicals via water sonolysis and H<sub>2</sub>O<sub>2</sub> cleavage.

Additionally, there are several benefit effects of these combined techniques as follows;

- Cavitation effects enhancing temperature and pressure
- Good cleaning of catalyst surface
- The increment of mass transport of the catalyst and solution
- The addition of surface area of catalyst
- The improvement of direct reaction with the photogenerated surface holes and electrons under cavitation (Parag and Pandit, 2004)
- The increment in decomposing hydrophobic parts of organic pollutant which unlikely occur in the photocatalytic activity. (He, 2009)

The combined processes of photocatalysis with sonolysis (sonophotocatalysis) using an ultrasound source of 20 kHz in degradation of these herbicides was also carried out by Bahena (Bahena *et al.*, 2008). Results showed more than 90% degradation of

alazine and gesaprim, commercial herbicides, in TiO<sub>2</sub> suspensions under UV light (15 W, 352 nm) and ultrasound. The study of alachlor degradation profiles was recorded by measuring the concentration of the active compounds present in the alazine (alachlor and atrazine) and gesaprim (atrazine) by HPLC as a function of irradiation time (sound and/or light). Mineralization of these herbicides was studied by the decrease of total organic carbon and chemical oxygen demand. The results showed that alachlor was completely mineralized. At 150 min of irradiation time, over 80% of chemical oxygen demand abatement was attained for both herbicides with sonophotocatalysis. The combined effects of sonolysis greatly enhanced the photocatalytic degradation of the herbicides. This activity followed pseudo-first order kinetics and the rate constant was increased by the combined effect of sonolysis.

### 2.6.1 Synergistic effect of sonophotocatalysis

In different processes consisting of sonocatalysis, photocatalysis and sonophotocatalysis, the decay rate of organic compound was evaluated in terms of reaction rate. The reaction rate of combined sonocatalysis and photocatalysis is generally greater than the sum of two processes. It can be normalized difference between the rate constant of two processes in terms of synergy as explained in equation 2.24.

$$\text{Synergetic effect} = \frac{k_{vis+us+TiO_2} - (k_{us+TiO_2} + k_{vis+TiO_2})}{(k_{us+TiO_2} + k_{vis+TiO_2})} \quad (2.24)$$

Where,  $k_{vis+US+TiO_2}$  is pseudo first order rate constant under combined system of sonolysis and photocatalysis in visible light,  $k_{US+TiO_2}$  is pseudo-first-order rate constant under sonocatalysis and  $k_{vis+TiO_2}$  is pseudo-first-order rate constant under photocatalysis in visible light.

## 2.7 Influences of sonophotocatalytic activity

### 2.7.1 Effect of the catalyst loading

In order to obtain the optimum catalyst loading, varying the amount of catalyst loading in the different range can be performed under ultrasonic irradiation and visible light irradiation simultaneously. It appears that the degradation of organic pollutants improved gradually with the increase of the amount of catalyst loading until it reached optimum value. It can be explained that when low amounts of catalyst is used, the rate of reaction on the catalyst surface area is limited, due to the proportion of catalyst loading to the reaction rate (Bejarano-Pe´rez *et al.*, 2007). However, using catalyst concentration higher than the optimum slightly reduces the degradation rate because of diminished light irradiation passing through the sample. Furthermore, the aggregation of catalyst particles at high concentration affects the amount of active site areas on the surface of catalyst. It reduces the sonophotocatalytic degradation rate.

### 2.7.2 Effect of pH

The pH is a complex parameter as it is involved in the ionization state of the surface, as shown in equations (2.25) and (2.26), as well as to that of reactants and products such as acids and amines:



There are three possible mechanisms contributing to organic pollutant degradation: hydroxyl radical attack, direct oxidation by the positive hole, and direct reduction by the electron in the conducting band depending on the nature of the substrate and pH (Kaur and Singh, 2007).

The surface charge of  $TiO_2$  (pzc of  $TiO_2$ ) can be employed to describe the effect of pH on the photocatalytic reaction. It relates to the electrostatic attraction of the positive

and negative charge of  $\text{TiO}_2$  with the ionization of organic pollutants. The strong adsorption and weak adsorption can be influenced by the surface charge of  $\text{TiO}_2$  (Kaur and Singh, 2007).

For example, in acidic solution,  $\text{TiO}_2$  is attracted by the presence of inorganic anions forming a layer of charged barriers around the  $\text{TiO}_2$  particles. It hinders the collision between the alachlor molecule and the  $\text{TiO}_2$  particles that retard the alachlor degradation (Wong and Chu, 2003).

### **2.7.3 Effect of ultrasonic intensity**

The application of ultrasonic sound generating OH and  $\text{O}_2$  radicals, and increasing the mass transfer rate are utilized to assist the photocatalytic activities of degradation of organic pollutant. The reaction rate increases substantially when the illuminated catalysts are simultaneously sonicated. In addition, parameters such as frequency, power intensity and amplitude were studied by Wayment *et al.*, (2002) and Neppoliana *et al.*, (2002).

## **2.8 Design of Experiment (DoE)**

The photocatalytic degradation of organic pollutants has been frequently investigated in the kinetic expression of reaction, the mechanism of reactions, and also the mineralization of pollutants. The traditional one-factor-at-a-time method was generally employed to determine the influence of parameters involving in the assessment one factor at a time as controlling all other constants. This method consumes time and cost of experiment as well as ignores the interactions between effects of variables and also provides misguided prediction of optimum photocatalytic degradation efficiency (Raya *et al.*, 2009; Sakkas *et al.*, 2010).

Therefore, design of experiment is an approach to do experiments systematically. Its benefits are to save time and money due to the reduction of the number of experiments and to maximize significance. Response surface methodology (RSM) based on DoE could be applied to determine precisely the effect of the variables on

the reaction by varying all the factors simultaneously in a systematic manner. This method verifies relationships between several independent variables and one or more dependent variables. This experimental design in photocatalytic reactions plays an important role in the ability of reaching the optimum of the catalytic reaction.

There are four DoEs including full three level factorial designs, central composite design (CCD), Doehlert design and Box–Behnken design (BBD), commonly applied in the photocatalytic study. The advantages and disadvantage of each DoE method are presented in Table 2.6.

Table 2.6 Comparison of four DoEs in RSM

Method	Advantages	Disadvantages
Full three level factorial designs	Accurately predicting the response	Need large number of experimental runs
Central composite design (CCD)	Accurately fitting quadratic response models	Need time consuming design with large numbers of factors
Doehlert design	Requiring few experimental points	Need more complex experimental design
Box–Behnken design (BBD)	Accurately fitting quadratic response models, requiring fewer number of runs for 3 factors	Not benefit for 4 or more factors

For example, a multivariable center composite design (CCD) based on response surface methodology was applied to estimate the individual and interaction factors including pH, TiO<sub>2</sub> loading, oxygen concentration and light flux. This technique reaches to the optimum condition of photocatalytic degradation of methylparaben (Lin *et al.*, 2009). In addition, an overview of the most relevant applications is depicted at Table 2.7.

Table 2.7 Examples of photocatalytic degradation using RSM

Compound	Photocatalytic Process	Selected variables	DoE and optimization techniques	Reference
Diuron	H <sub>2</sub> O <sub>2</sub> /Fe(II)/UV	Pesticide dose, hydrogen peroxide dose, ferrous ion dose Fe(II)	Box–Behnken design	Catalkaya <i>et al.</i> , 2007
Diuron and Linuron	Fe(II)/H <sub>2</sub> O <sub>2</sub> /UV	Hydrogen peroxide dose and iron	Central composite Design	Farre <i>et al.</i> , 2006
Alachlor	Fe(II)/H <sub>2</sub> O <sub>2</sub> /UV	Temperature 20–50 °C, iron concentration 2–20 mg L <sup>-1</sup> , illuminated volume 11.9–59.5% of total	Central composite design without star points	Gernjak <i>et al.</i> , 2006
2,4-Dimethyl aniline	Fe <sup>3+</sup> exchanged zeolite Y/ H <sub>2</sub> O <sub>2</sub> /UV	Fe <sup>3+</sup> concentration and H <sub>2</sub> O <sub>2</sub> concentration	Factorial matrices 2 <sup>2</sup> and Doehlert matrices	Rios-Enriquez <i>et al.</i> , 2004

Reference: Sakkas *et al.* 2010

### 2.8.1 Box–Behnken design (BBD)

The BBD technique is a three-level design based upon the combination of two-level factorial designs and incomplete block designs. The number of experiments required (N) is given by  $N = 2k(k-1) + C_0$ , where k is the number of variables and  $C_0$  is the number of center points. The main advantage of using BBD is that this design avoids extreme conditions of experiments. BBD is a spherical design with excellent predictability within the spherical design space and requires fewer experiments than other technique with the same number of factors. Compared to other methods, the BBD technique is considered as the most suitable for evaluating quadratic response surfaces. In addition, the BBD technique is rotatable or nearly rotatable regardless of the number of factors under consideration.

In application of DoEs in photocatalytic process, the study of the Box-Benken technique of the phenol photocatalytic degradation by  $\text{TiO}_2$  nanoparticles were investigated using four variables such as titanium dioxide ( $\text{TiO}_2$ ) catalyst size,  $\text{TiO}_2$  concentration, dissolved oxygen (DO) concentration and phenol concentration (Raya *et al.*, 2009).

## CHAPTER III

### METHODOLOGY

The main objective of this study concerns the degradation of alachlor on S-doped TiO<sub>2</sub> photocatalytic and sonophotocatalytic activity. The experiments are divided into three parts as shown in Figure 3.1. The catalyst characterization is studied first to provide us the idea of the studied material. Then, the comparison of photocatalysis and sonophotocatalysis is carried out to ensure that the set-up system is worked properly. After that, the detail study will be investigated.

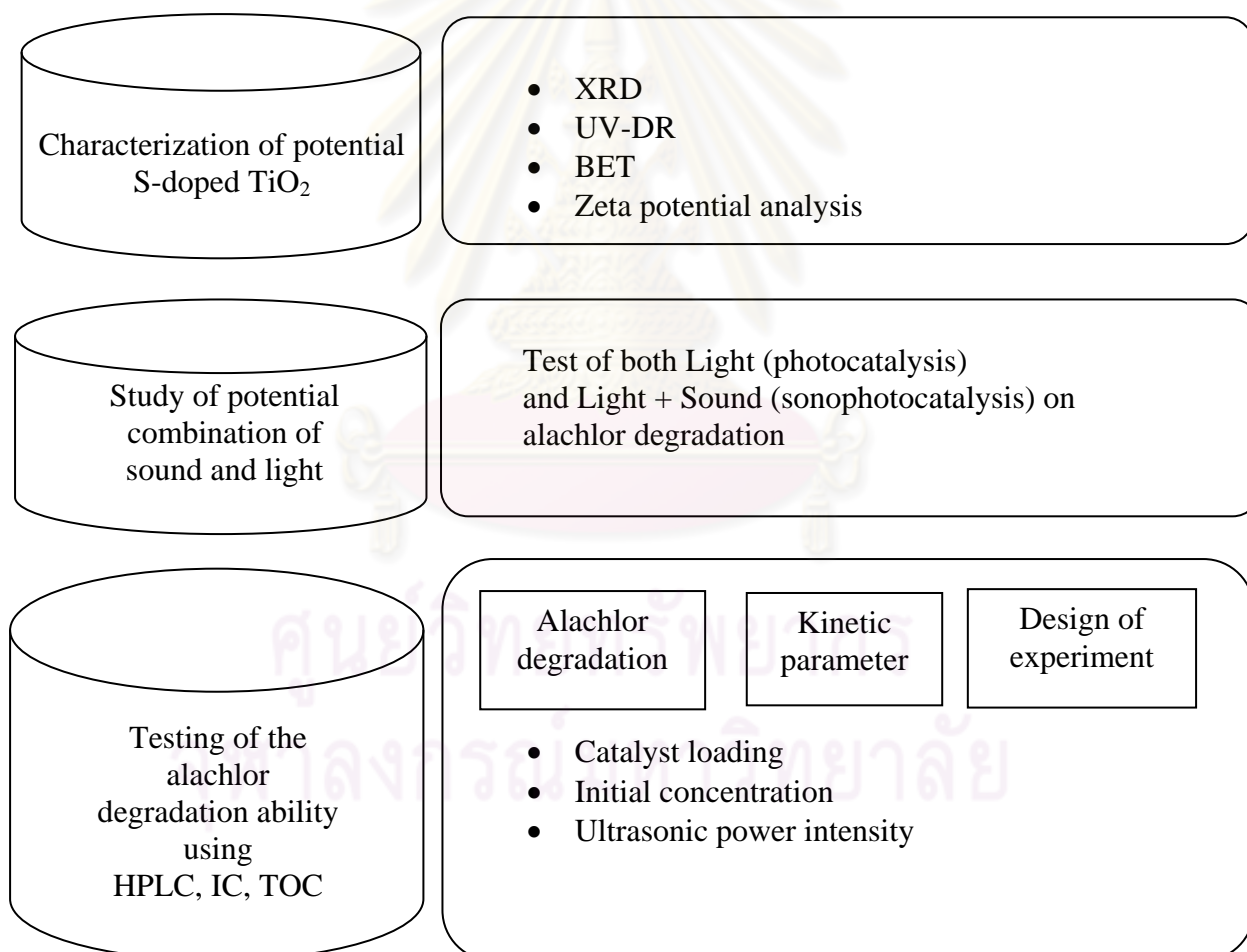


Figure 3.1 The experimental framework of this study

## 3.1 Chemicals and instrumentation

### 3.1.1 Chemicals

- Alachlor (2-chloro-2-,6-diethyl-N-(methoxymethyl) acetanilide) supplied by Supelco (USA)
- TiO<sub>2</sub> Degussa P25 (mixture containing approximately 75% anatase and 25% rutile with a high surface area of about 50 m<sup>2</sup> g<sup>-1</sup>) was purchased from Evonik Degussa Industry
- S-doped TiO<sub>2</sub> catalysts were provided by Prof. Teruhisa Ohno (Ohno *et al.*, 2004)
- FeSO<sub>4</sub> supplied by Carlo Erba Co.
- CuSO<sub>4</sub> supplied by Carlo Erba Co.
- H<sub>2</sub>SO<sub>4</sub> supplied by Carlo Erba Co.
- H<sub>2</sub>O<sub>2</sub> supplied by Carlo Erba Co.
- K<sub>2</sub>S<sub>2</sub>O<sub>8</sub> supplied by Carlo Erba Co.
- HPLC grade acetonitrile from Labscan
- HPLC grade water from Labscan

### 3.1.2 Instrumentation

- X-ray diffractometer (Bruker axs D8, Germany)
- UV-Visible spectrophotometer (Shimazu UV-1201, Japan)
- UV-Visible spectrophotometer (Jusco 608, Japan)
- UV-Visible diffuse reflectance spectrophotometer (Hitachi 3501, Japan)
- N<sub>2</sub> adsorption-desorption analyzer (Quantachrom Autosorp-1, USA)
- Scanning electron microscope (model: Supra 25) with US Phoenix EDX
- High performance liquid chromatograph (HPLC Agilent Technologies 1200 series detector and 1100 series pump and controller)
- Ion chromatograph (Dix-4000, Dionex Co.)
- 500 W xenon arc lamp (Shanghai Dian Guang Device Ltd.)
- JB420 and JB450 cutoff filter (China Nantong Yinxing Optical Co. Ltd.)
- A 20 kHz ultrasonic processor 500 W (Sonic Model: VC 505)

## 3.2 Catalyst characterization

S-doped TiO<sub>2</sub> and pure TiO<sub>2</sub> (Degussa P25) were characterized by an X-ray diffractometer (XRD), UV-Vis diffuse reflectance spectrophotometer, Brunauer-Emmett-Teller method (BET), Scanning Electron Microscopy/ Energy Dispersive Spectroscopy (SEM/EDX), Transmission Electron Microscopy (TEM) and the zeta potential technique.

### 3.2.1 X-ray diffractometer (XRD)

The crystal structure and crystal size of S-doped TiO<sub>2</sub> powders were determined by using a powder X-ray diffractometer, Bruker D8, equipped with a Cu K $\alpha$  radiation source. All of the powder samples were run at an angle of  $2\Theta$  from 20° to 80° with a step size of 0.02° and a time step of 2.0 sec to assess the matrix structure.

The average crystallite sizes for the catalyst samples were calculated by applying the Scherrer equation to the full-width at half-maximum of the (101) crystal plane of anatase TiO<sub>2</sub> by the following equation 3.1.

$$D_{Scherrer} = \frac{k\lambda}{\beta \cos \theta} \quad (3.1)$$

Where,  $k$  equals to 0.9, a shape factor for spherical particles;  $\lambda$  is the X-ray wavelength ( $\lambda = 0.154$  nm);  $\theta$  is the Bragg angle (radian); and  $\beta = B - b$ , the line broadening.  $B$  is the full width of the direction line at half the maximum intensity, and  $b = 0.042$  is the instrumental broadening, (Demeestere *et al.*, 2005).

The mass fraction values of anatase and rutile were calculated by the following equation 3.2 (Jho *et al.*, 2008)

$$\% A = \frac{100}{(1 + 1.265 \frac{I_R}{I_A})} \quad (3.2)$$

Where A is mass fraction of anatase in particle catalyst,  $I_R$  is maximum intensity of the rutile phase, and  $I_A$  is the maximum intensity of the anatase phase.

### 3.2.2 UV-Vis diffuse reflectance spectrophotometer

The absorbance spectra of S-doped TiO<sub>2</sub> powders were determined by UV–VIS diffuse reflectance spectroscopy (DRS-UV) using Hitachi U-3010 (Japan) spectrophotometer with an integrating sphere. BaSO<sub>4</sub> was used as a reference.

The diffuse reflectance spectra of the photocatalyst powders, together with those of the pure rutile and anatase powders of TiO<sub>2</sub> (P25), are calculated. The band gap energies of the catalysts were calculated using the following equation 3.3.

$$E_g = hc/\lambda \quad (3.3)$$

where,  $E_g$  is the energy gap (eV),  $h$  is Plank's constant,  $c$  is the velocity of light ( $m s^{-1}$ ), and  $\lambda$  is the wavelengths of the absorption edges (nm) (Surolia *et al.*, 2007).

### 3.2.3 The Brunauer-Emmett-Teller method (BET)

Nitrogen adsorption and desorption isotherms were obtained for the surface area using Quantachrome, Autosorb I. The physical characteristics of the samples were determined by the BET method at  $-196^\circ\text{C}$  under a relative pressure of 0.02-0.3 with an Autosorb-I analyzer. Before the BET analysis, each sample was degassed in a vacuum at a heat of  $250^\circ\text{C}$  for 3 hrs. The fitting of the straight part of the  $p/V(p-p_0)$  versus  $p/p_0$  curve was applied to measure the surface area. The adsorption isotherms of nitrogen were collected at  $-196^\circ\text{C}$  using approximately 20 values of relative pressure ranging from 0.05 to 0.99. The pore size and pore size distribution of each sample was measured.

### **3.2.4 Scanning Electron Microscopy/Energy Dispersive Spectroscopy (SEM/EDS)**

After coating the samples surface with a thin layer of gold, surface morphology and particle size were studied using a scanning electron microscope (model: Supra 25) with US Phoenix EDX attachment. In SEM, an electron beam was scanned across the surface of the sample, making the electrons strike the sample. The detected specific signals can be compiled into an image or elemental composition of the sample. Interaction of the primary beam with atoms in the sample causes shell transitions that result in the emission of an X-ray. The emitted X-ray has an energy characteristic of the parent element. The detection and measurement of the energy result in elemental analysis (Energy Dispersive X-ray Spectroscopy or EDS). This technique can provide rapid qualitative or, with adequate standards, quantitative analysis of the elemental composition with a sampling depth of 1-2 microns. Element mapping is applied by X-rays to generate form maps or line profiles, showing the elemental distribution on a sample's surface.

### **3.2.5 Transmission Electron Microscopy (TEM)**

The power of sample was developed in the colloid form. The colloidal sample form was deposited on a copper grid. For the TEM analysis, the deposited sample on the copper grid is dried and transferred to a TEM (model: JEOL JEM-2010 instrument with 200 kV of acceleration voltage). The magnification used in this measurement was 25k to 100k. The samples for TEM analysis were dispersed in absolute ethanol by sonication, dropped on a copper carbon only grid and dried at 70°C with UV lamp.

### **3.2.6 Zeta potential technique**

The mobility distribution of a dispersion of charged particles as subjected to an electric field was measured by zeta potential technique. The quantification of the magnitude of the surface charge at the double layer widely applied.

The zeta potential and surface charge of powders were determined by using an electrophoretic light scattering spectrophotometer, Malvern ZS90. The pH of the sample

solution was adjusted using 0.1 M NaOH and/or 0.1 M HCl before adding into the sample cell. The measurements were performed at 25°C. Each sample value is the average of three time measurements. The range of zeta potential was -30 mV to 30 mV.

### 3.3 Photocatalytic and sonophotocatalytic activities

#### 3.3.1 Photocatalytic activities

In order to compare the photocatalytic activities of S-doped TiO<sub>2</sub> to that of pure TiO<sub>2</sub> (Degussa, P-25), their effects on alachlor degradation rates were investigated by varying the wave length of the light source within the visible range, initial concentration, catalyst loading and rate expression. The photocatalytic degradation of alachlor was carried out under the following conditions:

- As presented in Figure 3.2, the 80 mL pyrex glass reactor was equipped with cooling system to maintain temperature in the solution at 23-25°C.
- The initial alachlor solution of 10 mg L<sup>-1</sup> (3.7 x 10<sup>-5</sup> M) was prepared by diluting from the stock solution to obtain a solubility in water of 240 mg L<sup>-1</sup>, and a solution pH was adjusted to be 7.
- 80 mg of catalyst, equivalent to catalyst loading 1g<sub>catalyst</sub> L<sup>-1</sup> solution, was suspended in a synthetic wastewater contaminated alachlor. To obtain equilibrium adsorption between solid and alachlor, the mixed solution was placed in the dark for 30 min.
- The suspended sample was photoirradiated using a 500-W Xenon lamp which emits both UV and visible light over a wide range of wavelengths.
- To limit the irradiation wavelength, the light beam was passed through a JB420 and a JB450 cutoff filter (China Nantong Yinxing Optical Co. Ltd.) to cut off the wavelengths that were shorter than 420 nm and 450 nm respectively.

- A sample was collected for every 15 min in the beginning phase and every 30 min and every 30 min after the time on stream. Samples were filtered by passing through 0.45  $\mu\text{m}$  pore size membrane filters to remove all the catalyst powder and other contaminants.

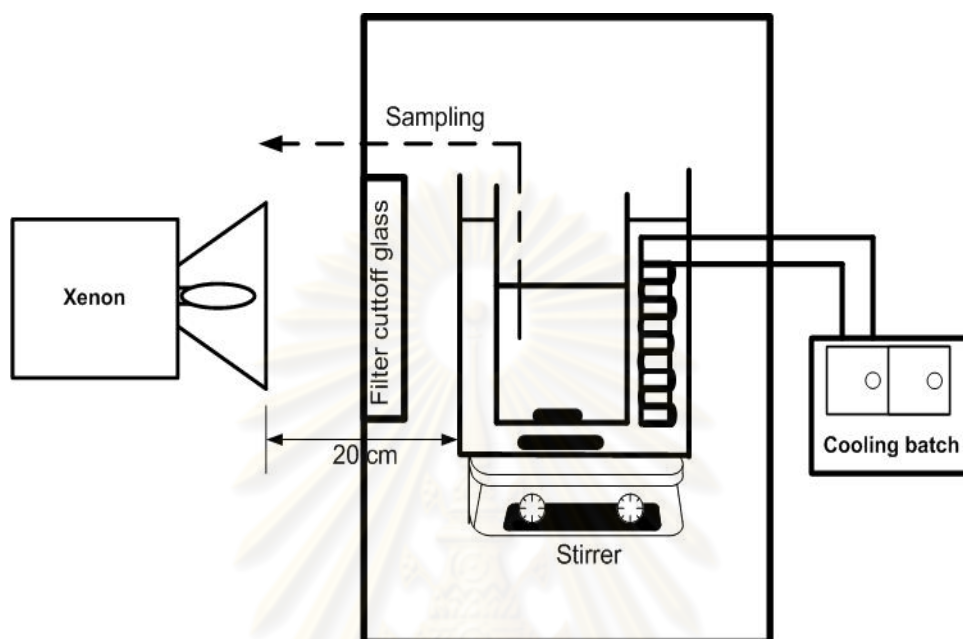


Figure 3.2 A schematic diagram of the photocatalytic experimental setup

### 3.3.2 Sonophotocatalytic activities

The combined process comprising both photocatalysis and sonolysis was systematically determined by comparing the alachlor degradation efficiency of the individual processes. To study the impact of sonophotocatalytic activity on the degradation of alachlor by S-doped  $\text{TiO}_2$ , the effects of the ultrasonic power, catalyst loading, and oxidizing agents in both  $\text{H}_2\text{O}_2$  and  $\text{K}_2\text{S}_2\text{O}_8$  were evaluated. The sonophotocatalytic degradation of alachlor was carried out under following conditions:

- As presented in Figure 3.3, the 80 mL pyrex glass reactor was equipped with cooling system to maintain temperature in the solution at 23-25°C.

- An initial alachlor solution of  $10 \text{ mg L}^{-1}$  ( $3.7 \times 10^{-5} \text{ M}$ ) was prepared by diluting from the stock solution to obtain a solubility in the water of  $240 \text{ mg L}^{-1}$ , and the solution pH was 7.
- 80 mg catalyst, equivalent to catalyst loading  $1 \text{ g}_{\text{catalyst}} \text{ L}^{-1}$  solution, was suspended in synthetic wastewater contaminated alachlor. To obtain equilibrium adsorption between solid and alachlor, the mixed solution was placed in dark for 30 min.
- The suspended sample was photoirradiated using a 500-W Xenon lamp which emits both UV and visible light over a wide range of wavelengths.
- To limit the irradiation wavelength, the light beam was passed through a JB450 cutoff filter (China Nantong Yinxing Optical Co. Ltd.) to cut off the wavelengths that were shorter than 450 nm.
- A 500 W ultrasonic processors (Sonic Model: VC 505) was used as an source of ultrasound at ultrasonic frequency of 20 kHz.
- A sample was collected for every 15 min in the beginning phase and every 30 min and every 30 min after the time on stream. Samples were filtered by passing through  $0.45 \text{ }\mu\text{m}$  pore size membrane filters to remove all catalyst powder and other contaminants.

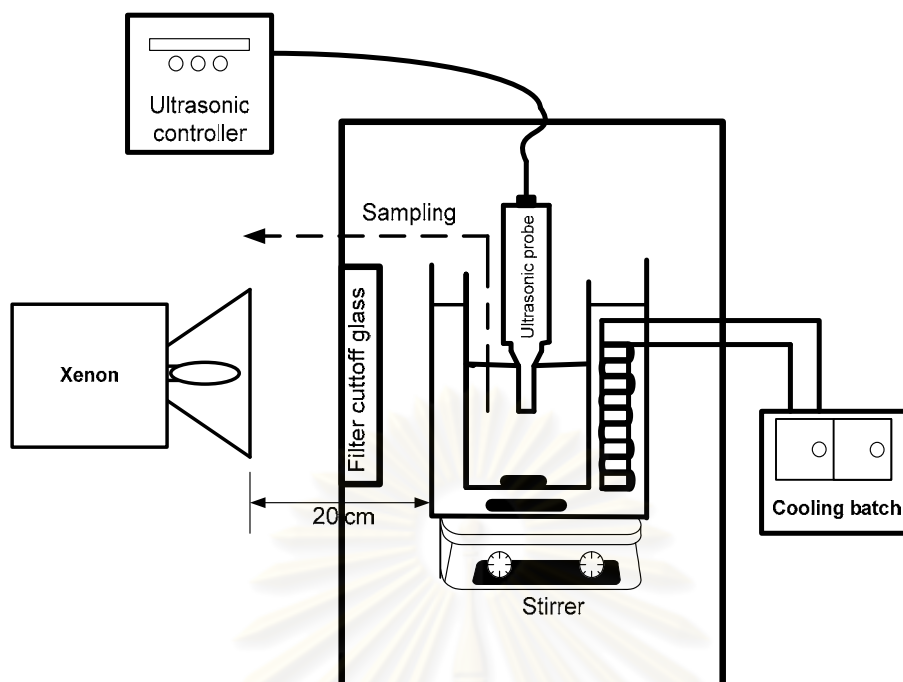


Figure 3.3 A schematic diagram of the sonophotocatalytic experimental setup

### 3.4 Analysis methods

#### 3.4.1 Alachlor

The alachlor that remained after photoirradiation was collected over each time interval. The amount of alachlor was determined using an HPLC comprised with an Agilent Technologies 1200 series detector and Agilent Technologies 1100 series pump and controller. A hypersil C18 ODS 4.0 x 125 mm 5 micron column was employed in this analysis. A maximum absorption wavelength of 197 nm was used to measure the alachlor concentration corresponding to five standard points. The 60% of the mobile phase composed of acetonitrile, while the other 40% was of distilled–deionized water at a flow rate of 1.0 mL min<sup>-1</sup>.

#### 3.4.2 Total organic carbon (TOC)

A TOC analyzer was used to perform a high sensitivity quantitative analysis of the total organic and inorganic carbon contaminations with high sensitivity. The total organic carbon in the solution was measured with a TOC analyzer with auto-sampler Model 1051,

equipped with TOC Analyzer Model 1010, and a computer for monitoring. The chemical compounds consists of sodium persulfate ( $\text{Na}_2\text{S}_2\text{O}_8$ ), phosphoric acid ( $\text{H}_3\text{PO}_4$ ) potassium biphthalate (KHP) and the carrier gas was nitrogen gas (ultra high purity grade).

Before the TOC measurement was taken, the essential reagents including water reagent, sodium persulfate reagent ( $100 \text{ g L}^{-1}$ ), and 5% phosphoric acid reagent were prepared. Nitrogen gas was injected through the TOC analyzer until the TOC measurement stabilized, which was observed when the IR (Infrared) signal reached between 4,000-8,000. To verify the standard, the  $R^2$  value of five levels of potassium biphthalate standard plot did not fall below 0.95. The Detection limit ranged from 2 ppb to 125 ppm.

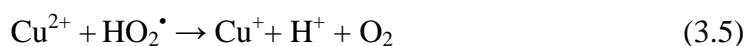
### 3.4.3 Ion analysis

The collected sample was filtered using a  $0.45 \mu\text{m}$  syringe filter before the ion analysis was performed. The water-soluble inorganic ions ( $\text{Cl}^-$ ,  $\text{NO}_2^-$ ,  $\text{NO}_3^-$  and  $\text{SO}_4^-$ ) were analyzed by an ion chromatograph (Dix-1000, Dionex Co.) equipped with a conductivity detector. For the anion analysis, a mixture ( $2.7 \text{ mM Na}_2\text{CO}_3$  and  $0.3 \text{ mM NaHCO}_3$ ) was prepared. The five standard curves with the standard ion solution (Dionex Co.) were applied to check the concentration of remaining organic ions.

### 3.4.4 Quantitative determination of active radicals

In the quantitative determination of active radicals, a modified Fricke dosimeter was used to determine the overall concentration of reactive oxygen species in irradiated aqueous suspensions of the catalyst. It consisted of  $5 \text{ mM}$  of  $\text{FeSO}_4$  (Fisher),  $10 \text{ mM}$  of  $\text{CuSO}_4$  (Fisher), and  $20 \text{ mM}$  of  $\text{H}_2\text{SO}_4$  (Fisher). During the reaction of  $\text{Fe}^{2+}$  with reactive oxygen species  $\text{Fe}^{3+}$  ion was produced, and the latter was quantified by spectrophotometry (Shimadzu 1201) at the wavelength of  $304 \text{ nm}$ . Standard quartz cuvettes with the path length of  $1 \text{ cm}$  were used. The absorbance by  $\text{Fe}^{3+}$  was correlated with the concentration of  $\text{Fe}^{2+}$  reacted and further used for calculations (Davydov *et al.* 2001). This determination was based on the conversion of two-valent into three-valent iron ions. Two-valent iron ions can react with reactive oxygen species of both hydroxyl and

hydroperoxyl radical forming two three-valent iron ions per electron-hole pair scavenged according to the following reaction schemes:



These reactions proceed even though the hydroxyl radicals are absent.

### 3.5 Design of Experiments (DoE)

In studies on photocatalytic degradation of organic pollutants, many researchers emphasized the individual effects of their factors, which were varied one at a time as the other factors remained constant. The interaction data of these factors were absolutely neglected. In order to find out interaction effects among all experimental factors, response surface methodology (RSM) has been widely applied experimental technique. Due to the large number of experiments and complicated data analysis, a systematical study of all these factors would be quite difficult to achieve. Hence response surface methodology based on the Box-Behnken design (BBD) was used to find out the optimal condition for sonophotocatalytic degradation of alachlor. This technique was the most appropriate for evaluating quadratic response surfaces and also avoiding extreme condition effects. All main parameters, including initial alachlor concentration, ultrasonic intensity, and amount of catalyst loading, were statistically investigated.

To optimize the photocatalytic degradation of alachlor, Box-Beknhen was applied in the experimental design. The initial concentrations of alachlor ranged from 1 mg L<sup>-1</sup> to 5 mg L<sup>-1</sup>. The catalyst loading was 0.5-2.5 g L<sup>-1</sup>. Ultrasonic power irradiation varied from 14w to 44w in an 80 mL volume of reactor. The sonophotocatalytic degradation of alachlor was carried out under the following conditions:

- As presented in Figure 3.3, the 80 mL pyrex glass reactor was equipped with cooling system to maintain temperature in the solution at 23-25°C.

- Initial alachlor solutions of  $1 \text{ mg L}^{-1}$  to  $5 \text{ mg L}^{-1}$  were prepared by diluting the stock solution to obtain a solubility in water of  $240 \text{ mg L}^{-1}$ , and a solution pH of 7.
- 40 mg to 200 mg of S-doped  $\text{TiO}_2$ , which equals to  $0.5 - 2.5 \text{ g}_{\text{catalyst}} \text{ L}^{-1}$  was suspended in a synthetic wastewater contaminated alachlor. To obtain equilibrium adsorption between solid and alachlor, the mixed solution was placed in dark for 30 min.
- The suspended sample was photoirradiated using a 500-W Xenon lamp (Shanghai Dian Guang Device Ltd.) which emitted both UV and visible light over a wide range of wavelengths.
- To limit the irradiation wavelength, the light beam was passed through a JB420 cutoff filter (China Nantong Yinxing Optical Co. Ltd.) to cut off the wavelengths that were shorter than 420 nm.
- A 20-kHz, 500 W ultrasonic processors (Sonic Model: VC 505) was used as the ultrasound source. It was varied from 14w to 44w in the 80 mL volume reactor.
- A sample was collected for every 30 min after the time on stream. The samples were filtered by passing through  $0.45 \mu\text{m}$  pore size membrane filters to remove the catalyst powder and other contaminants.

In this study, BBD was selected to evaluate how to optimize of the photocatalytic degradation of alachlor. The desired outcomes were be the coefficients for a mathematical model using a regression analysis technique as well as model data to checking the adequacy of the model. The response function and the experimental data (on the percent removal of alachlor) were evaluated statistically using Minitab 15 (trial version).

## CHAPTER IV

### RESULTS AND DISCUSSION

This chapter discusses the results of characterization with S-doped TiO<sub>2</sub>, photocatalytic activity, and sonophotocatalytic activity and response surface method.

#### 4.1 Characterization results

S-doped TiO<sub>2</sub> and pure TiO<sub>2</sub> (Degussa P25) were characterized by X-ray diffraction (XRD), diffuse reflectance spectroscopy measurement (DRS-UV), Brunauer, Emmett, and Teller (BET), Transmission Electron Microscopy (TEM) and Zeta potential technique.

##### 4.1.1 X-ray diffraction spectra (XRD)

XRD patterns of S-doped TiO<sub>2</sub> and TiO<sub>2</sub> are presented in Figure 4.1. The anatase phase of TiO<sub>2</sub> ( $2\theta = 26.8$ ) was observed in both materials. The rutile phase was not much presented in S-doped TiO<sub>2</sub>. The ratio of the rutile and the anatase was lower in S-doped TiO<sub>2</sub> (less than 7:93) compared to TiO<sub>2</sub> (20:80), calculated using equation (3.2). From the main peak of anatase using (1 0 1), the average crystallite sizes can be calculated using Scherrer's equation to the full-width at half-maximum of the (101) crystal plane of anatase TiO<sub>2</sub> (equation 3.1). It was observed that S-doped TiO<sub>2</sub> formed smaller crystallite sizes (12 nm) compared to TiO<sub>2</sub> itself (20-21 nm) tabulated in Table 4.1. The results of crystal sizes are similar to what was reported in several papers. It is expected that higher content of anatase phase and smaller crystallite size could enhance the potential of photocatalytic reaction.

##### 4.1.2 UV-Visible diffuse reflectance spectra

The diffuse reflectance spectra of the S-doped TiO<sub>2</sub> photocatalyst powders, together with those of pure rutile and anatase powders (Degussa, P25), are shown in Figure 4.2. It is interesting to notice that photoadsorption of S-doped TiO<sub>2</sub> was stronger than its pure TiO<sub>2</sub> (P25) in both UV region and visible region. It was also observed that the spectra of the samples displayed a red shift in the band gap transition. The catalyst

should have the ability to respond to the whole light. The results of band gap energies shown in Table 4.1 were calculated by equation 3.3.

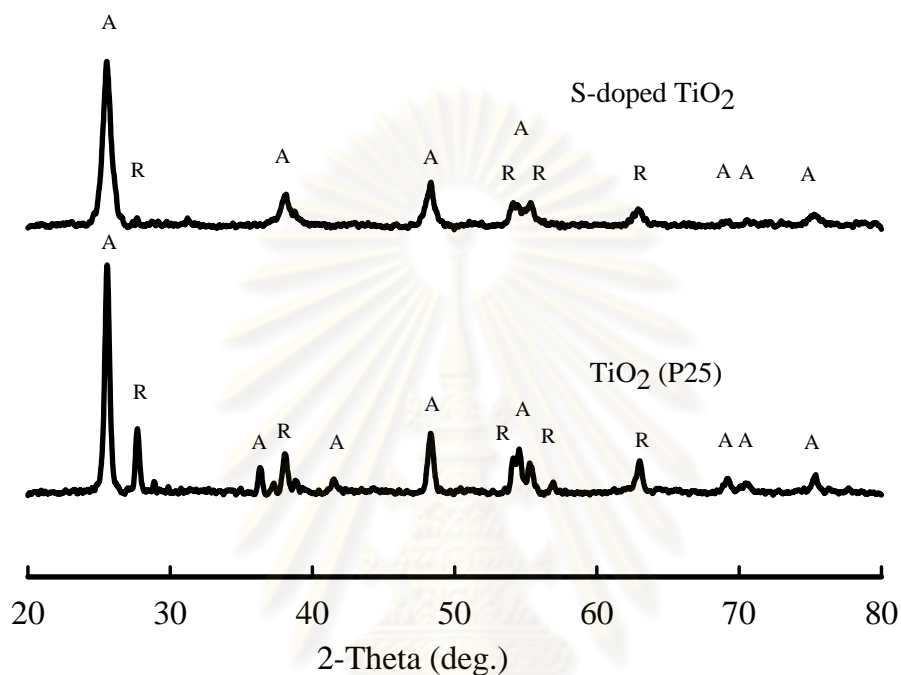


Figure 4.1 XRD patterns of S-doped  $\text{TiO}_2$  and  $\text{TiO}_2$  (P25)

Table 4.1 Physical characteristics of S-doped  $\text{TiO}_2$  and pure  $\text{TiO}_2$

	Surface area ( $\text{m}^2 \text{g}^{-1}$ )	Crystallite size (nm)	rutile:anatase ratio	Absorption edge (nm)	Band gap energy (eV)
$\text{TiO}_2$	50	20	20:80	390	3.18
S-doped $\text{TiO}_2$	87	12	7:93	393	3.16

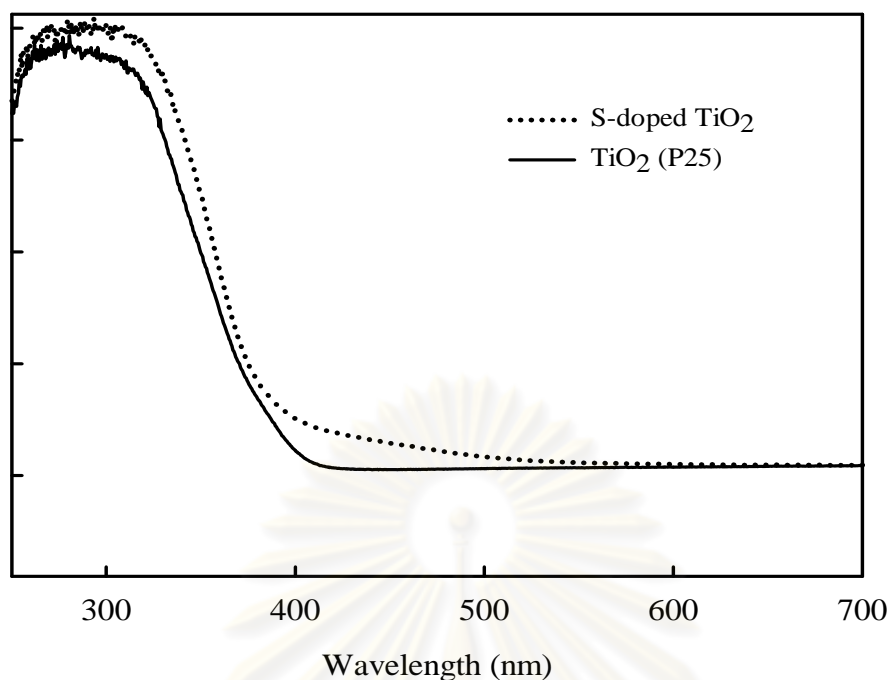
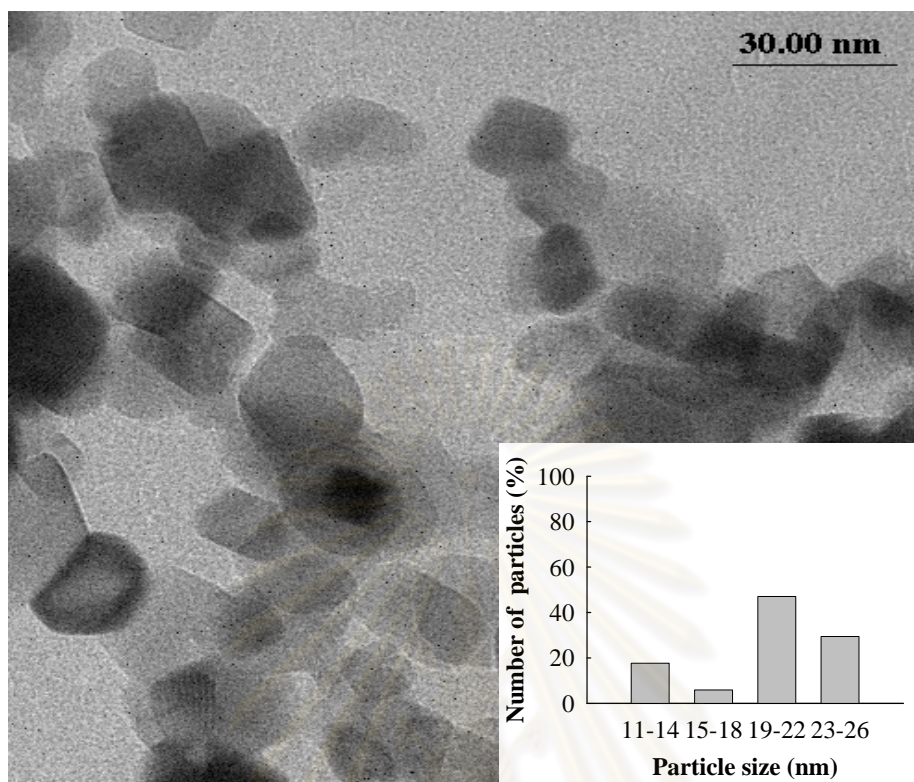


Figure 4.2. Diffuse reflectance spectra of S-doped TiO<sub>2</sub> and TiO<sub>2</sub> (P25)

#### 4.1.3 Transmission Electron Microscopy

Particle size of S-doped TiO<sub>2</sub> is confirmed by TEM images as shown in Figure 4.3. The image shows that particles of TiO<sub>2</sub> are relatively larger than that of S-doped TiO<sub>2</sub>. The particles of S-doped TiO<sub>2</sub> were more dispersed than particles of TiO<sub>2</sub> (P25). Particle distributions for both catalysts are presented in the inserted figures in each image. Particle size of P25 fell in 14-25 nm while that of S-doped TiO<sub>2</sub> fell in 5-15 nm. The image showed smaller particles of S-doped TiO<sub>2</sub> result in higher surface area, which agrees with the surface area measurement. In addition, the surface area of TiO<sub>2</sub> of S-doped TiO<sub>2</sub> measured by BET Technique is 50 m<sup>2</sup> g<sup>-1</sup> (Table 4.1). In Figure 4.3, some portion of particles is smaller than the crystallite size of TiO<sub>2</sub>. This might be due to other contaminants presenting in the material. Some researchers claimed that those small particles (~ 10-17 nm examined by TEM) which are smaller than TiO<sub>2</sub> (P25) (average a crystallite size ~ 20 nm, examined by XRD) may present in amorphous form as similar results as Ohno *et al.*, 2001. The same evidence was seen in S-doped TiO<sub>2</sub> sample. It was observed that some particles representing are smaller size (~ 5-11 nm examined by TEM) than the crystallite sizes obtained from XRD (~ 12 nm).

a)



b)

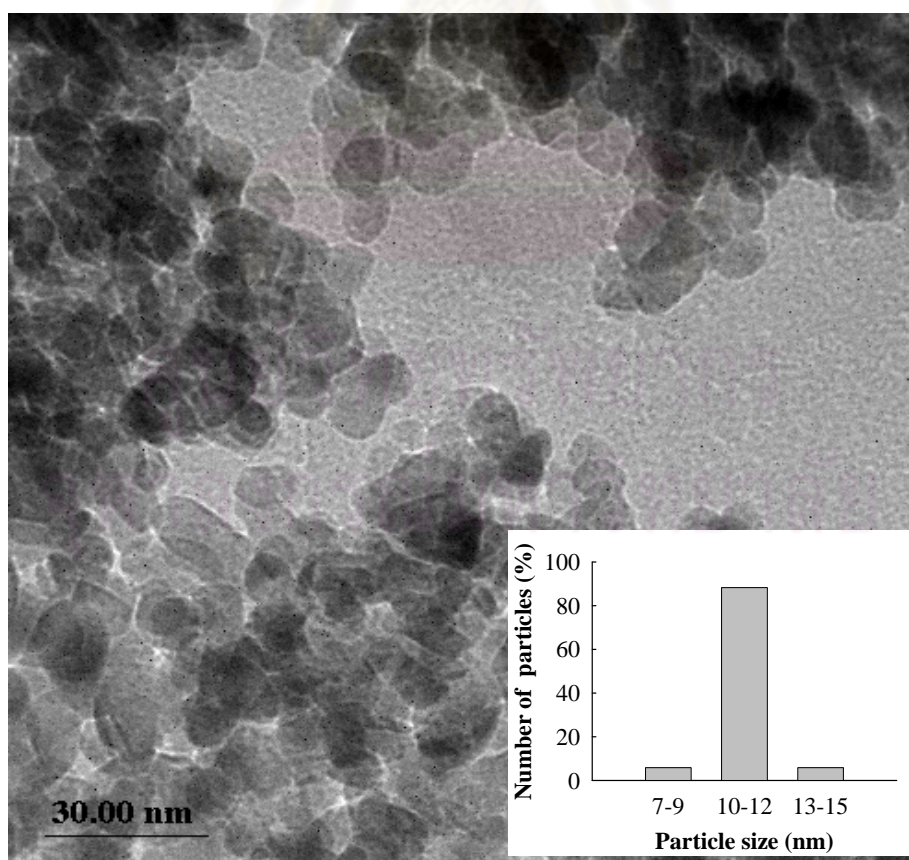


Figure 4.3 TEM images of (a) TiO<sub>2</sub> (P25) and (b) S-doped TiO<sub>2</sub>

#### 4.1.4 Point of zero charge (pzc)

The pH influences the surface charge of the semiconductor, thereby affecting the interfacial electron transfer and the photoredox process. It can be described on the basis of point of zero charge of S-doped TiO<sub>2</sub>. The point of zero charge of S-doped TiO<sub>2</sub> was at pH 5.6. The surface of TiO<sub>2</sub> was positively charged at pH values less than 5.6, and negatively charged at pH values higher than 5.6 as presented in Figure 4.4. Therefore, initial pH was fixed at 7 based on the zero-point charge of S-doped TiO<sub>2</sub> at pH 5.6. This means that pH over 5.6 would be suitable for alachlor degradation. In addition, a condition higher than pH 7 would not be applicable to perform the reaction, since H<sub>2</sub>O<sub>2</sub>, produced from sanitation, was unstable and readily decay into water and oxygen in alkaline solution (Wong *et al.*, 2003)

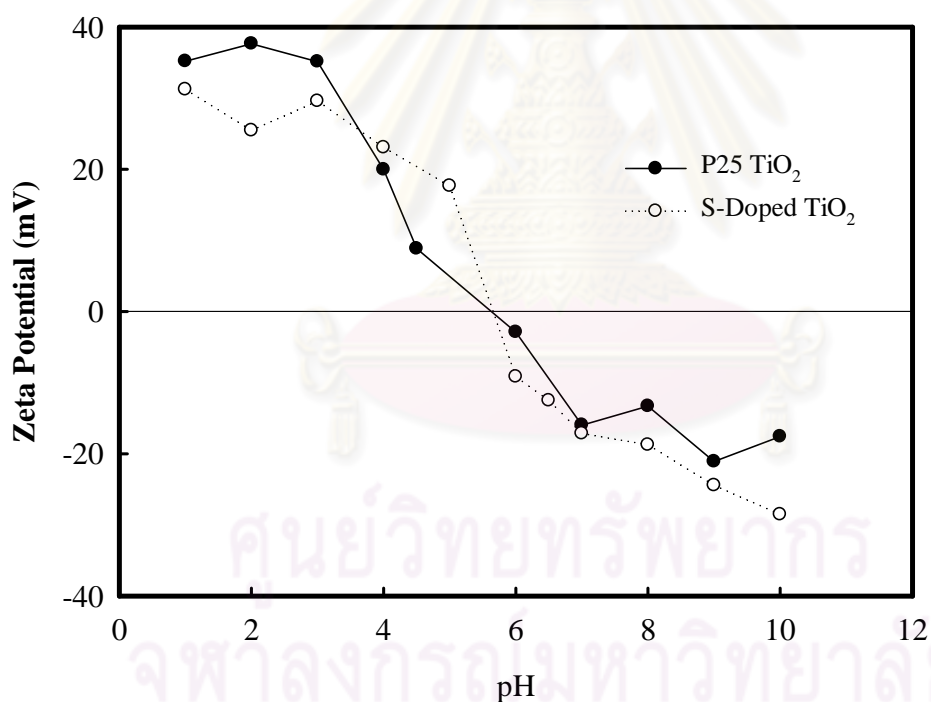


Figure 4.4 Zeta potential of TiO<sub>2</sub> (P25) and S-doped TiO<sub>2</sub>

## 4.2 Photocatalytic activities for alachlor degradation

This section discusses the study of photocatalytic activity of alachlor degradation by S-doped TiO<sub>2</sub> under visible light. The photodegradation of pure TiO<sub>2</sub> (P25) and S-doped TiO<sub>2</sub> was compared in different wavelength of generated light source. The effects of operating factors including initial concentration of alachlor, and catalyst loading were investigated. In addition, the synergistic effect of combined systems of photocatalysis and sonolysis was also described.

The alachlor concentration profiles decrease proportionally to time, as shown in Figure 4.5. The decline of alachlor concentration under UV condition was concave (Figure 4.5a), while those under visible region study were in straight trend lines (Figure 4.5b, c). It is obvious that the kinetics of those setups should be different. The degradation under UV should be described by first-order kinetics otherwise by zero-order kinetics. However, it is difficult for the comparison view point. In this case, the experimental data has been plotted against first-order kinetics. The first-order kinetics can be accepted only if the regression least squares for each data group were failed in the high satisfactory ( $R^2 > 0.9$ ). The expression of first-order kinetic is converted for the evaluation as follows;

$$\ln\left(\frac{C_0}{C}\right) = k_{app}t \quad (4.1)$$

Where  $k_{app}$  is the apparent rate constant,  $t$  is the irradiation time,  $C_0$  is initial concentration of alachlor, and  $C$  as the effluent concentration of alachlor.

In order to compare the efficiency of two photocatalysts (pure TiO<sub>2</sub> (P25) and S-doped TiO<sub>2</sub>), the degradation of alachlor under visible light was studied as shown in Figure 4.5. The decay of alachlor was studied in three patterns of light irradiation wavelength, including whole wavelength range, cutoff 420 and cutoff 450 nm. The test was carried out with catalyst loading of 1 g L<sup>-1</sup> solution. The photo-degradations of alachlor with reaction time are shown in Figure 4.5 for all cases. . It was observed that TiO<sub>2</sub> performed better than S-doped TiO<sub>2</sub> under UV light because of the mixed-phase TiO<sub>2</sub> that the electron transfer from rutile to anatase phase can reduce the recombination of photogenerated charges (Lei *et al.*, 2008). While, in Figure 4.2, TiO<sub>2</sub>

absorbs UV less than that of S-doped TiO<sub>2</sub>. However the ratio of anatase and rutile of TiO<sub>2</sub> is much higher comparing to S-doped TiO<sub>2</sub>.

However, the activities of both catalysts were somewhat the same, when performed under light wavelength greater than 420 nm. Finally, when low wavelength (< 450 nm) of light was eliminated, the concentration profile of alachlor gradually decreased with TiO<sub>2</sub> while it largely decreased with S-doped TiO<sub>2</sub>. This might be caused by the higher absorbance in visible light for S-doped TiO<sub>2</sub>.

The photocatalysis rate constants of S-doped TiO<sub>2</sub> were  $2.96 \times 10^{-3} \text{ min}^{-1}$  and  $1.3 \times 10^{-3} \text{ min}^{-1}$  at irradiation at wavelength longer than 420 and 450 nm respectively which is higher than the rate constant of pure TiO<sub>2</sub> (P25). As a result, S-doped TiO<sub>2</sub> is an effective catalyst for alachlor degradation under visible light region.

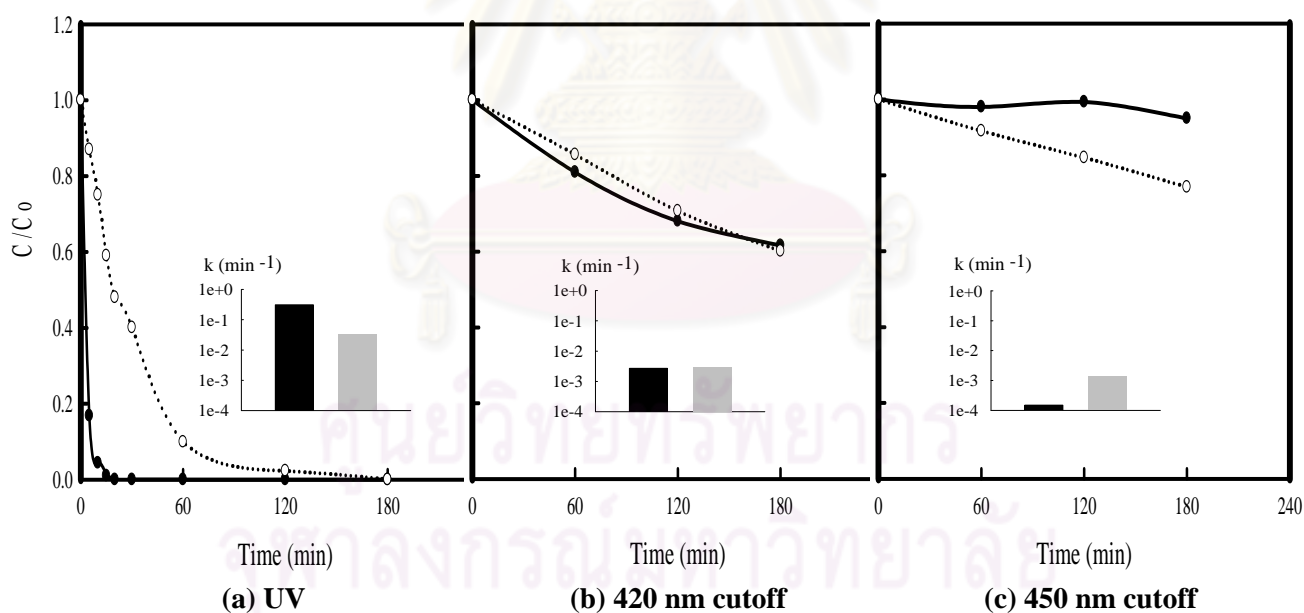


Figure 4.5 Concentration profiles and rate constants based on pseudo-first-order expression of photocatalytic degradation of alachlor over S-doped TiO<sub>2</sub> (gray color bar and dotted line) or TiO<sub>2</sub> (P25) (black color bar and black line) with different cutoff filters with 500 W xenon lamp (a) no cutoff  $\lambda$  filter (b) 420 nm cutoff  $\lambda$  filter (c) 450 nm cutoff  $\lambda$  filter

### 4.2.1 Effect of catalyst concentration

Photocatalytic reaction depends on the amount of catalyst loading in the solution. Amount of catalyst loadings were varied from 0.5 g to 2.0 g<sub>catalyst</sub> per 1 L of solution. The test was carried out only in visible light region ( $\lambda > 450$  nm). The degradation profiles of alachlor are presented in Figure 4.6. It shows that the higher amount of catalyst corresponded to higher alachlor degradation. This behavior was observed until the ratio of the amount of catalyst to solution reached 1.5 g L<sup>-1</sup>, an optimal catalyst loading. The reaction rate for each loading was clarified by rate constant values, based on pseudo-first order kinetics. The values were presented in the inserted table in Figure 4.6. When the ratio of catalyst to solution was beyond the optimal catalyst loading, the concentration profile (loading of 2.0 g L<sup>-1</sup>) was matched to its optimal one (loading of 1.5 g L<sup>-1</sup>). The reaction rate beyond this loading based on alachlor concentration would present similar to the maximum value. However, considering the reaction rate based on the catalyst amount, it would be declined. The reason was that high amount of catalyst may lower the light intensity, causing light scattering and blocking of irradiation of light through the whole catalyst in the solution.

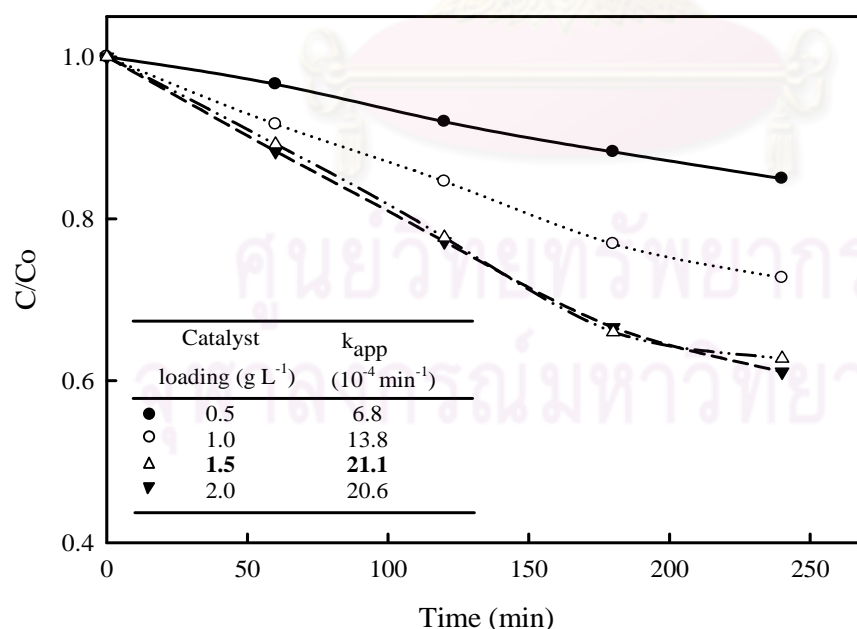


Figure 4.6 Concentration profiles and the apparent rate constant of alachlor degradation for different catalyst loadings by S-doped TiO<sub>2</sub> = 1.0 g L<sup>-1</sup> (cutoff  $\lambda$  filter at 450 nm)

### 4.2.2 Influence of initial concentration

The experiment was performed by varying alachlor initial concentration in the range 5 – 20 mg L<sup>-1</sup> under the conditions of 1 g<sub>catalyst</sub> L<sup>-1</sup> catalyst loading, initial pH of 7. In the photocatalytic activity under visible light of S-doped TiO<sub>2</sub>, a pseudo first-order reaction rate of the alachlor concentration can be described in terms of Langmuir–Hinshelwood (L–H) expression under small amount of alachlor adsorption on TiO<sub>2</sub>. The most common method for analyzing kinetic parameters ( $k_{app}$  and  $K_{ad}$ ) is linear least squares (LES) method, as presented in equation 4.2 – 4.3.

The study of a Langmuir–Hinshelwood (LH) kinetic model is applied for reactions appearing at a solid–liquid interface due to the importance of substrate preadsorption on a provided photocatalyst. This kinetic model can be expressed in LH kinetic rate as shown in equation 4.2 and 4.3.

$$r_0 = -\frac{dC}{dt} = \frac{k_{app} K_{ad} C_{initial}}{1 + K_{ad} C_{initial}} \quad (4.2)$$

$$\frac{1}{r_0} = \frac{1}{k_{app}} + \frac{1}{k_{app} K_{ad} C_{initial}} \quad (4.3)$$

Where  $k_{app}$  represents the apparent reaction rate constant, mg L<sup>-1</sup> min<sup>-1</sup>

$K_{ad}$  is the apparent adsorption equilibrium constant L mg<sup>-1</sup>

$C_{initial}$  is the initial concentration of the substrate mg L<sup>-1</sup> (Yano *et al.*, 2005).

In order to prove that the photodecomposition followed the LH kinetic model, variation of initial concentration of organic pollutants was conducted. A linear expression can be suitably obtained by plotting the reciprocal initial rate against the reciprocal initial concentration. The initial rate ( $r_0$ ) was obtained following the Simpson's one-third rule as appendix C.3 (Fogler, 2005).

From a plot of  $r_0^{-1}$  VS  $C_{initial}^{-1}$  (shown in Figure 4.7), it shows a good linearity having  $R^2 = 0.99$ . This provides the equilibrium constant for adsorption of alachlor and the apparent rate constant as 0.0585 L mg<sup>-1</sup> and 0.0423 mg L<sup>-1</sup> min<sup>-1</sup>, respectively.

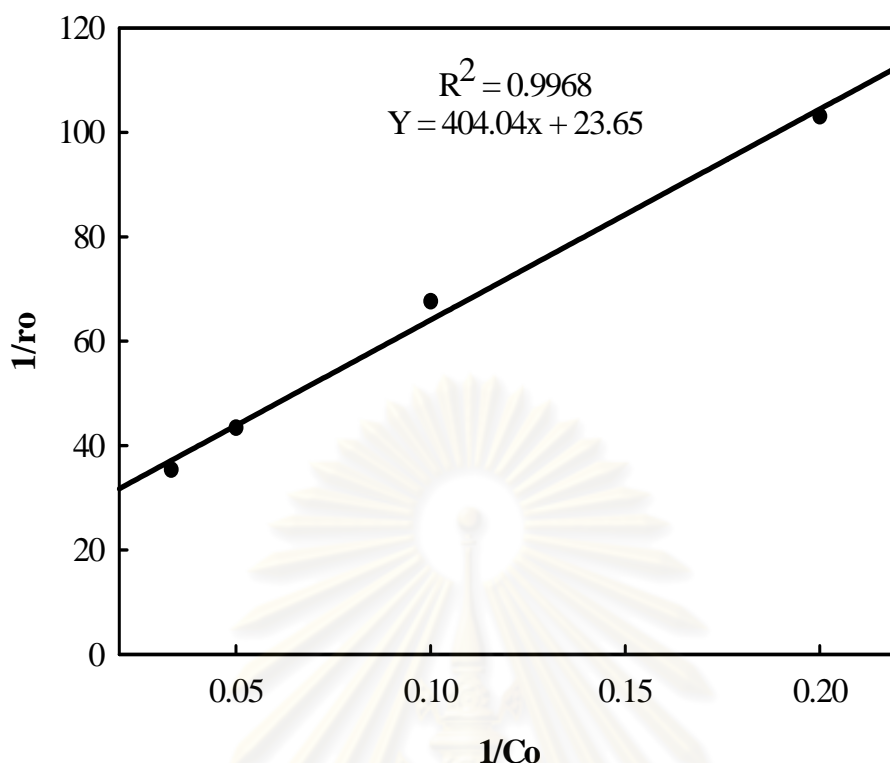


Figure 4.7 Linear plot of Langmuir–Hinshelwood (L–H) expression:alachlor 10 mg L<sup>-1</sup>, pH= 7, S-doped TiO<sub>2</sub> = 1.0 g L<sup>-1</sup>

#### 4.2.3 Synergistic effect of sonophotocatalysis

The photocatalytic activity and the sonophotocatalytic activity ofalachlor degradation with both catalysts (TiO<sub>2</sub> (P25), and S-doped TiO<sub>2</sub>) were investigated. The study was carried out using 20 kHz sonication system with 1 g<sub>catalyst</sub> L<sup>-1</sup> catalyst loading and an initial pH of 7. The results showed that the degradation ofalachlor with these catalysts followed the pseudo-first-order reaction rate law, as shown in Figure 4.8. The rate constants ( $k_{app}$ ) could be determined from the corresponding slopes. It was found that the  $k_{app}$  obtained from TiO<sub>2</sub> (P25) and from S-doped TiO<sub>2</sub> under visible light alone were 0.0002, and 0.0014 min<sup>-1</sup>, respectively while the  $k_{app}$  from TiO<sub>2</sub> (P25) and from S-doped TiO<sub>2</sub> using combination of sonication with visible light were 0.0019 and 0.0045 min<sup>-1</sup>. As seen, TiO<sub>2</sub> (P25) did little to enhance degradation under visible light. This is due to the extremely low light absorbance capacity of TiO<sub>2</sub> (P25) in the visible light region, proving that TiO<sub>2</sub> (P25) is not effective in the visible light region. In contrast, the reaction activity of the S-doped TiO<sub>2</sub> catalyst in the visible light region observed was seven times higher compared to that of TiO<sub>2</sub> (P25). These results agreed

with the results reported on the degradation of methylene blue and isopropanol (Ohno *et al.*, 2004). It is believed that the physical properties in the higher surface area and smaller size particles of S-doped TiO<sub>2</sub> should be taken into account making it the better choice over TiO<sub>2</sub> (P25), as presented in Table 4.1. Other factors include the absorption edges and energy bandgap capacity of S-doped TiO<sub>2</sub> which provided it a higher capacity for light absorption in the visible light region.

When sonication was simultaneously employed, the reaction rates of both catalysts increased, as shown in Figure 4.8. This was due to both the sonolytic and photocatalytic oxidation processes generating free radicals that attacked organic compounds synergistically. For example, water molecules split ultrasonically into free radicals, whereas in photocatalytic oxidation with titanium dioxide as the catalyst, electrons in the conduction band ( $e_{cb}^-$ ) and holes in the valence band ( $h_{vb}^+$ ) were produced under the light irradiation as expressed in equation 4.4 – 4.6.



Moreover, in the presence of sonication, cleaning the catalyst surface and increasing the mass transport of the reactants directly affect the degradation rate. To evaluate whether there is any synergetic effect of sonication on a photocatalytic reaction or not, an expression based on pseudo-first order rate constant for each condition was employed as shown in equation 2.24. If the additional effect is taken place, the value obtained from equation 2.24 will be zero, meaning that the activity of sonication and photocatalysis are independent. In this case, it was found that the synergetic effect increases the reaction rate of TiO<sub>2</sub> (P25) and S-doped TiO<sub>2</sub> by 5% and 11%, respectively. This confirmed the potential of S-doped TiO<sub>2</sub> to alachlor degradation under visible light.

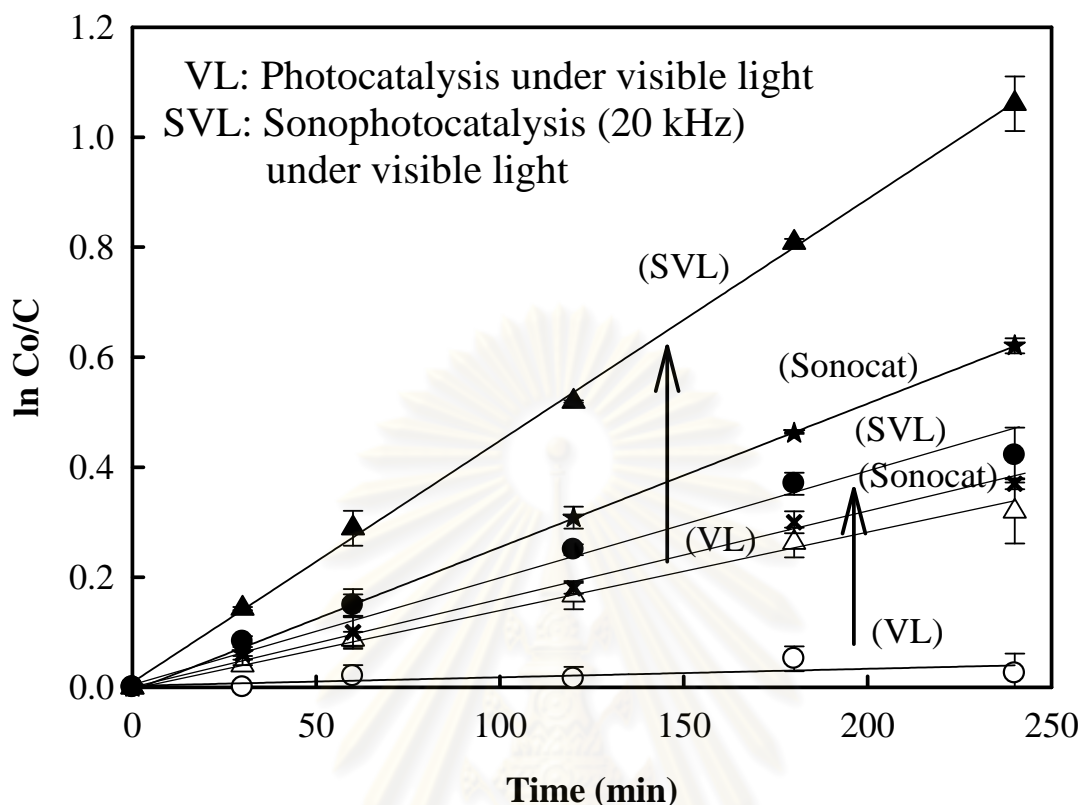


Figure 4.8. Pseudo-first-order profiles of alachlor degradation over  $\text{TiO}_2$  (P25) (Round) and S-doped  $\text{TiO}_2$  (Triangle);  $1 \text{ g}_{\text{catalyst}} \text{ L}^{-1}$  at an initial pH of 7 sonocatalysis (US+S-doped  $\text{TiO}_2$ ), sonophotocatalysis (US+light+S-doped  $\text{TiO}_2$ ): catalyst ( $1 \text{ g L}^{-1}$ ), alachlor ( $10 \text{ mg L}^{-1}$ ), (black cross:  $\text{TiO}_2$  (P25)) (black star: S-doped  $\text{TiO}_2$ ) sonocatalysis (US+S-doped  $\text{TiO}_2$ ) catalyst ( $1 \text{ g L}^{-1}$ ), alachlor ( $10 \text{ mg L}^{-1}$ )

Table 4.2 presents the photocatalytic degradation of alachlor in the past decade. It was found that all conditions set for the studies were only under UV light with  $\text{TiO}_2$  (P25) catalyst. As observed, the degradation rate under UV is much higher than under visible light. The alachlor concentrations used in both researchers (Bahena *et al.* 2008 and Penuela *et al.* 1996) were different that were not directly comparable. Therefore, it should be an interesting study on this reaction by applying ultrasonic condition simultaneously with photocatalysis

Table 4.2 Comparisons of kinetic rate constants of alachlor degradation

	Alachlor			
	$k_{app}$ ( $\text{min}^{-1}$ )			
	This study <sup>a</sup>		Bahena <sup>b</sup> <i>et al.</i> 2008	Penuela <sup>c</sup> <i>et al.</i> 1996
	TiO <sub>2</sub> (P25)	S doped TiO <sub>2</sub>	TiO <sub>2</sub> (P25)	TiO <sub>2</sub> (P25)
Sonolysis	-	-	0.089	-
Photolysis	-	-	0.071	0.017
Photocatalysis	0.0002	0.0014	0.113	0.053
Sonophotocatalysis	0.0014	0.0045	0.173	-

Remark: <sup>a</sup>Alachlor  $3.7 \times 10^{-5}$  M,  $1 \text{ g L}^{-1}$  TiO<sub>2</sub> (P25) and S doped TiO<sub>2</sub>, Xenon lamp (500W, cutoff 450 nm)

<sup>b</sup>Alachlor  $1.46 \times 10^{-4}$  M,  $0.2 \text{ g L}^{-1}$  TiO<sub>2</sub> (P25), UV lamp (15 W, 352 nm)

<sup>c</sup>Alachlor  $30\text{-}60 \text{ }\mu\text{g L}^{-1}$ ,  $0.15 \text{ g L}^{-1}$  TiO<sub>2</sub> (P25), a xenon arc lamp with UV special glass filter (Hanau, Germany)

### 4.3 Sonophotocatalytic activities for alachlor degradation

S-doped TiO<sub>2</sub> has been confirmed as an effective catalyst under visible light, discussed in 4.2. It was employed in the study of sonophotocatalytic degradation of herbicides applied in within the visible region. In this section, parameters generally effecting photocatalysis are investigated in this section. The effects of catalyst concentration, initial concentration of alachlor and ultrasonic power were conducted. Moreover the addition of persulfate solution, hydrogen peroxide solution as oxidizing agents effecting on alachlor degradation was included.

#### 4.3.1 Effect of the catalyst concentration

To determine the optimal catalyst loading value, a range of  $0.5\text{--}2.0 \text{ g}_{\text{catalyst}} \text{ L}^{-1}$  was tested. In this part of the study, S-doped TiO<sub>2</sub> is the only focus. The concentration profiles of alachlor degradation are presented in Figure 4.9. It was found that degradation improved gradually at increasing catalyst loading, until it reaches its

optimal value of  $1 \text{ g}_{\text{catalyst}} \text{ L}^{-1}$ . The reaction rate is proportional to the amount of catalyst loaded in the lower range of loading. It could be explained that when a low amount of  $\text{TiO}_2$  ( $0.5 \text{ g}_{\text{catalyst}} \text{ L}^{-1}$ ) was used, the rate of reaction was limited by  $\text{TiO}_2$  surface area itself. After increasing the catalyst concentration higher than  $1 \text{ g}_{\text{catalyst}} \text{ L}^{-1}$ , the degradation rate was reduced slightly. This was due to higher the solution opacity and light scattering that occurred. Consequently, they lessened the light passing through the sample. However, the concentration profiles were not much different. It might be possible for sonication to eliminate the aggregation of catalyst particles (Kaur *et al.*, 2007). Finally, the degradation rate constants were ranked according to the catalyst loading of  $1 > 1.5 \sim 2.0 > 0.5 \text{ g}_{\text{catalyst}} \text{ L}^{-1}$ , as shown in the inserted table in Figure 4.9.

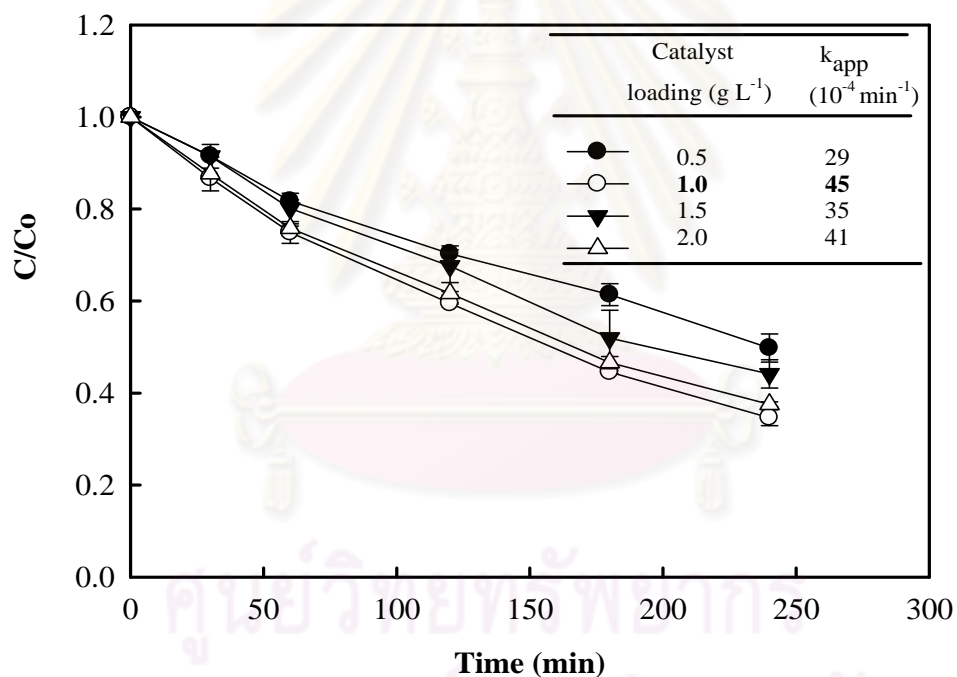


Figure 4.9 Effect of catalyst loading of S-doped  $\text{TiO}_2$  on 20 kHz in visible light; where  $C_{\text{initial}} = 10 \text{ mg L}^{-1}$ , S-doped  $\text{TiO}_2$  loading =  $1 \text{ g L}^{-1}$ , 13 W ultrasonic power, light  $> 450 \text{ nm}$  and  $\text{pH} = 7$

#### 4.3.2 Effect of ultrasonic power

In sonolysis, there are two factors, frequency and power density, must be considered. In a previous study, the rate of alachlor sonodegradation was approximately 25 times

faster at 300 kHz under argon saturation than it was at 20 kHz with the same input energy (Wayment *et al.*, 2002). However, there has been no evidence revealing the effects of power density on alachlor sonodegradation. In this work, therefore, ultrasonic power density was studied using range of 13–43 W in 80 mL reactor volume with a fixed frequency of 20 kHz. The percentages of alachlor degradation in 4 hr period were observed to be 65, 75, 80 and 85% at the power densities of 13, 23, 33 and 43 W, respectively, as shown in Figure 4.10. It could be concluded that the high amount of OH radicals generated by cavitation bubbles played a key role in increasing the mass transport between the solution phase and catalyst surface, thus improving the sonophotocatalytic activity. It means that the degradation rate depended on ultrasonic power applied to reactor agreeing with the result obtained by Neppoliana *et al.* (2002). For the further study, ultrasonic power density of 13 W is utilized because it is to save energy consumption and to emphasize on the study of heterogeneous reaction later than homogeneous reaction.

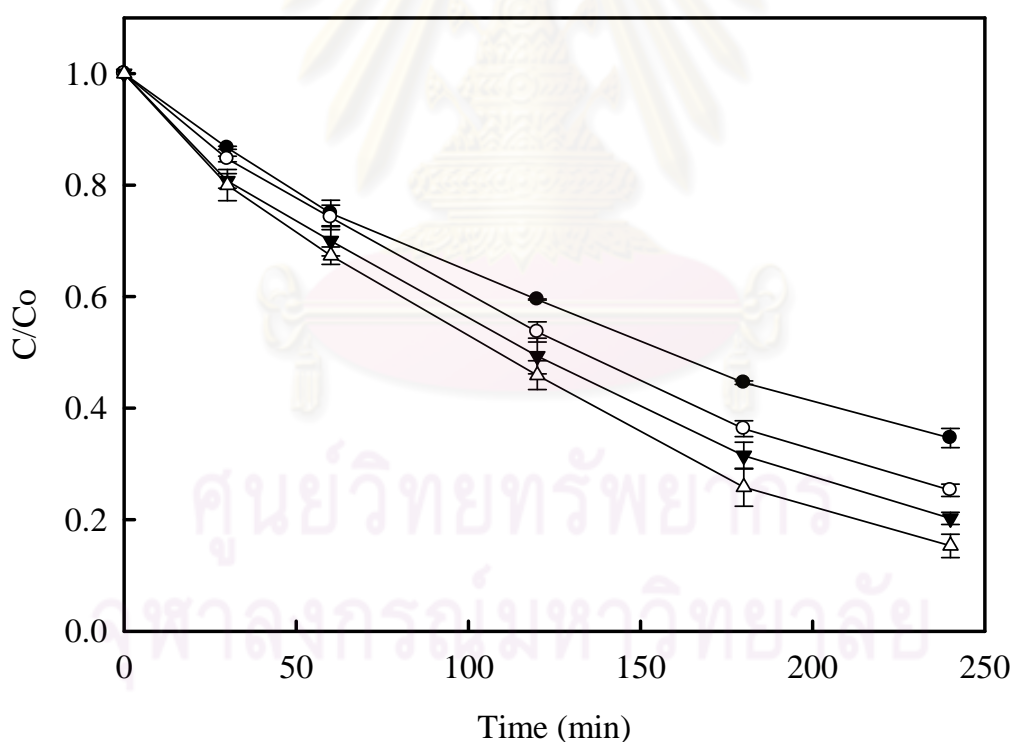


Figure 4.10 Effect of ultrasound power (●, 13 W; ○, 23 W; ▼, 33 W; and △, 43 W) on sonophotocatalytic where  $C_{\text{initial}} = 10 \text{ mg L}^{-1}$ , S-doped  $\text{TiO}_2$  loading =  $1 \text{ g L}^{-1}$ , light  $> 450 \text{ nm}$  and  $\text{pH} = 7$

### 4.3.3 Kinetic model for sonophotocatalytic activity

The experiment was performed by varying the initial alachlor concentration, from 5 to 30 mg L<sup>-1</sup> under the optimal conditions of 1 g<sub>catalyst</sub> L<sup>-1</sup> catalyst loading, an initial pH of 7, and 20 kHz with 13 W sonication, as shown in Figure 4.11. The experimental data can be fitted with pseudo-first-order as expressed in equation 4.1. The R<sup>2</sup> is greater than 0.97. The rate constant of the variation of initial alachlor concentration from 5, 10, 20 30 mg L<sup>-1</sup> are 0.0077, 0.0045, 0.0022, and 0.0016 min<sup>-1</sup>. The reaction rate increased with reducing the initial concentration of alachlor. Due to the decrease of the active sites of catalyst, generated OH radical is small. Consequently, it could cause the lower removal efficiency. Moreover the applied ultrasonic power per unit of pollutant is small when the amount of initial concentration increases. Therefore the ultrasound also generated less OH radical and less energy of mass transfer to direct reaction in the alachlor solution.

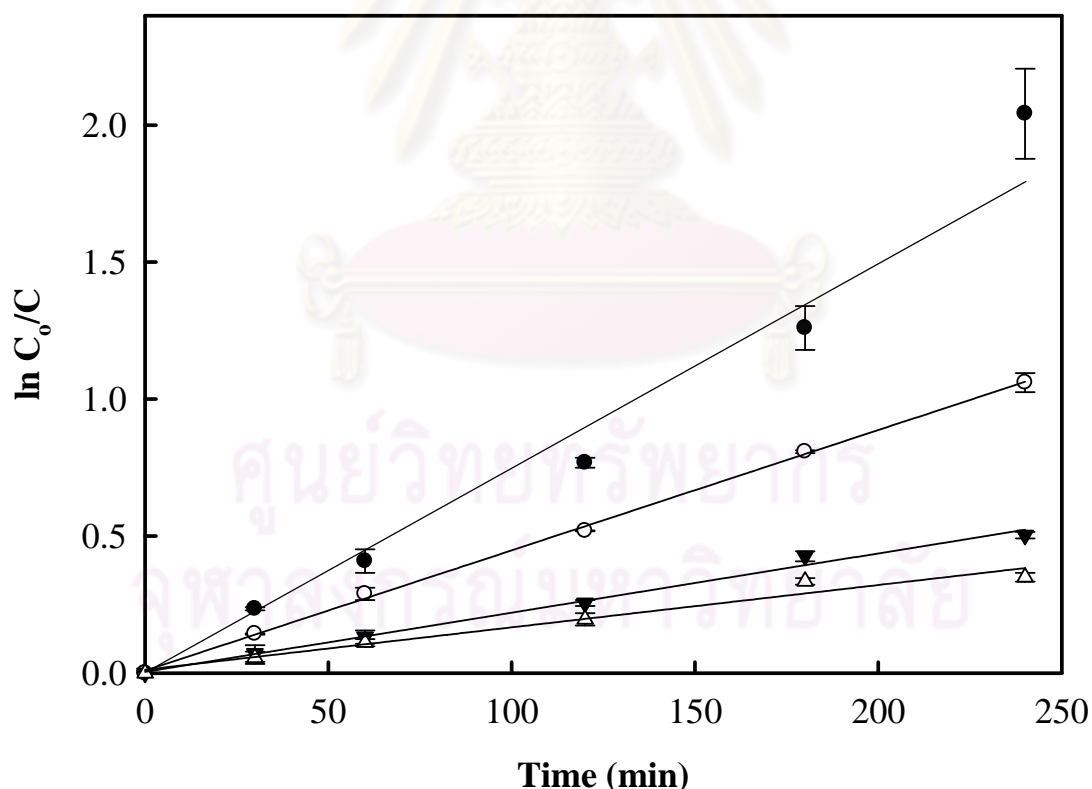
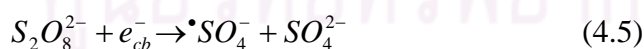


Figure 4.11 Influence of  $C_{\text{initial}}$  on the sonophotocatalytic degradation of alachlor by S-doped TiO<sub>2</sub> (● 5 mg L<sup>-1</sup>, ○ 10 mg L<sup>-1</sup>, ▼ 20 mg L<sup>-1</sup>, Δ 30 mg L<sup>-1</sup>), where  $C_{\text{initial}} = 10$  mg L<sup>-1</sup>, S-doped TiO<sub>2</sub> loading = 1 g L<sup>-1</sup>, 13 W ultrasonic power, light > 450 nm and pH = 7

#### 4.3.4 Effect of K<sub>2</sub>S<sub>2</sub>O<sub>8</sub> addition

Alachlor sonophotocatalytic degradation was carried out by varying the K<sub>2</sub>S<sub>2</sub>O<sub>8</sub> concentration, 0.1–5 mM as illustrated in Figure 4.12a,b, while other parameters were set at the considered conditions ( $C_{\text{initial}} = 10 \text{ mg L}^{-1}$ ,  $1 \text{ g}_{\text{catalyst}} \text{ L}^{-1}$ , pH of 7, and 13 W of ultrasonic power). In that presence of K<sub>2</sub>S<sub>2</sub>O<sub>8</sub>, the sonophotocatalytic system was considerably faster than it was in the absence of K<sub>2</sub>S<sub>2</sub>O<sub>8</sub>. It was found that the higher K<sub>2</sub>SO<sub>8</sub> concentrations presented higher alachlor degradation rate, until K<sub>2</sub>S<sub>2</sub>O<sub>8</sub> reached its optimal concentration (K<sub>2</sub>S<sub>2</sub>O<sub>8</sub> Conc. = 0.5 mM). In addition, the optimal concentration provided for the complete degradation of alachlor within 120 min., as shown in Figure 4.12 (a). Using pseudo-first order degradation, the rate constants were determined to be 0.012, 0.025, 0.042, 0.026, and 0.030 min<sup>-1</sup> for the persulfate medium concentrations of 0.1, 0.25, 0.5, 1, 5 mM, respectively. This provided the optimal K<sub>2</sub>S<sub>2</sub>O<sub>8</sub> concentration dose of 0.5 mM.

In the presence of K<sub>2</sub>S<sub>2</sub>O<sub>8</sub>, S<sub>2</sub>O<sub>8</sub><sup>2-</sup> can be reduced to sulfonate and its radicals (SO<sub>4</sub><sup>-</sup>, <sup>•</sup>SO<sub>4</sub><sup>-</sup>) under both photo-thermal activity and sonolytic activity through thermolytic cleavage. Sulfonate and its radicals can readily react with H<sub>2</sub>O thus forming more <sup>•</sup>OH radicals. This hydroxyl radical, which is a strong oxidant, can attack organic pollutant, increasing the degradation rate. The mechanism can be expressed as follows (Neppoliana *et al.*, 2002; Osajima *et al.*, 2008);



However, an overdose of the K<sub>2</sub>S<sub>2</sub>O<sub>8</sub> solution retarded the degradation rate. In this case, sulfate anion was dominated in the solution. This excess anion could be adsorbed on the catalyst surface. Since the surface of catalyst was occupied, the reaction would perform homogeneously itself without the assistance of photocatalysis, resulting in the inhabitation of catalyst surface and alachlor species attaching to one another.

However, an overdose of the  $K_2S_2O_8$  solution retarded the degradation rate due to the excess sulfate anion concentration which was adsorbed on the catalyst surface. It inhibited catalyst andalachlor from attaching to one another.

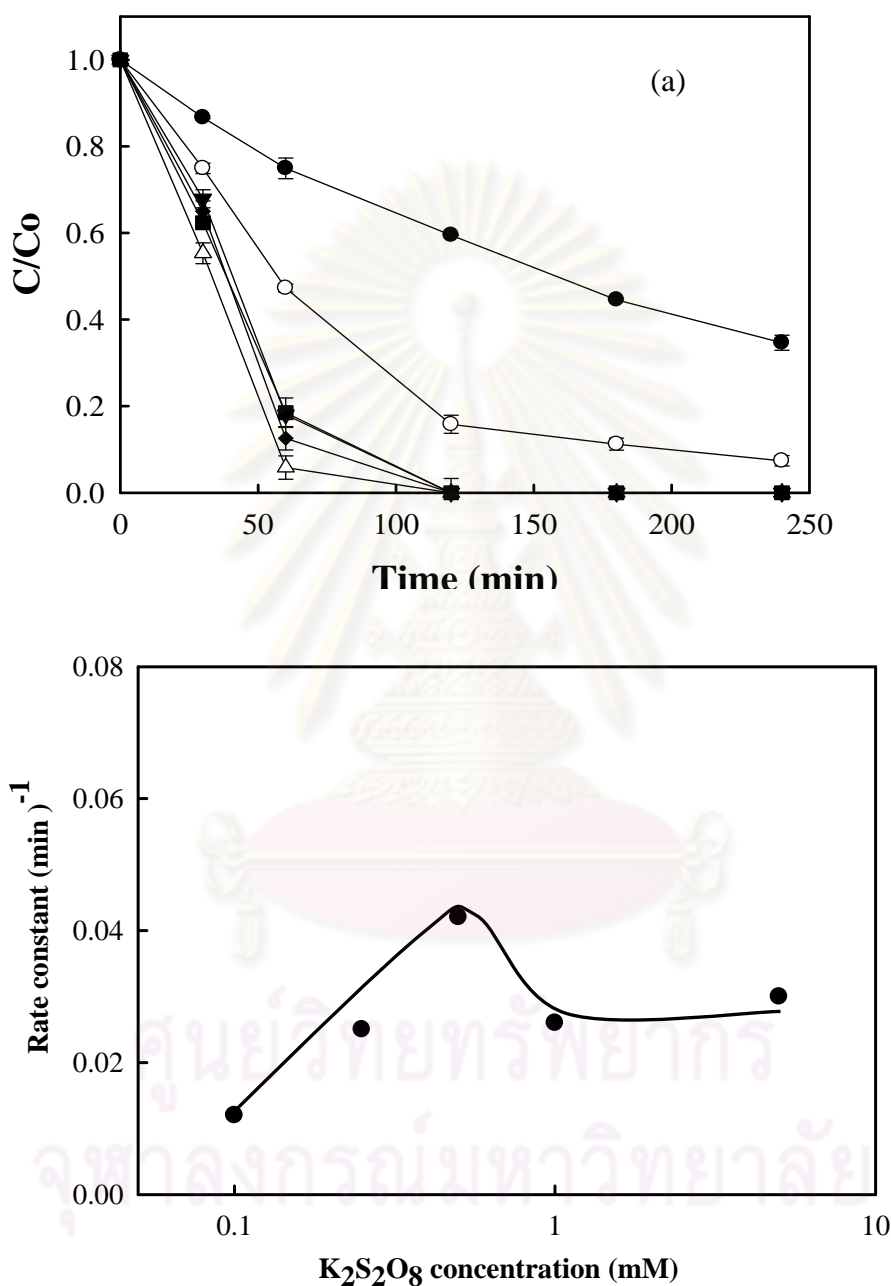


Figure 4.12 (a) Sonophotocatalytic degradation ofalachlor under the irradiated S-doped  $TiO_2$  with various concentrations of persulfate solutions (● without  $K_2S_2O_8$ , ○ 0.1 mM, ▼ 0.25 mM, Δ 0.5 mM, ■ 1.0 mM, and ◆ 5.0 mM) where  $C_{initial} = 10 \text{ mg L}^{-1}$ , 13 W ultrasonic power, light  $> 450 \text{ nm}$  and  $pH = 7$ . (b) The rate constant ofalachlor degradation with various concentrations of persulfate solutions.

### 4.3.5 Effect of H<sub>2</sub>O<sub>2</sub> addition

To examine the effect of adding H<sub>2</sub>O<sub>2</sub> on the alachlor degradation under sonophotocatalytic activity, different H<sub>2</sub>O<sub>2</sub> concentrations were applied. The experiments were conducted by varying the H<sub>2</sub>O<sub>2</sub> concentrations from 0.5-50 mM. In this part of the study, a suspension of 1 g L<sup>-1</sup> S-doped TiO<sub>2</sub> and 10 mg L<sup>-1</sup> alachlor at pH 7 under visible light with wave length longer than 450 nm were fixed condition. The degradation profiles were shown in Figure 4.13. It was noticed that degradation of alachlor in sonophotocatalytic activity with the addition of 0.5 mM H<sub>2</sub>O<sub>2</sub> was faster in first 30 min comparing to the activity without H<sub>2</sub>O<sub>2</sub>. The degradation of alachlor gradually declined after 120 minutes of treatment. Since all profiles almost overlapped to each other, H<sub>2</sub>O<sub>2</sub> had no significant effect on alachlor sonophotocatalytic degradation within the range used in this study. These results were found to be similar to the literature presented by Wong *et al.*, 2003. This is because H<sub>2</sub>O<sub>2</sub> is not stable and decays rapidly into oxygen and water. As a result, no improvement in alachlor degradation rate could be detected.

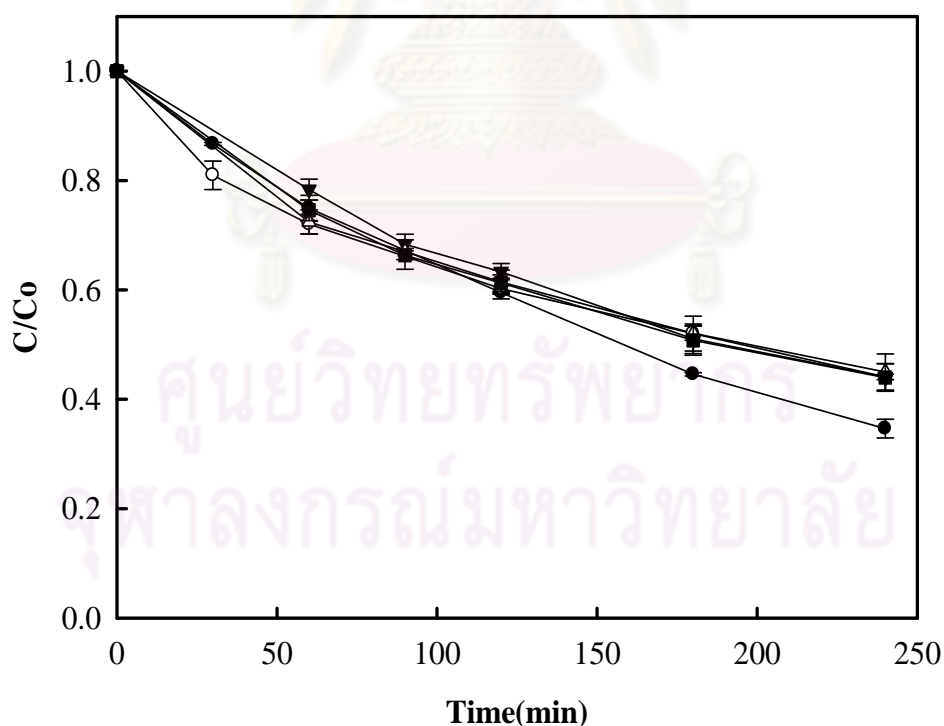


Figure 4.13 Sonophotocatalytic degradation of alachlor under the irradiated S-doped TiO<sub>2</sub> with various concentrations of H<sub>2</sub>O<sub>2</sub> (● without H<sub>2</sub>O<sub>2</sub>, ○ 0.5 mM, ▼ 1.0 mM, △ 10.0 mM, and ■ 50.0 mM) C<sub>initial</sub> = 10 mg L<sup>-1</sup>, S-doped TiO<sub>2</sub> loading = 1 g L<sup>-1</sup>, 13 W ultrasonic power, light > 450 nm and pH = 7

#### 4.3.6 Mineralization study

The mineralization of alachlor by different treatment processes of S-doped TiO<sub>2</sub> such as photocatalysis, sonocatalysis and sonophotocatalysis were investigated by tracking the TOC concentration. The comparisons in terms of the degradation activity ( $C/C_0$ ) are presented in Figure 4.14a. The mineral decay ratios of TOC/TOC<sub>0</sub> as a function of time are shown in Figure 4.14b.

A TOC reduction could be observed in every studied condition. In the controlled experiment, TOC was reduced by only 29% under photocatalytic system and 28% under sonolytic system within 480 min. In contrast, TOC reduction on sonophotocatalysis was considerably higher than that of individual system like photocatalysis and sonocatalysis system during the same period of treatment time. Due to the effect of ultrasound irradiation, the higher sonophotocatalytic mineralization of alachlor was achieved by comparing to its photocatalysis and sonocatalysis. In addition, TOC reduction was considerably increased to 59% in sonophotocatalysis with out persulfate and to 65% with the addition of persulfate solution. This means that the decay of alachlor by sonophotocatalytic activity with the presence of persulfate solution was enhanced substantially.

As a whole, the sonophotocatalytic system together with the persulfate solution showed the best systematic results in terms of alachlor degradation and TOC reduction. A few peaks appeared in HPLC analysis after 480 min reaction time; however in this study these peaks were not quantified. Consequently, these little intermediate products may not be totally mineralized to CO<sub>2</sub>, as presented by remaining TOC in the system. In the study by Wong and Chu *et al.* (2003), remaining intermediates were less hazardous compared to initial alachlor itself.

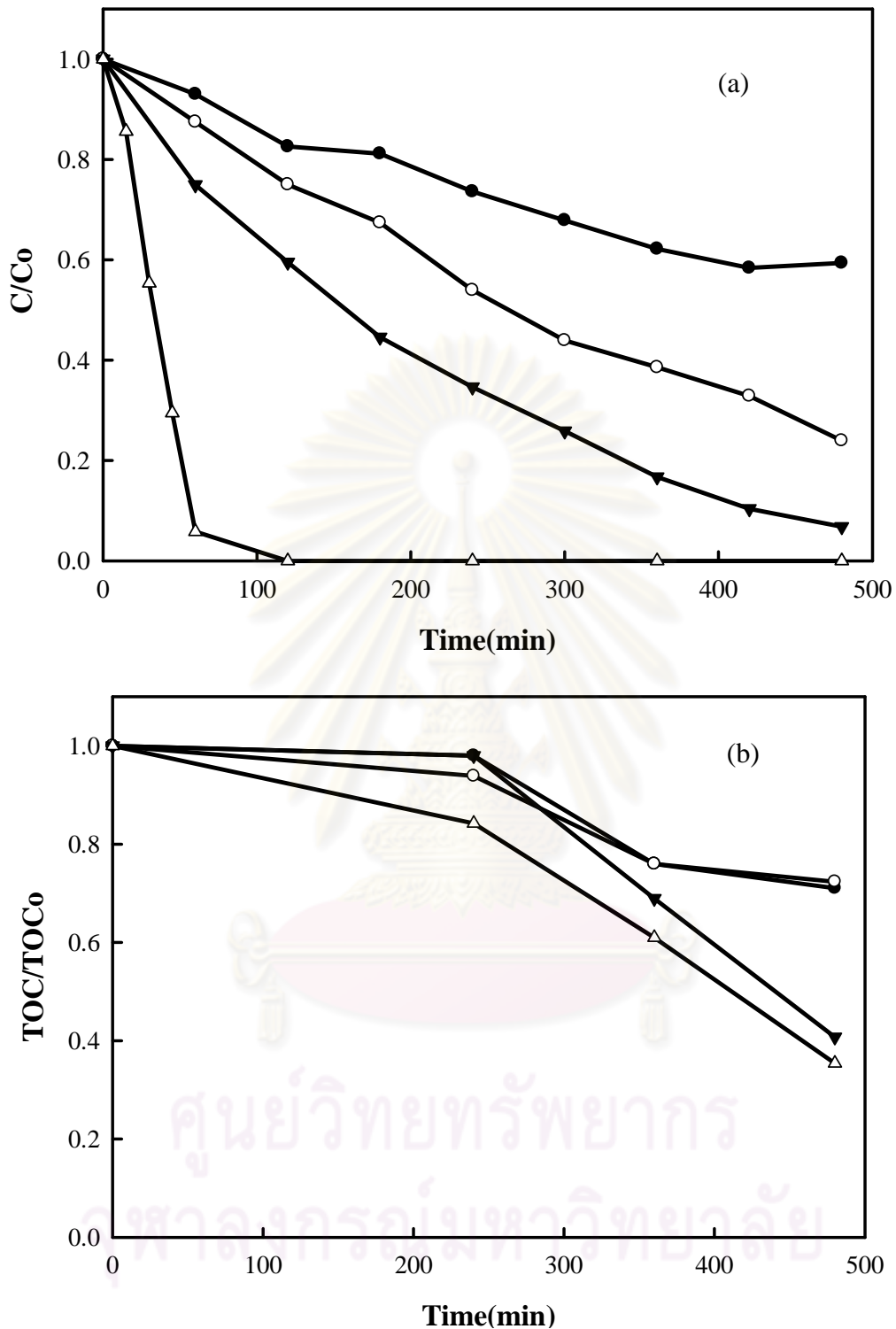


Figure 4.14 (a) alachlor degradation (● photocatalysis, ○ sonocatalysis, ▼ sonophotocatalysis, Δ sonophotocatalysis with adding 0.5 mM K<sub>2</sub>S<sub>2</sub>O<sub>8</sub>) and (b) TOC reduction (● photocatalysis, ○ sonocatalysis, ▼ sonophotocatalysis, Δ sonophotocatalysis with adding 0.5 mM K<sub>2</sub>S<sub>2</sub>O<sub>8</sub>) where C<sub>initial</sub> = 10 mg L<sup>-1</sup>, S-doped TiO<sub>2</sub> loading = 1 g L<sup>-1</sup>, 13 W ultrasonic power, light wavelength > 450 nm and pH =

### 4.3.7 Hydroxyl radical

It is difficult to determine hydroxyl radicals generated in the system. In this study, a comparison in measurement has been used. One of the practical methods is “The Fricke dosimetry”. It is a method based on the conversion of two-valent into three-valent iron ions. Two-valent iron ions can react with reactive oxygen species of both hydroxyl and hydroperoxyl radical forming two three-valent iron ions per electron-hole pair scavenged as show in equation 3.4 to 3.7. As seen, the detected amount cannot use to represent active radicals, since some of them can be consumed by  $\text{Cu}^{2+}$ . Therefore, only relative hydroxyl radicals produced in the system is taken account.

In Figure 4.15, it is found that the generation of  $\text{Fe}^{3+}$  in sonophotocatalysis was higher than that in both photocatalysis and sonocatalysis. Relatively, sonophotocatalysis produced more hydroxyl radical than either sonocatalysis or photocatalysis itself. This result would support the higher activity on sonophotocatalysis beyond other techniques.

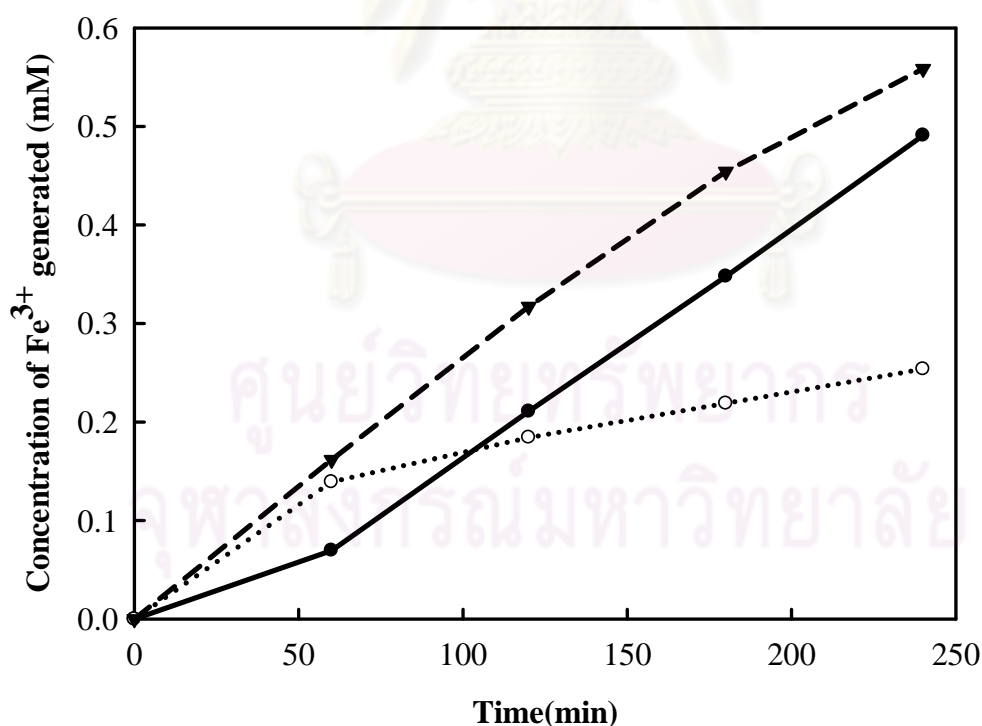


Figure 4.15 Comparison of the photocatalytic and sonophotocatalytic oxidation of  $\text{Fe}^{2+}$  over S-doped  $\text{TiO}_2$  (○, photocatalysis; ●, sonocatalysis; ◄ sonophotocatalysis) where  $C_{\text{initial}} = 10 \text{ mg L}^{-1}$ , S-doped  $\text{TiO}_2$  loading =  $1 \text{ g L}^{-1}$ , 13 W ultrasonic power, light wavelength  $> 450 \text{ nm}$  and  $\text{pH} = 7$

### 4.3.8 Inorganic ion concentration

Since alachlor contains chemical species (Cl and N) which could eventually present in form of ions dissolved in water, the balance of those species had to be conducted. The ion concentration ( $\text{Cl}^-$ ,  $\text{NO}_2^-$  and  $\text{NO}_3^-$ ) of related species are measured and shown in Figure 4.16. The results revealed the formation of  $\text{Cl}^-$ ,  $\text{NO}_2^-$  and  $\text{NO}_3^-$  from the mineralization of organic chlorine and nitrogen compounds, which are connected to alachlor molecule. The formation rate of  $\text{Cl}^-$  and  $\text{NO}_3^-$  comes from the oxidation of the side chain of the alachlor molecule which happened more easily than the cleavage of the ring. Nitrogen was principally mineralized into nitrate. Nitrite ions were initially generated, but they were quickly oxidized to nitrate, and the formation rate of  $\text{NO}_2^-$  was very slow (Qu *et al.*, 2004). It shows similar results as the degradation mechanism of the photocatalytic process, in which the decay pathways may include dechlorination, hydroxylation, dealkylation, scission of the C-O bond, and N-dealkylation (Chu *et al.*, 2004).

Base on the amount of initial alachlor using 10 mg, total amount of N and Cl was 1.8 mg. At the end of the 480 min test, the total amount of N and Cl from total ion amount dissolved in the water was 0.4 mg. There is 78% of amount of N and Cl elements in the solution, relating to the intermediate still remains in the solution, as previous discussion.

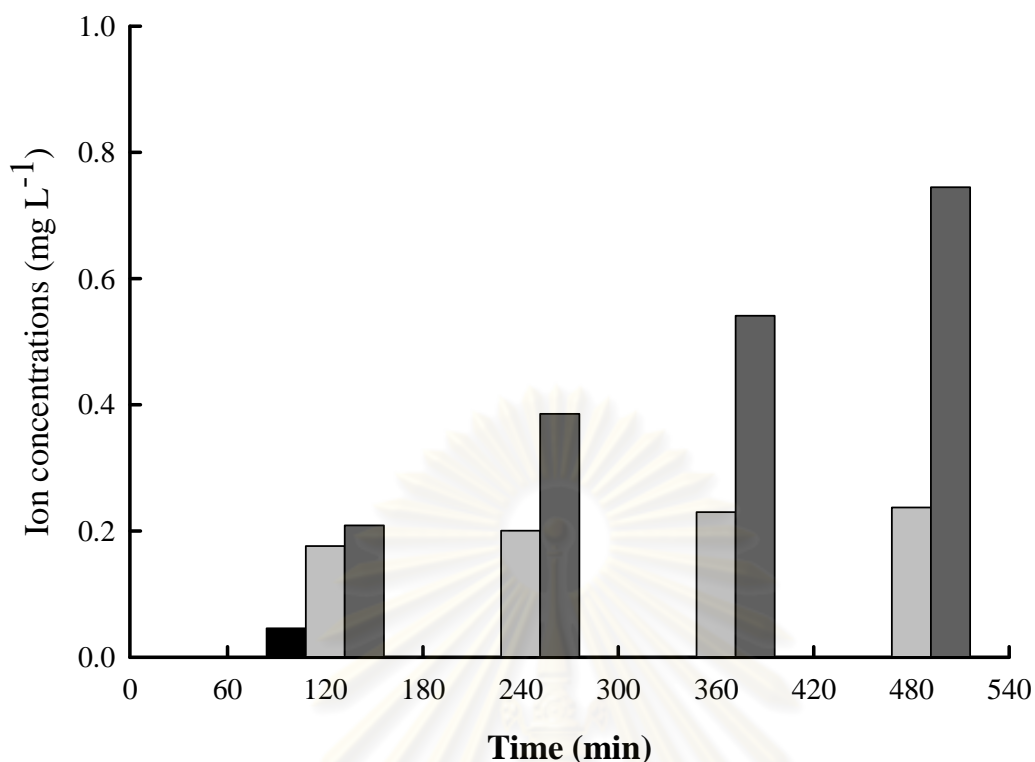


Figure 4.16 Inorganic ion concentration produced from the sonophotocatalytic oxidation of alachlor over S-doped TiO<sub>2</sub> (NO<sub>2</sub><sup>-</sup>; black bar, Cl<sup>-</sup>; grey bar, NO<sub>3</sub><sup>-</sup>; dark grey bar) where C<sub>initial</sub> = 10 mg L<sup>-1</sup>, S-doped TiO<sub>2</sub> loading = 1 g L<sup>-1</sup>, 13 W ultrasonic power, light > 450 nm and pH = 7

#### 4.4 Design of experiment (DoE)

The study the individual effect of each parameter, such as initial concentration (5-30 mg L<sup>-1</sup>), catalyst loading, and ultrasonic power, was evaluated. It was found that the lower initial concentration, the higher alachlor removal was observed. The lower initial concentration of alachlor (1-5 mg L<sup>-1</sup>) was presently interested. However, it is questionable that whether the removal efficiency is individual or interactive from other factors. The study of interaction on each parameter by DoE was highly interested.

Response surface model base on BoX-Behnken was applied to determine the simple and interactive effects of operating variables ofalachlor removal. It consists of analysis of variance and fitting model, adequacy check of the model, optimization conditions and response surface analysis, and verification of model and experimental confirmation.

A three factor level of BBD with three central points of factors was applied to investigate the optimal operating factor. Table 4.3 concluded the method of low level, medium level and maximum level for each factor of the design. The three factors were assigned as  $X_1$  (initial concentration ofalachlor),  $X_2$  (catalyst loading),  $X_3$  (ultrasonic power intensity). The experiments were performed randomly in order to prevent any systematic bias of the results. This design included 30 experiments separated to three blocks: low and high as presented in Table 4.3 and Table 4.4. The coefficients of the mathematic model, which expresses the percent removal ofalachlor (response) as a function of the experimental condition (independent variable), were calculated by a regression analysis technique.

**Table 4.3 Experimental range and levels of independent variables**

Independent variable	Factor $X_i$	Range and level		
		-1	0	+1
Initial concentration ofalachlor ( $\text{mg L}^{-1}$ )	$X_1$	1	3	5
Catalyst loading ( $\text{mg L}^{-1}$ )	$X_2$	500	1500	2500
Ultrasonic power intensity (w in 80 mL)	$X_3$	24	34	44

**Table 4.4 Design matrix for experimental factors and responses at different factor levels**

Run	Factor			Response
	Initial concentration (mg L <sup>-1</sup> )	Catalyst Loading (mg L <sup>-1</sup> )	Power intensity (W in 80 mL)	Percent removal
1	1	1500	44	81.0
2	3	2500	24	47.2
3	5	1500	24	32.2
4	3	2500	24	47.2
5	3	500	44	48.7
6	1	1500	24	74.6
7	1	2500	34	88.3
8	5	500	34	33.9
9	3	1500	34	51.7
10	3	1500	34	50.5
11	3	1500	34	48.4
12	5	2500	34	37.2
13	5	2500	34	37.0
14	5	1500	44	39.2
15	5	500	34	34.8
16	3	2500	44	51.8
17	3	500	24	39.6
18	1	2500	34	89.0
19	3	2500	44	57.0
20	1	1500	44	83.7
21	5	1500	24	32.0
22	3	1500	34	49.0
23	3	500	44	47.8
24	1	1500	24	75.7
25	3	1500	34	47.6
26	5	1500	44	42.4
27	1	500	34	72.0

(Continued) Table 4.4 Design matrix for experimental factors and response at different factor levels

Run	Factor			Response
	Initial concentration (mg L <sup>-1</sup> )	Catalyst Loading (mg L <sup>-1</sup> )	Power intensity (W in 80 mL)	
28	1	500	34	76.8
29	3	1500	34	47.1
30	3	500	24	39.8

#### 4.4.1 Analysis of variance (ANOVA) and fitting model

ANOVA results of the model presented in Table 4.5 indicate that the model equation can adequately be used to describe the sonophotocatalytic degradation of alachlor under a wide range of operating conditions. F-value of 305.44 which is greater than that of the tabular F 0.01(9, 20) value (3.46) implies that the model is significant. It can be adequately applied for the sonophotocatalytic degradation of alachlor. The experimental data revealed that the model is statistically significant with linear, quadratic and interaction terms due to value of “P” less than 0.050 indicating a 95% confidence interval. The “Lack-of-Fit F-value” of 1.67 is lower than that of F 0.01(3, 17) value (5.19) indicating that the Lack-of-Fit is not significant relative to the pure error (Murugesan *et al.*, 2007).

The linear, quadratic and interaction model results give excellent details of the relationships between the independent variable and the response. The predicted expression of percentage removal of alachlor is obtained in equation 4.8 and Table 4.6.

$$\begin{aligned}
 \% \text{ Alachlor removal} = & 49.050 - 22.025X_1 + 3.831X_2 + 3.956X_3 + 9.894X_1^2 \\
 & - 0.319X_2^2 - 1.344X_3^2 - 2.875X_1X_2 - 0.375X_1X_3 \\
 & - 0.338X_2X_3
 \end{aligned} \tag{4.8}$$

Be concerned that, the predicted expression is limited to the parameter range of this study (initial concentration ofalachlor: 1-5 mg L<sup>-1</sup>, catalyst loading: 500-2500 mg L<sup>-1</sup> and ultrasonic power intensity 24-44 W in 80 mL).

**Table 4.5 ANOVA results of the experimental responses**

Source	DF	Seq SS	Adj SS	Adj MS	F	P
Regression	9	9077.27	9077.27	1008.59	305.44	0.000
Linear	3	8246.90	8246.90	2748.97	832.50	0.000
Square	3	762.21	762.21	254.07	76.94	0.000
Interaction	3	68.16	68.16	22.72	6.88	0.002
Residual Error	20	66.04	66.04	3.30		
Lack-of-fit	3	15.06	15.06	5.02	1.67	0.210
Pure Error	17	50.98	50.98	3		
Total	29	9143.31				

Table 4.6 presents the P-value for each parameter. The P-value is used to verify the significance of each of the coefficients and the t-value with the estimated factor. The higher t-value and smaller P-value indicate that the effect is more significant to the corresponding coefficient. In this experiment, the initial concentration, catalyst loading, and ultrasonic power intensity strongly affectalachlor removal efficiency. This consideration is under the criteria of P-value less than 0.05.

**Table 4.6 Coefficients of each factor on response surface model**

Term	Coef	Se Coef	T	P
Constant	49.05	0.7419	66.118	0.000
Initial Conc.	-22.025	0.4543	-48.482	0.000
Cat. Loading	3.831	0.4543	8.433	0.000
Power Intensity	3.956	0.4543	8.709	0.000
Initial Conc.*Initial Conc.	9.894	0.6687	14.796	0.000
Cat. Loading*Cat. Loading	-0.319	0.6687	-0.477	0.639
Power Intensity*Power Intensity	-1.344	0.6687	-2.01	0.058
Initial Conc.*Cat. Loading	-2.875	0.6425	-4.475	0.000
Initial Conc.*Power Intensity	0.375	0.6425	0.584	0.566
Cat. Loading*Power Intensity	-0.338	0.6425	-0.525	0.605

The correlation efficient of the model ( $R^2$ ) was 0.9889. Since the interactions of some parameters did not exist but only parameters interacted between initial concentration and catalyst loading did exist. The model could be adjusted and expressed in equation 4.8.

$$\begin{aligned} \% \text{Alachlor removal} = & 49.050 - 22.025X_1 + 3.831X_2 + 3.956X_3 + 9.894X_1^2 \\ & - 2.875X_1X_2 \end{aligned} \quad (4.8)$$

A new correlation coefficient of the adjusted model was found to be 0.9864, which was still acceptable. This also supported that the previous experimental on power intensity could be conducted individually. However, the interaction between initial concentration and catalyst loading might divert the model more or less, not in significantly (based on small coefficient presented).

#### 4.4.2 Adequacy check of the model

To ensure that the approximating model provides an adequate predicted data to the actual system, an adequacy check of the predicted model is an important part of the data analysis. The model results comply with the assumptions of the analysis of variance (ANOVA) as shown in the normal probability and studentized residuals plots (Figure 4.17). The normal probability plot presents that the residuals follow a normal distribution with all points following a straight line. The normality of apparent problems does not occur as a result of the absence of an apparent S-shaped curve.

The plot between residuals and predicted data is shown in Figure 4.18. All of residuals are ranged in the interval of  $\pm 3.50$ . It means that the plot shows a random scatter in which the variance of observed data is constant with respect to all of the responses (Korbahti *et al.*, 2008).

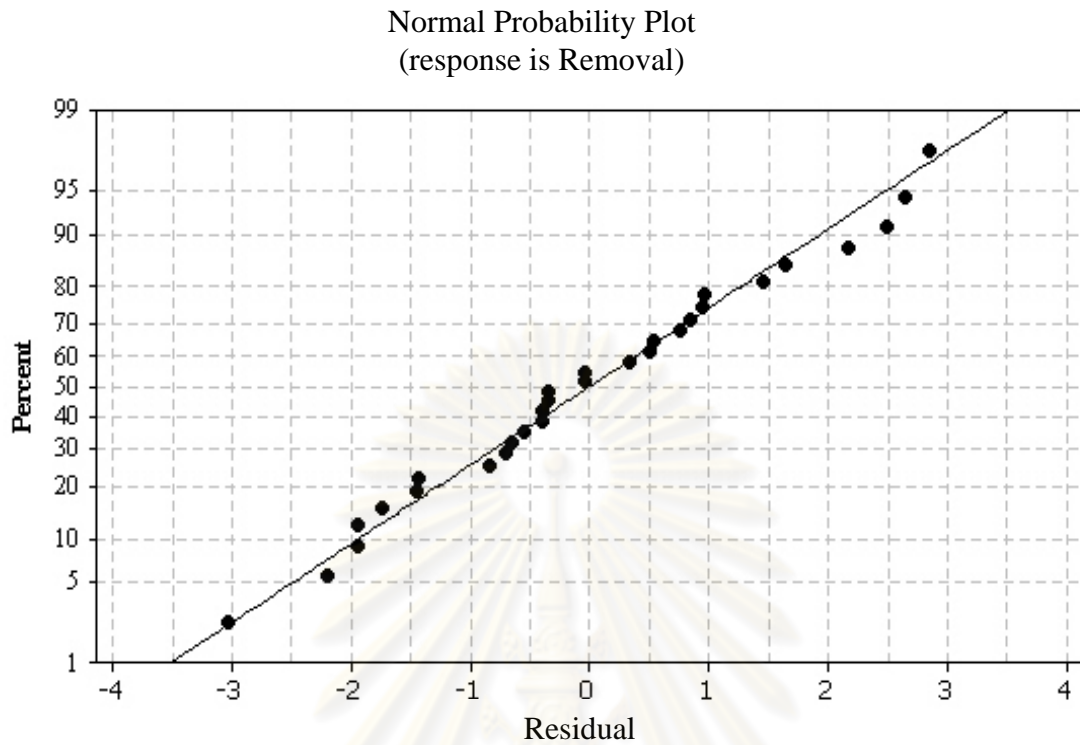


Figure 4.17 An normal probability plot of the experimental data foralachlor removal

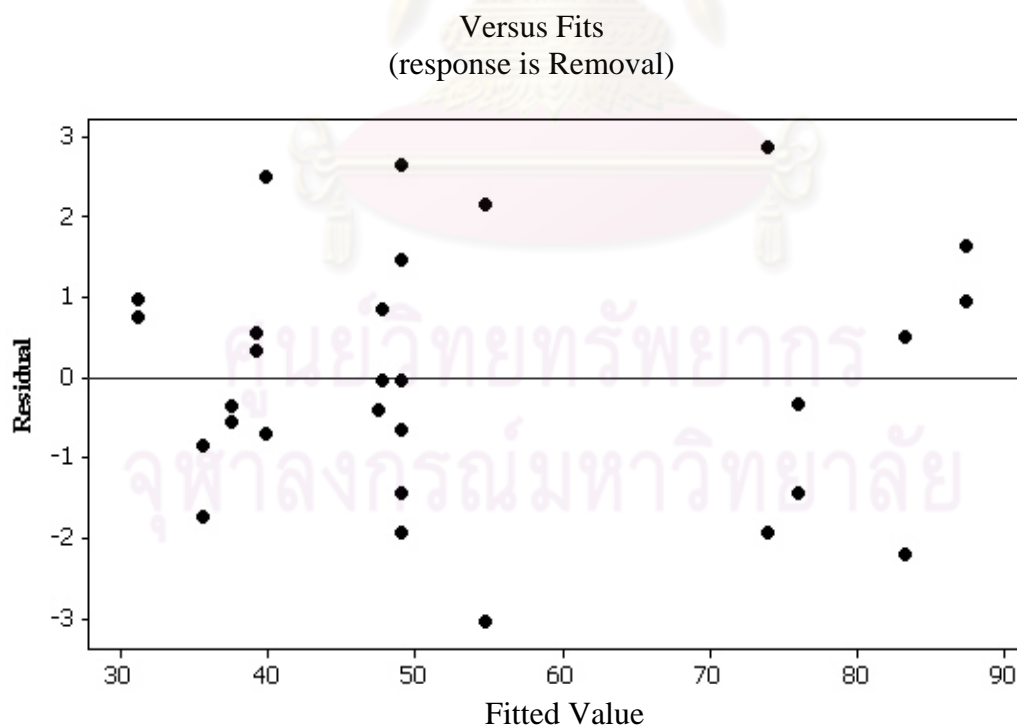


Figure 4.18 Histogram internally studentized residuals and normal % probability plot foralachlor removal

#### 4.4.3 Main and interaction effect and response surface analysis

Main effect plots display important factors including initial alachlor concentration, catalyst loading, and ultrasonic power intensity as shown in Figure 4.19. It presents that the removal efficiency of alachlor increased with increasing catalyst loading from 500 to 1500 mg L<sup>-1</sup> and then increased slightly from 1500 to 2500 mg L<sup>-1</sup>. The high amount of catalyst generated more free radicals which can increase alachlor degradation. On the other hand, increased catalyst loading hindered the light from passing to activate the catalyst. In the contour plot of effect of ultrasonic power intensity, the removal efficient of alachlor linearly improves with power intensity up to 30 W.

As shown in Figure 4.19, the results illustrated that the removal efficiency of alachlor decreased with decrease in the initial alachlor concentration. Due to the increase of the equilibrium adsorption of the alachlor onto the active sites of catalyst surface, the small amount of OH radical, which is an active oxidant, is generated. It causes the lower removal efficiency (Cho and Zoh, 2007).

As a result of higher ultrasonic power intensity which initiates the stronger acoustic cavitations effect, alachlor removal efficiency improves with the increase of ultrasonic power intensity (Zhang and Zheng, 2009).

Main Effects Plot for Removal  
Data Means

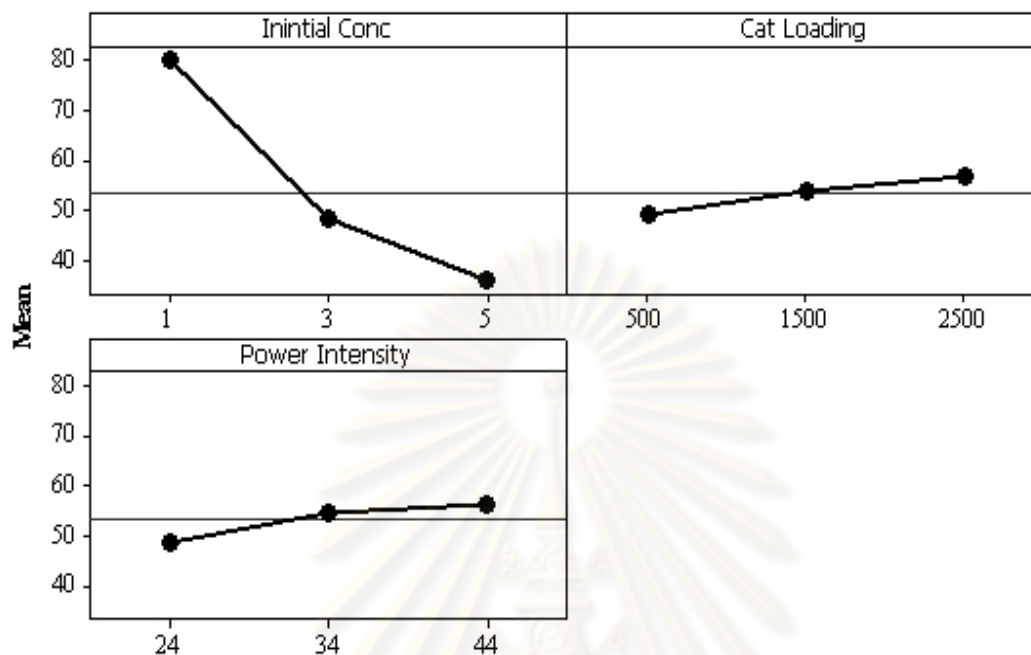


Figure 4.19 Main effect of matrix plots of experimental factors for percentage removal ofalachlor in a three factors, three levels Box-Benkhen design

In order to study the interaction effect of initialalachlor concentration, catalyst loading, ultrasonic power intensity is plotted in the term of two-factor interaction effect as shown in Figure 4.20. The results of all interaction plots indicated that there is interaction between initialalachlor concentration and catalyst loading which is similar to the results of ANOVA results as presented in Table 4.3. The P-value of interaction between initialalachlor concentration and catalyst loading was less than 0.05 suggesting significance at 95% confidence level.

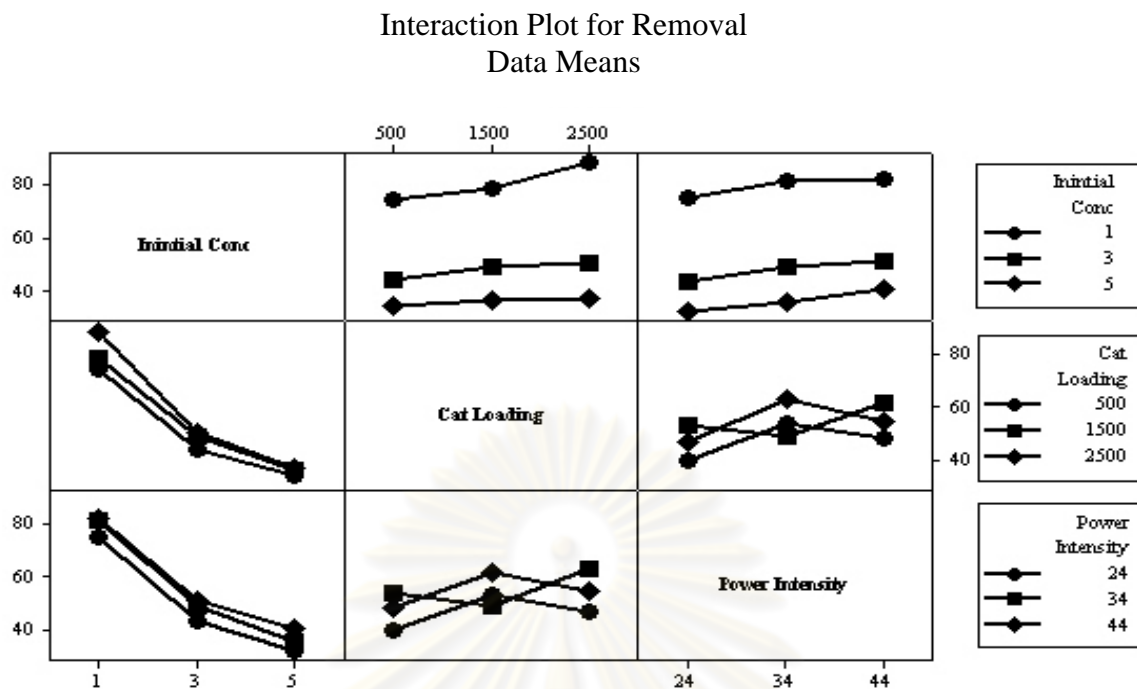


Figure 4.20 Two-factor interaction of matrix plots of experimental factors for percentage removal ofalachlor in a three factors, three levels Box-Benken design

Figures 4.21-4.23 present contour and three-dimensional (3D) plots for the predicted responses and the experimental factors. In all of the six plots in each response, if the model has more than two factors, one factor was set constant for each diagram. In Figure 4.21 and 4.22, the response of catalyst loading and initialalachlor concentration plots shows the interaction effect which presentsalachlor removal efficiency decreased with decrease in initialalachlor concentration. It also increases with catalyst loading as reflected in the plot of interaction effect in catalyst loading and initialalachlor concentration, shown in Figure 4.20.

จุฬาลงกรณ์มหาวิทยาลัย

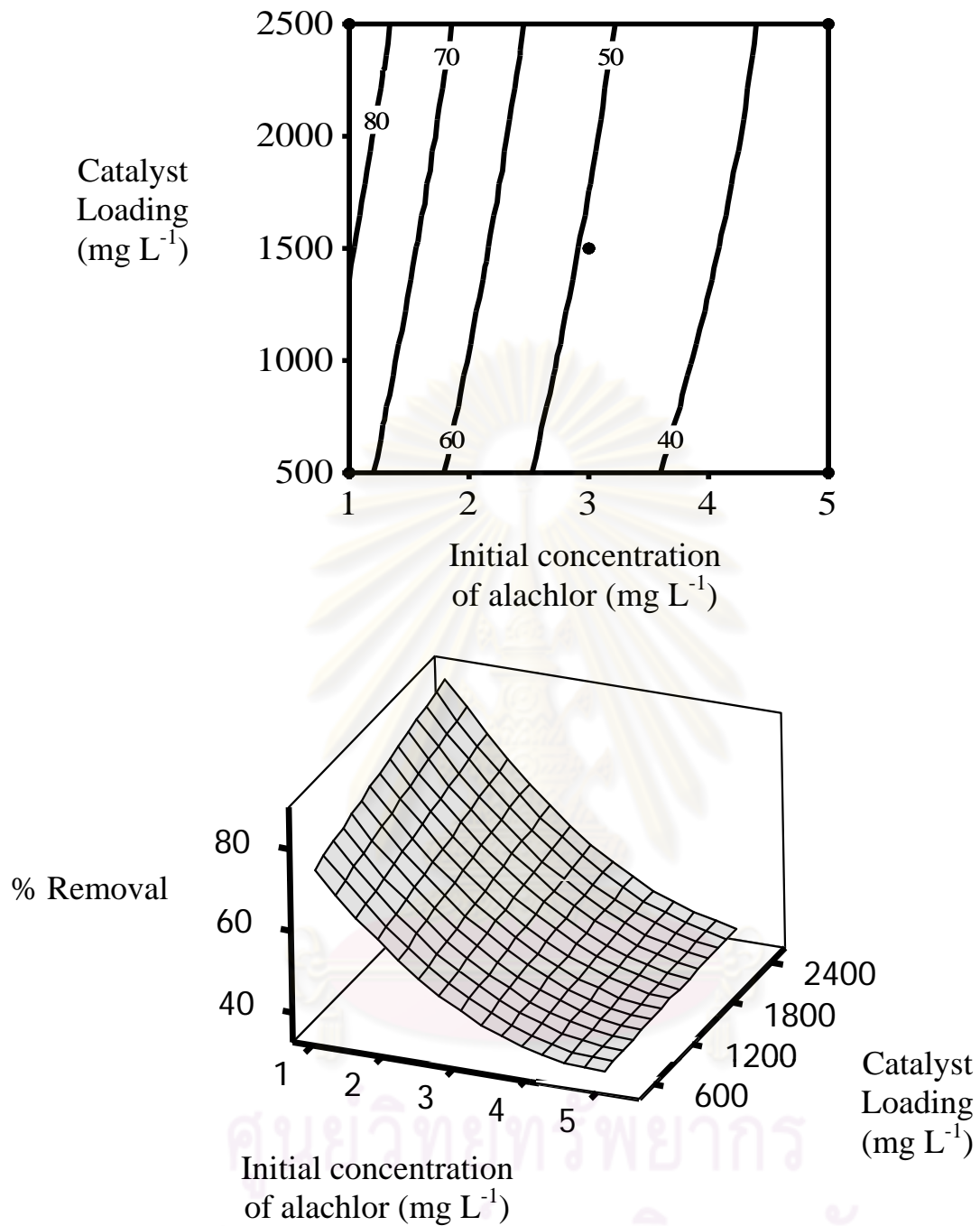


Figure 4.21 Contour plot and surface plot of response for catalyst loading and initial concentration

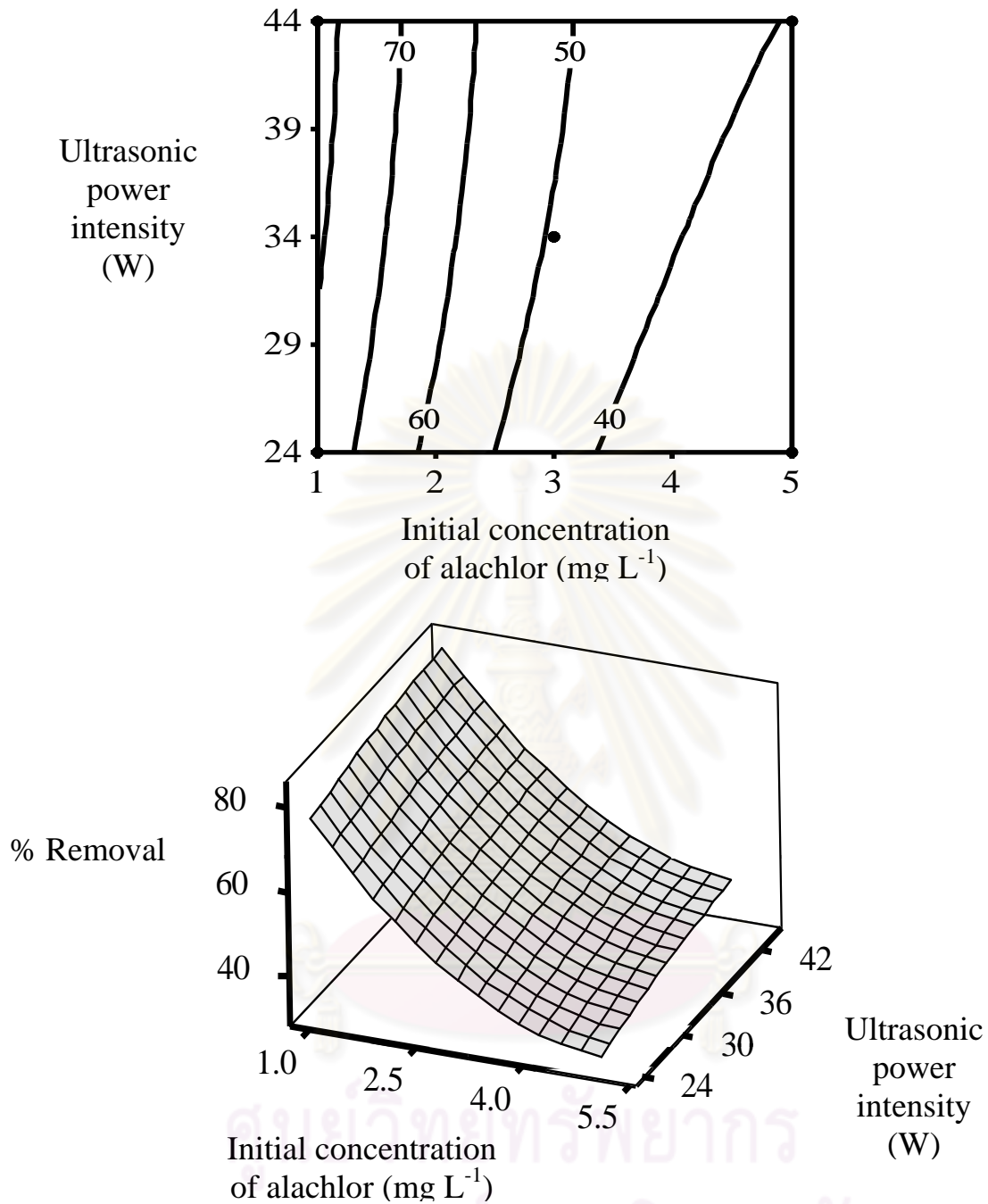


Figure 4.22 Contour plot and surface plot of response for ultrasonic power intensity and initial concentration

When ultrasonic power is applied, the alachlor removal efficiency also increased as presented in Figure 4.22 and 4.23. It can be summarized that ultrasonic power improves the alachlor removal efficiency as the same result of main effect as shown in Figure 4.20.

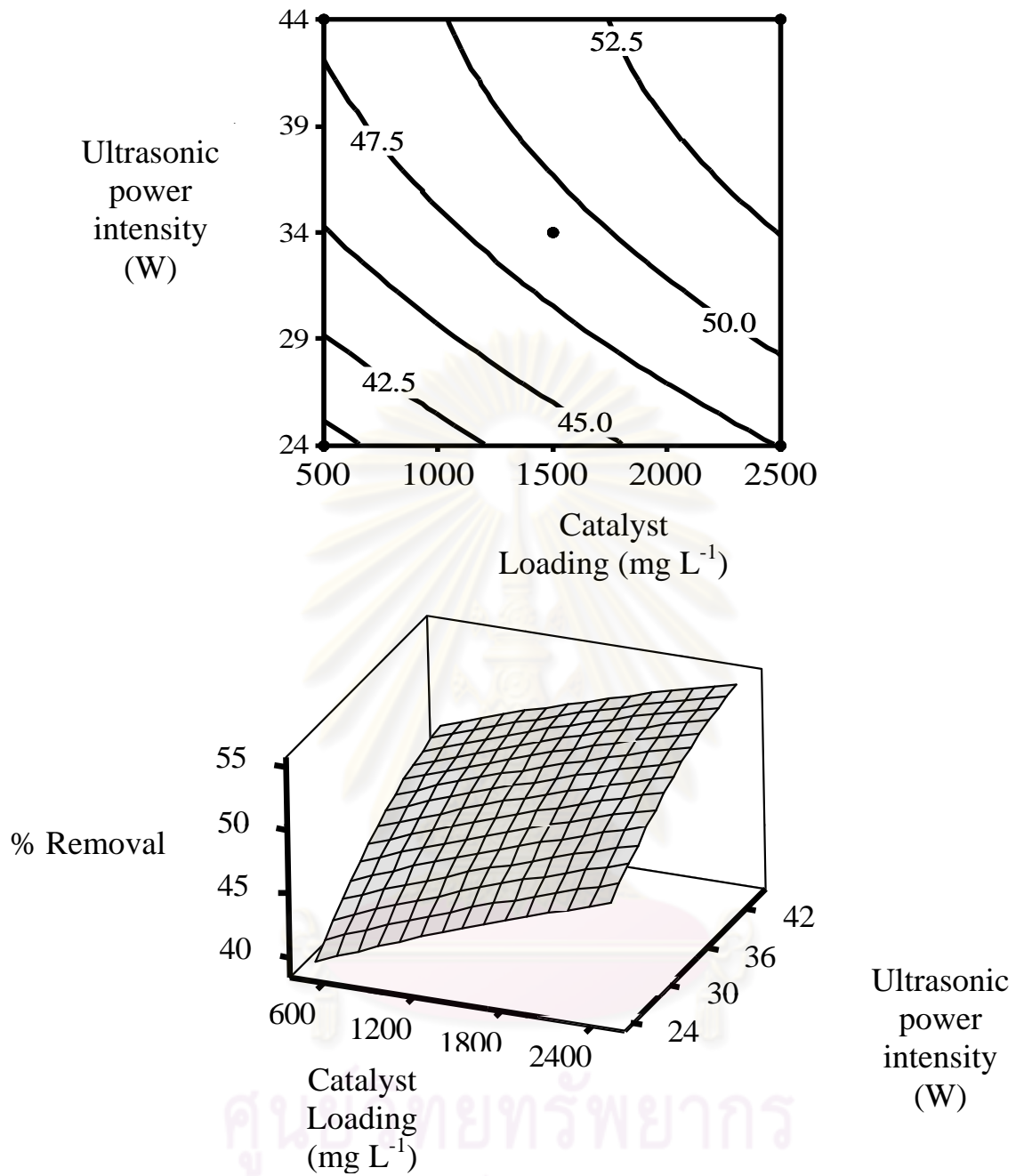


Figure 4.23 Contour plot and surface plot of response for ultrasonic power intensity and catalyst loading

#### 4.4.4 Optimization

After the study of main and interaction effects have been already conducted, optimization was carried out by numerical optimization function in the Minitab software. The options including lower, upper and target for the optimization were set at 85% alachlor removal efficiency respectively. The optimal conditions at 85% alachlor removal as presented in Figure 4.24 were recorded at 1 mg L<sup>-1</sup> alachlor concentration using 1.785 g L<sup>-1</sup> S doped TiO<sub>2</sub> and 44 w ultrasonic power .

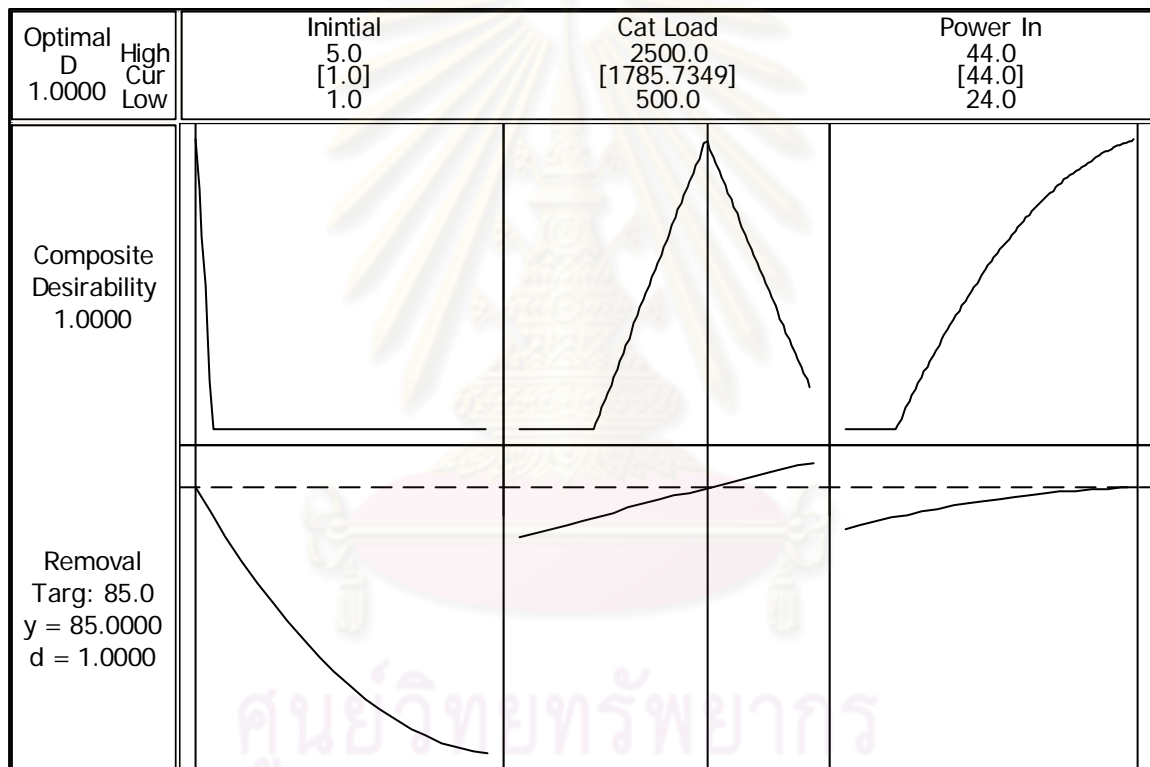


Figure 4.24 Optimality plot to locate optimum factor levels for maximized response

#### 4.4.5 Verification of model

It further proves that the response of the predicted conditions reasonably agree with the experimental values. There are four critical conditions used for validation and adequacy of the predicted results as presented in Table 4.7 and Figure 4.25. The three triplicate values of four observed values indicate that the predicted values of adjusted

model were more close to the experimental values comparing to values from predicted model.

Table 4.7 Comparison of experimental and predicted values of four responses at the optimal levels predicted by RSM

Initial concentration ofalachlor (mg L <sup>-1</sup> )	Catalyst loading (mg L <sup>-1</sup> )	Ultrasonic power intensity (W in 80 mL)	Predicted value (%) (Predicted model)	Predicted Value (%) (Adjusted model)	Observed value (%)
1.61	859	24	60.0	61.5	63.2±2.2
1.46	2013	24	70.5	71.0	71.2±2.9
1	1785	44	85.0	86.8	87.2±2.6
1	2500	44	89.3	91.6	91.6±1.9

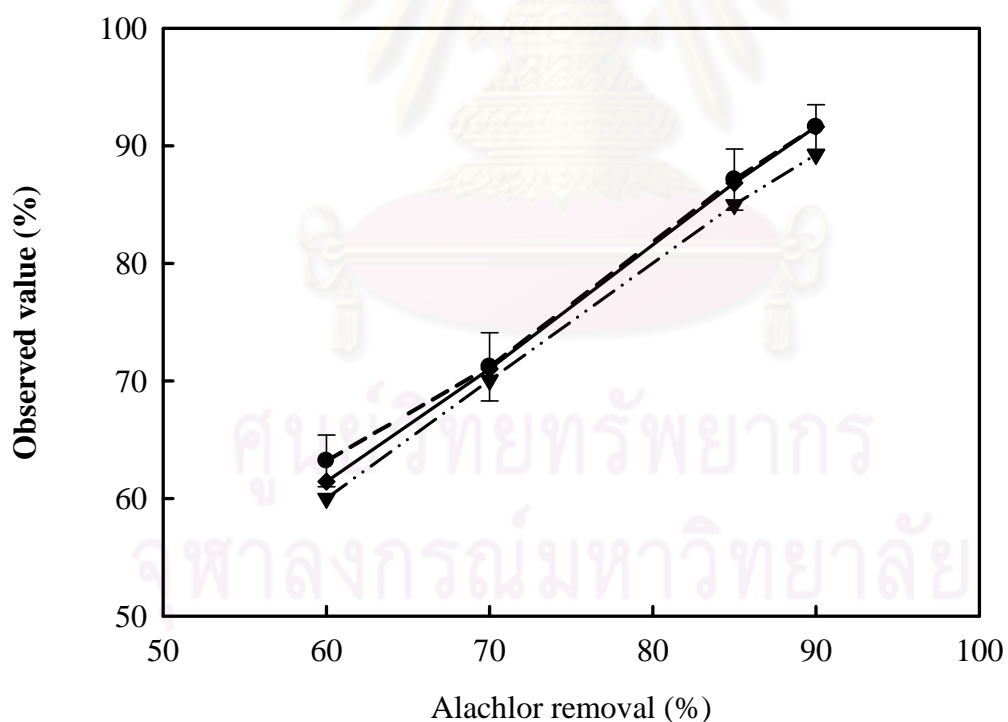


Figure 4.25 Comparison of experimental and predicted values (predicted model and adjusted model) of four responses: observed value (●), predicted value (▼) adjusted value (◆)

## CHAPTER V

### CONCLUSIONS

#### 5.1 Conclusions

5.1.1 The properties of S-doped TiO<sub>2</sub> were characterized and found that it was strong adsorption properties under visible region, small crystallite size (12 nm) and high relative surface area (87 m<sup>2</sup> g<sup>-1</sup>).

5.1.2 The photocatalytic activities of alachlor by S-doped TiO<sub>2</sub> under visible light at wavelengths longer than 450 nm were relatively faster than using pure TiO<sub>2</sub> (P25). Langmuir–Hinshelwood (L–H) expression describes alachlor degradation in terms of initial concentration of alachlor and initial reaction rate. In addition, ultrasonic power usually generates hydroxyl radicals and generally increases mass transfer for chemical oxidation. Significant improvement in the degradation rate of alachlor was shown with a synergistic effect of 11%.

5.1.3 In sonophotocatalytic activity of alachlor degradation by S-doped TiO<sub>2</sub> under visible light, the results presented that both photocatalysis and sonophotocatalysis were found to follow pseudo-first-order rate law. The rate constant of sonophotocatalytic activities for alachlor degradation by S-doped TiO<sub>2</sub> was two times higher than its activity of TiO<sub>2</sub> (P25). It was found that the rate constant increased by decreasing initial concentration of alachlor that could be explained by the Langmuir–Hinshel wood model. At 10 mg L<sup>-1</sup> initial alachlor concentration, the reaction rate was proportional to the amount of catalyst loading until it reached the optimum point at 1 g L<sup>-1</sup>. It was also observed that pH in solution slightly influences the rate of alachlor degradation. In applying ultrasonic irradiation, the degradation rate of alachlor increased as power input of ultrasonic sound increased. In addition, degradation of alachlor was probably not influenced by the addition of hydrogen peroxide whereas the alachlor degradation in presence of K<sub>2</sub>S<sub>2</sub>O<sub>8</sub> was faster considerably than that in the same system without K<sub>2</sub>S<sub>2</sub>O<sub>8</sub>. Mineralization of alachlor under sonophotocatalytic activity was also discussed. The sonophotocatalytic degradation of alachlor also produced inorganic ions remaining in solution. The reasons that Fe<sup>2+</sup> can react with both OH<sup>•</sup> and H<sub>2</sub>O<sub>2</sub> generated by

ultrasound. The dechlorination of alachlor involved the generation of  $\text{Cl}^-$  ions and the N dealkylation involved the formation of  $\text{NO}_2^-$  and  $\text{NO}_3^-$  ions. On the Fricke reaction measurement, the result presents that the effect of ultrasound enhances photocatalytic activity of alachlor degradation by generating more hydroxyl radicals.

5.1.4 The experimental design of S doped  $\text{TiO}_2$  sonophotocatalytic degradation of alachlor under visible light was achieved by response surface methodology based on Box-Behnken design. The correlation coefficient ( $R^2$ ) between the experimental data and model data was 0.98. The optimum operating conditions were of alachlor concentration,  $1.785 \text{ g L}^{-1}$  catalyst loading and  $0.55 \text{ W m L}^{-1}$  ( $44 \text{ W}$  in  $80 \text{ mL}$ ) to achieve 85% alachlor removal in 1 hr. In addition, the model results proposed that ultrasonic power increased the alachlor removal efficiency. It can be concluded that response surface methodology based on Box-Behnken design presented a precise and reliable technique to optimize the operating condition of alachlor degradation of sonophotocatalytic activities.

## 5.2 Recommendations

5.2.1 The pathway of alachlor degradation and intermediated evaluation on S-doped  $\text{TiO}_2$  sonophotocatalytic activity were not included in this study. It is suggested that the pathway of alachlor degradation should be identified.

5.1.2 This study focused on the alachlor degradation under synthesis light source. It would be better to study this reaction in the solar light.

5.1.3 From the TEM images, particles which is smaller than the crystallize size of  $\text{TiO}_2$  was found. This is an unusual case. EDX technique should be use to indentify what they are.

## REFERENCES

- Augugliaro, V., Litter, M., Palmisano, L. and Soria, J. The combination of heterogeneous photocatalysis with chemical and physical operations: A tool for improving the photoprocess performance. Journal of Photochemistry and Photobiology C: Photochemistry Reviews 7 (2006) : 127–144
- Bahena C.L., Marti´nez S.S. and Guzma´n D.M. Sonophotocatalytic degradation of alazine and gesaprim commercial herbicides in TiO<sub>2</sub> slurry. Chemosphere 71 (2008) : 982–989.
- Bejarano-Pe´rez, N. and Sua´rez-Herrera, M.F. Sonophotocatalytic degradation of congo red and methyl orange in the presence of TiO<sub>2</sub> as a catalyst. Ultrasonics Sonochemistry 14 (2007) : 589–595.
- Catalkaya, E.C. and Kargi, F. Effects of operating parameters on advanced oxidation of diuron by the Fenton’s reagent: a statistical design approach. Chemosphere 69 (2007) : 485–492.
- Chen, L.C., Tsai F.R. and Huang C.M. Photocatalytic decolorization of methyl orange in aqueous medium of TiO<sub>2</sub> and Ag-TiO<sub>2</sub> immobilized on gamma-Al<sub>2</sub>O<sub>3</sub>. Journal Photochemistry Photobiology A: Chemistry 170(1) (2005) : 7–14.
- Chen, X. and Mao, S.S. Titanium dioxide nanomaterials: synthesis, properties, modifications, and applications. Chemical Reviews 107 (2007) : 2891-2959.
- Chen, X. Synthesis and investigation of novel nanomaterials for improved photocatalysis. Phd Dissertation Department of Chemistry, Case Western Reserve University, 2005.
- Cho, I.H. and Zoh, K.D. Photocatalytic degradation of azo dye (Reactive Red 120) in TiO<sub>2</sub>/UV system: Optimization and modeling using a response surface methodology (RSM) based on the central composite design. Dyes and Pigments 75 (2007) : 533-543.
- Chu W. and Wong C.C. Study of herbicide alachlor removal in a photocatalytic process. Industrial & Engineering Chemistry Research 43 (2004) : 5027-5031.
- Davydov, L., Reddy, E.P., France, P. and Smirniotis P.G. Sonophotocatalytic destruction of organic contaminants in aqueous systems on TiO<sub>2</sub> powders. Applied Catalysis B: Environmental 32 (2001) : 95–105.

- Demeestere K., Dewulf J., Ohno T., Salgado P.H. and Langenhove H.V. Visible light mediated photocatalytic degradation of gaseous trichloroethylene and dimethyl sulfide on modified titanium dioxide. Applied Catalysis B: Environmental 61 (2005) : 140–149.
- Department of Agriculture Thailand Report on hazardous chemicals imported into Thailand (2004) [Online] Available from: <http://www.dao.go.th>, April 10, 2009.
- Farre, M.J., Domenech, X. and Pera, J. Assessment of photo-Fenton and biological treatment coupling for Diuron and Linuron removal from water. Water Research 40 (2006) : 2533–2540.
- Flynn, H. Physics of Acoustic Cavitation in Liquids. Physical Acoustics (W.P. Mason ed). Vol. IB. New York: Academic Press, 1964.
- Fogler, H. S. Elements of chemical reaction engineering Prentice-Hall, Englewood Cliffs, New Jersey, 2005
- Food and Agriculture Organization of the United Nations (FAO), Regional Office for Asia and the Pacific. Implementation, Monitoring and Observance International Code of Conduct on the Distribution and Use of Pesticides, Proceeding of Asia Regional Workshop. (2005) FAO Regional Office for Asia and the Pacific, Bangkok, Thailand
- Fujishima, A. and Zhang X. Titanium dioxide photocatalysis: present situation and future approaches. Comptes Rendus Chimie 9 (2006) : 750–760.
- Gernjak, W., Fuerhacker, M., Fernández-Ibañez, P., Blanco, J., Malato, S. Solar photo-Fenton treatment process parameters and process control. Applied Catalysis B: environmental 64 (2006) : 121–130.
- He, Y. Sonochemistry and advance oxidation processes: Synthesis of nanoparticles and degradation of organic pollutants Phd Thesis Chemistry University of Melbourne, Australia, 2009.
- Himaman, W. Examination of Soil bacteria capable of degrading herbicides alachlor and Oxyfluorfen Master Thesis Biological Science Chiangmai University, 1998.
- Jho, J.H., Kim, D.H., Kim, S.J. and Lee, K.S. Synthesis and photocatalytic property of mixture of anatase and rutile TiO<sub>2</sub> doped with Fe by mechanical alloying process. Journal of Alloys and Compounds 459 (2008) : 386-389.
- Kaur, S. and Singh, V. Visible light induced sonophotocatalytic degradation of Reactive Red dye 198 using dye sensitized TiO<sub>2</sub>. Ultrasonics Sonochemistry 14 (2007) : 531–537.

- Kellogg, R.L., Bagdon, J. and Wallace, S. An information aid for assessing possible NRCS involvement in the State Management plan process for regulation of pesticides. National resource conservation service, Department of agriculture, United States, 1998.
- Korbahti, K.B. and Rauf, M.A. Response surface methodology (RSM) analysis of photoinduced decoloration of toluidine blue. Chemical Engineering Journal 136 (2008) : 25–30.
- Lei, S., Duan, W. Highly active mixed-phase TiO<sub>2</sub> photocatalysts fabricated at low temperature and the correlation between phase composition and photocatalytic activity Journal of Environmental Sciences 20 (2008): 1263–1267
- Lin, Y., Ferronato, C., Deng, N., Wua, F. and Chovelon, J.M. Photocatalytic degradation of methylparaben by TiO<sub>2</sub>: Multivariable experimental design and mechanism. Applied Catalysis B 88 (2009) : 32–41.
- Linsebigler, A.L., Lu, G. and Yates, J.T., Jr. Photocatalysis on TiO<sub>2</sub> surfaces: principles, mechanisms, and selected results. Chemical Reviews 95 (1995) : 735.
- Liu, S. and Chen, X. A visible light response TiO<sub>2</sub> photocatalyst realized by cationic S-doping and its application for phenol degradation. Journal of Hazardous Materials 152 (2008) : 48–55.
- Mason, T.J. and Lorimer, J.P. Applied Sonochemistry: Uses of Power Ultrasound in Chemistry and Processing. Wiley-VCH Verlag GmbH & Co. KGaA, 2002.
- Malato, S. Blanco, J., Vidal, A. and Richter, C. Photocatalysis with solar energy at a pilot-plant scale: An overview. Applied Catalysis B: Environment, 37 (2002) : 1-15
- Miltner, R.J., Fronk, C.A. and Speth, T.F. Removal of Alachlor from Drinking Water. Proc. Nat'l Conference on Environ. Engineering, ASCE. Orlando, FL (1987).
- Miltner, R.J., Baker, D.B., Speth, T.F. and Fronk, C.A. Treatment of seasonal pesticides in surface waters. Journal American Water Works Association 81 (1989) : 43-52.
- Ministry of Public Health. Bureau of Epidemiology Annual epidemiological surveillance report 2005. [Online] available from: [http://203.157.15.4/Annual/Annual48/Part2/Table/Table9\\_36.html](http://203.157.15.4/Annual/Annual48/Part2/Table/Table9_36.html), December 15, 2009.
- Murugesan, K., Dhamija, A., Nam, I.H., Kim, Y.M. and Chang, Y.S. Decolourization of reactive black 5 by laccase: Optimization by response surface methodology. Dyes and Pigments 75 (2007) : 176-184.

- Neppoliana B., Junga H., Choia H., Leea J.H. and Kang J.W. Sonolytic degradation of methyl tert-butyl ether: the role of coupled fenton process and persulphate ion. Water Research 36 (2002) : 4699–4708.
- Ohno, T., Sarukawa, K., Tokieda, K. and Matsumura, M. Morphology of a TiO<sub>2</sub> photocatalyst (Degussa, P-25) consisting of anatase and rutile crystalline phases. Journal of Catalysis 203 (2001): 82–86
- Ohno T., Akiyoshi M., Umebayashi, T., Asai, K., Mitsui T. and Matsamura M. Preparation of S-doped TiO<sub>2</sub> photocatalysts and their photocatalytic activities under visible light. Applied Catalysis A 265 (2004) : 115–121.
- Orme S., and Kegley S. Pesticide database. In Pesticide Action Network. Pesticide Action Network North America, San Francisco, 2005.
- Osajima, J.A., Ishiki, H.M. and Takashima, K. The photocatalytic degradation of Imazapyr. Monatshefte fur Chemie 139 (2008) : 7–11.
- Panapitukkul, N., Pengnoo, A., Siriwong, C., and Chatupote, W. Hydrogeomorphological control on ground water quality in the rattaphum catchment (Songkhla lake basin), Thailand. Water, Air, and Soil Pollution: Focus 5 (2005) : 149–163.
- Panuwet, P., Prapamontol, T., Chantara, S., Thavornyuthikarn, P., Montesano, M.A., Whitehead, R.D. Jr., and Barrb D.B. Concentrations of urinary pesticide metabolites in small-scale farmers in Chiang Mai Province, Thailand. Science of the Total Environment 407 (2008) : 655-668.
- Parag, R. G., and Pandit, A. B. A review of imperative technologies for wastewater treatment II: hybrid methods. Advances in Environmental Research 8 (2004) : 553–597.
- Penuela, G. A. and Barcelo, D. Comparative degradation kinetics of alachlor in water by photocatalysis with FeCl<sub>3</sub>, TiO<sub>2</sub> and photolysis, studied by solid-phase disk extraction followed by gas chromatographic techniques. Journal of Chromatography A 754(1–2) (1996) : 187–195.
- Paola, A. D., Cufalo, G., Addamo, M., Bellardita, M., Campostrini, R., Ischia, M. Ceccato, R., and Palmisano, L. Photocatalytic activity of nanocrystalline TiO<sub>2</sub> (brookite, rutile and brookite-based) powders prepared by thermohydrolysis of TiCl<sub>4</sub> in aqueous chloride solutions. Colloids and Surfaces A: Physicochem. Eng. Aspects 317 (2008) : 366–376

- Raya, S., Lalman, J. A. and Biswas, N. Using the Box-Benken technique to statistically model phenol photocatalytic degradation by titanium dioxide nanoparticles. Chemical Engineering Journal 150 (2009) : 15–24.
- Rengifo-Herrera, J.A., and Pulgarin C. Photocatalytic activity of N, S co-doped and N-doped commercial anatase TiO<sub>2</sub> powders towards phenol oxidation and E. coli inactivation under simulated solar light irradiation. Solar Energy 84 (2010) : 37–43.
- Rios-Enriquez, M., Shahin, N., Durán-De-Bazúa, C., Lang, J., Oliveros, E., Bossmann, S.H. Optimization of the heterogeneous Fenton-oxidation of the model pollutant 2,4-xylidine using the optimal experimental design methodology, Solar Energy 77 (2004) : 491–501.
- Ryu, C.S., Kim, M.S. and Kim B.W. Photodegradation of alachlor with the TiO<sub>2</sub> film immobilised on the glass tube in aqueous solution. Chemosphere 53 (2003) : 765–771.
- Sakkas, V.A., Islam, Md.A., Stalikas, C. and Albanis, T.A. Photocatalytic degradation using design of experiments: A review and example of the Congo red degradation. Journal Hazardous. Materials 175 (2010): 33–44
- Silva, A.M.T., Ekaterini, N., Carmo-Apolinario, A.C., Xekoukoulotakis, N.P. and Mantzavinos, D. Sonophotocatalytic/H<sub>2</sub>O<sub>2</sub> degradation of phenolic compounds in agro-industrial effluents. Catalysis Today 124 (2007): 232–239.
- Surolia, P.K., Tayade, R.J. and Jasra, R.V. Effect of Anions on the photocatalytic activity of Fe (III) salts impregnated TiO<sub>2</sub>. Industrial & Engineering Chemistry Research 46 (2007) : 6196-6203.
- Suslick, K.S. (Ed.). Ultrasound-Its Chemical, Physical and Biological Effect. VCH Publishers, Inc., New York, 1988, pp 228-239
- Tomlin, C.D.S. The Pesticide Manual, 11th Ed. British Crop Protection Council, 1997.
- US EPA Alachlor prevention, pesticides and toxic substances (7508C). Registration Eligibility Decision (R.E.D.) Facts EPA-738-F-98-018 December (1998)
- US EPA The incorporation of water treatment effects on pesticide removal and transformations in food quality protection act (FQPA) drinking water assessments October (2001)
- US EPA Alachlor National Primary Drinking Water Regulations, Technical Factsheet [Online] Available from: <http://www.epa.gov/ogwdw000/pdfs/factsheets/soc/tech/alachlor.pdf> , May 18, 2009.

- Wang H., Niu J., Long X. and He Y. Sonophotocatalytic degradation of methyl orange by nano-sized Ag/TiO<sub>2</sub> particles in aqueous solutions. Ultrasonics Sonochemistry 14 (2007) : 531–537.
- Wayment, D.G. Variable frequency sonochemistry Phd Dissertation the Graduate Faculty of Texas Tech University, 1997.
- Wayment, D.G., Dominick, J. and Casadonte Jr. Frequency effect on the sonochemical remediation of alachlor. Ultrasonics Sonochemistry 9 (2002) : 251–257.
- WHO/FAO Des Nations Unies Pour L' Alimentation Et L' Agriculture. Data sheets on pesticides No. 86 WHO/PCS/DS/96.86 Date of issue: July 1996
- Wong, C.C. and Chu W.<sup>a</sup> The direct photolysis and photocatalytic degradation of alachlor at different TiO<sub>2</sub> and UV sources the Examination of the Reaction Mechanism. Chemosphere 50 (2003) : 981–987.
- Wong, C. C. and Chu, W.<sup>b</sup> The hydrogen peroxide-assisted photocatalytic degradation of alachlor in TiO<sub>2</sub> suspensions. Environmental Science & Technology 37 (10) (2003) : 2310-2316.
- Yano, J., Matsuura, J., Ohura H. and Yamasaki S. Complete mineralization of propyzamide in aqueous solution containing TiO<sub>2</sub> particles and H<sub>2</sub>O<sub>2</sub> by the simultaneous irradiation of light and ultrasonic waves. Ultrasonics Sonochemistry 12 (2005) : 197–203.
- Zhang, Z. and Zheng, H. Optimization for decolorization of azo dye acid green 20 by ultrasound and H<sub>2</sub>O<sub>2</sub> using response surface methodology. Journal of Hazardous Materials 172 (2009) : 1388–1393.



**APPENDICES**

ศูนย์วิทยทรัพยากร  
จุฬาลงกรณ์มหาวิทยาลัย

## APPENDIX A

### Relationship Between particle velocity ( $v_A$ ) and acoustic pressure (P)

Consider an element (DEFG) of a liquid (Figure A1.) at a normal pressure of  $P$  and density of  $\rho$  subject to an applied acoustic wave of pressure  $P$

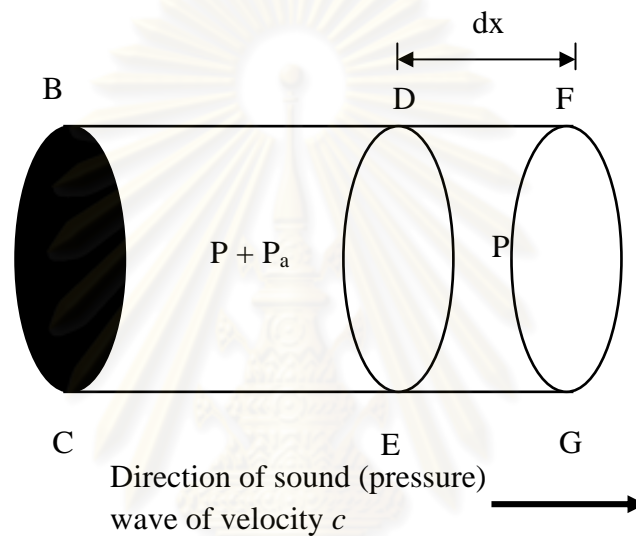


Figure A1. Element of liquid subjected to acoustic pressure.

Under the action of the excess pressure,  $P$ , the molecules in the element BC will be displaced in the direction of the wave, the velocity of particles increasing from zero at B to  $v$  at DE. The sound wave itself, of velocity  $c$ , will pass from DE to FG (i.e. through the distance  $dx$ ) in  $\frac{vc}{dx}$  seconds and hence the acceleration (velocity/time) of the particles in this volume element will, on average, be  $\frac{vc}{dx}$  since for such a small element  $v$  can be assumed to remain constant.

Obviously the force attained by these accelerating particles (= mass  $\times$  acceleration) derives from the excess pressure (=pressure  $\times$  area), such that:

$$(\rho A dx) \times \left(\frac{vc}{dx}\right) = (P) \times (A) \quad (\text{A.1})$$

i.e.  $\rho vc = P \quad (\text{A.2})$

or  $\frac{P}{v} = \rho c \quad (\text{A.3})$



ศูนย์วิทยทรัพยากร  
จุฬาลงกรณ์มหาวิทยาลัย

## APPENDIX B

### Characterization data

#### Zeta potential data

Table B.1 Average zeta potential (mV) of TiO<sub>2</sub> (P25), and S-doped TiO<sub>2</sub> samples.

TiO <sub>2</sub> (P25)		S-dopedTiO <sub>2</sub>	
pH	Avg. Zeta potential (mV)	pH	Avg. Zeta potential (mV)
10	-28.5	10	-17.6
9	-24.4	9	-21.1
8	-18.7	8	-13.3
7	-17.1	7	-16.0
6	-9.2	6	-2.9
5	17.7	4.5	8.9
4	23.1	4	20.0
3	29.6	3	35.1
2	25.5	2	37.7
1	31.2	1	35.2

ศูนย์วิจัยทันตวิทยา  
จุฬาลงกรณ์มหาวิทยาลัย

## APPENDIX C

### Standard calibration curve ofalachlor

#### C1. Calibration curve ofalachlor

Table C.1 Calibration curve data ofalachlor

No.	Concentration (mg L <sup>-1</sup> )	Area
1	12.36	2172.55
2	10.09	1779.75
3	6.41	1145.10
4	3.18	564.45
5	1.58	272.95
6	0.48	88.30
7	0.20	36.75

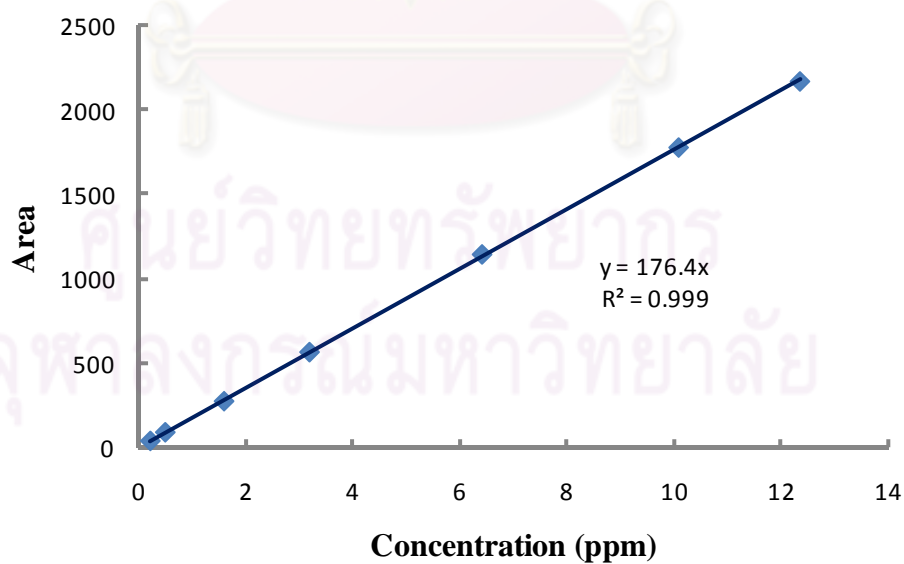


Figure C.1 Standard calibration curve ofalachlor

## C.2 Percentage of alachlor degradation

The removal efficiency of alachlor is calculated from the following formula:

$$\% \text{ degradation} = \frac{C_0 - C}{C_0} \times 100 \quad (\text{C.1})$$

where:  $C_0$  = the initial concentration of alachlor

$C$  = the concentration of alachlor in the time interval of irradiation

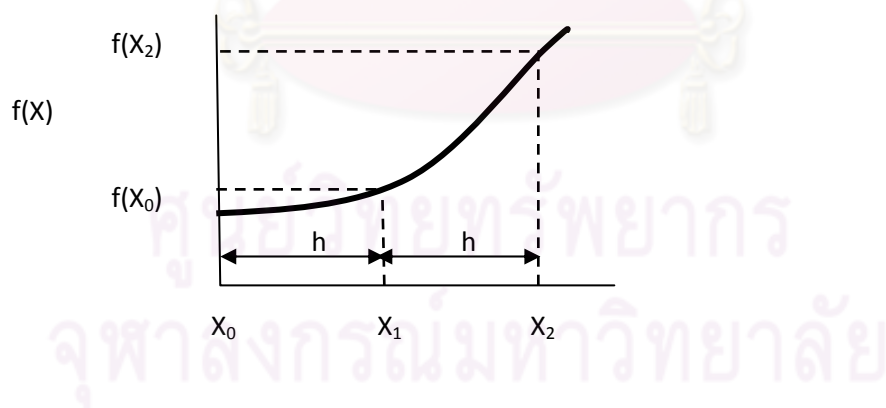
## C.3 Simpson's one-third rule (three-point)

A more accurate evaluation of the integral can be found with the application of Simpson's rule.

$$\int_{x_0}^{x_2} f(X) dX = \frac{h}{3} [f(X_0) + 4f(x_1) + f(X_2)] \quad (\text{C.2})$$

Where  $h = \frac{X_2 - X_0}{2}$

$$X_1 = X_0 + h$$



## APPENDIX D

### Results ofalachlor degradation

#### D1. Results of photocatalytic degradation of different catalyst concentration

Table D.1 photocatalyticalachlor degradation of different catalyst loading

Time (min)	C/C <sub>0</sub>			
	0.5 g L <sup>-1</sup> S-doped TiO <sub>2</sub>	1.0 g L <sup>-1</sup> S-doped TiO <sub>2</sub>	1.5 g L <sup>-1</sup> S-doped TiO <sub>2</sub>	2.0 g L <sup>-1</sup> S-doped TiO <sub>2</sub>
0	1.00	1.00	1.00	1.00
60	0.97	0.92	0.88	0.89
120	0.92	0.85	0.77	0.77
180	0.88	0.77	0.67	0.66
240	0.85	0.73	0.62	0.63

ศูนย์วิทยทรัพยากร  
จุฬาลงกรณ์มหาวิทยาลัย

Table D.2 photocatalytic alachlor degradation of different light sources

Time (min)	C/C <sub>0</sub>		C/C <sub>0</sub>	
	cutter of filter (420 nm)		cutter of filter (450 nm)	
	TiO <sub>2</sub> (P25)	S-doped TiO <sub>2</sub>	TiO <sub>2</sub> (P25)	S-doped TiO <sub>2</sub>
0	1.00	1.00	1.00	1.00
60	0.81	0.86	0.98	0.89
120	0.68	0.71	0.99	0.77
180	0.62	0.60	0.94	0.66

Continued Table D.2 photocatalytic alachlor degradation of different light sources

Time (min)	C/C <sub>0</sub>	
	No cutter of filter	
	TiO <sub>2</sub> (P25)	S-doped TiO <sub>2</sub>
0	1.00	1.00
5	0.17	0.87
10	0.04	0.75
15	0.01	0.59
20	0.00	0.48
30	0.00	0.40
60	0.00	0.10
120	0.00	0.02
180	0.00	0.00

Table D.3 photocatalytic alachlor degradation of different initial of alachlor concentration

Time (min)	Parameters			
	$C_0$ (mg L <sup>-1</sup> )	$r_0$ (mg L <sup>-1</sup> min <sup>-1</sup> )	$C_0^{-1}$ (L mg <sup>-1</sup> )	$r_0^{-1}$ (min L mg <sup>-1</sup> )
0	5	1.00	1.00	1.00
60	10	0.86	0.98	0.89
120	20	0.71	0.99	0.77
180	30	0.60	0.94	0.66

ศูนย์วิทยทรัพยากร  
จุฬาลงกรณ์มหาวิทยาลัย

Table D.4 photocatalytic alachlor degradation of different initial of alachlor concentration

Time (min)	S-doped TiO <sub>2</sub> ln(C <sub>0</sub> /C)		
	Photocatalysis	Sonocatalysis	Sonophotocatalysis
0	0.00±0.00	0.00±0.00	0.00±0.00
30	0.04±0.01	0.06±0.01	0.14±0.01
60	0.09±0.01	0.15±0.03	0.29±0.03
120	0.17±0.03	0.31±0.02	0.52±0.00
180	0.26±0.03	0.46±0.00	0.81±0.01
240	0.32±0.06	0.62±0.01	1.06±0.05

Continued Table D.4 photocatalytic alachlor degradation of different initial of alachlor concentration

Time (min)	TiO <sub>2</sub> (P25) ln(C <sub>0</sub> /C)		
	Photocatalysis	Sonocatalysis	Sonophotocatalysis
0	0.00±0.00	0.00±0.00	0.00±0.00
30	0.04±0.01	0.14±0.01	0.06±0.01
60	0.09±0.01	0.29±0.03	0.15±0.03
120	0.17±0.03	0.52±0.00	0.31±0.02
180	0.26±0.03	0.81±0.01	0.46±0.00
240	0.32±0.06	1.06±0.05	0.62±0.01

Table D.5 Sonophotocatalytic alachlor degradation of different catalyst loading (S-doped TiO<sub>2</sub>)

Time (min)	C/C <sub>0</sub>			
	0.5 g L <sup>-1</sup> S-doped TiO <sub>2</sub>	1.0 g L <sup>-1</sup> S-doped TiO <sub>2</sub>	1.5 g L <sup>-1</sup> S-doped TiO <sub>2</sub>	2.0 g L <sup>-1</sup> S-doped TiO <sub>2</sub>
0	1.00	1.00	1.00	1.00
30	0.92	0.87	0.93	0.90
60	0.82	0.77	0.82	0.76
120	0.70	0.59	0.65	0.62
180	0.61	0.45	0.48	0.48
240	0.50	0.33	0.42	0.37

ศูนย์วิทยทรัพยากร  
จุฬาลงกรณ์มหาวิทยาลัย

Table D.6 Sonophotocatalytic alachlor degradation of different ultrasonic powers

Time (min)	C/C <sub>0</sub>			
	13 W	23 W	33 W	43 W
0	1.0000±0.0000	1.0000±0.0000	1.0000±0.0000	1.0000±0.0000
30	0.8668±0.0026	0.8468±0.0050	0.8074±0.0130	0.8000±0.0280
60	0.7492±0.0237	0.7420±0.0220	0.7000±0.0270	0.6734±0.0157
120	0.5949±0.0012	0.5367±0.0180	0.4934±0.0320	0.4592±0.0260
180	0.4457±0.0031	0.3632±0.0140	0.3149±0.0240	0.2584±0.0340
240	0.3464±0.0172	0.2528±0.0110	0.2023±0.0110	0.1532±0.0210

ศูนย์วิทยทรัพยากร  
จุฬาลงกรณ์มหาวิทยาลัย

Table D.7 Sonophotocatalytic alachlor degradation of different initial of alachlor concentration

Time (min)	$\ln C_0/C$			
	5 mg L <sup>-1</sup>	10 mg L <sup>-1</sup>	20 mg L <sup>-1</sup>	30 mg L <sup>-1</sup>
0	0.0000±0.0000	0.0000±0.0000	0.0000±0.0000	0.0000±0.0000
30	0.2350±0.0054	0.1429±0.0021	0.0713±0.0304	0.0560±0.0224
60	0.4090±0.0426	0.2887±0.0224	0.1316±0.0242	0.1112±0.0134
120	0.7681±0.0183	0.5194±0.0014	0.2559±0.0110	0.1963±0.0224
180	1.2595±0.0798	0.8081±0.0048	0.4263±0.0184	0.3346±0.0119
240	2.0418±0.1642	1.0602±0.0351	0.5032±0.0117	0.3500±0.0161

ศูนย์วิทยทรัพยากร  
จุฬาลงกรณ์มหาวิทยาลัย

Table D.8 Sonophotocatalytic alachlor degradation of various concentration of persulfate solution

Time (min)	C/C <sub>0</sub>			
	without K <sub>2</sub> S <sub>2</sub> O <sub>8</sub>	0.1 mM K <sub>2</sub> S <sub>2</sub> O <sub>8</sub>	0.25 mM K <sub>2</sub> S <sub>2</sub> O <sub>8</sub>	0.5 mM K <sub>2</sub> S <sub>2</sub> O <sub>8</sub>
0	1.0000±0.0000	1.0000±0.0000	1.0000±0.0000	1.0000±0.0000
30	0.8668±0.0026	0.7493±0.0120	0.6789±0.0210	0.5533±0.0240
60	0.7492±0.0237	0.4728±0.0090	0.1802±0.0000	0.0583±0.0270
120	0.5949±0.0012	0.1580±0.0210	0.0000±0.0000	0.0000±0.0000
180	0.4457±0.0031	0.1124±0.0140	0.0000±0.0000	0.0000±0.0000
240	0.3464±0.0172	0.0738±0.0120	0.0000±0.0000	0.0000±0.0000

Time (min)	C/C <sub>0</sub>	
	1.0 mM K <sub>2</sub> S <sub>2</sub> O <sub>8</sub>	5.0 mM K <sub>2</sub> S <sub>2</sub> O <sub>8</sub>
0	1.0000±0.0000	1.0000±0.0000
30	0.6236±0.0120	0.6500±0.0240
60	0.1849±0.0340	0.1258±0.0270
120	0.0000±0.0000	0.0000±0.0000
180	0.0000±0.0120	0.0000±0.0000
240	0.0000±0.0000	0.0000±0.0000

Table D.9 Sonophotocatalytic alachlor degradation of various concentration of hydrogen peroxide solution

Time (min)	C/C <sub>0</sub>		
	without H <sub>2</sub> O <sub>2</sub>	0.5 mM H <sub>2</sub> O <sub>2</sub>	1.0 mM H <sub>2</sub> O <sub>2</sub>
0	1.0000±0.0000	1.0000±0.0000	1.0000±0.0000
30	0.8668±0.0026	0.8096±0.0260	0.7835±0.0190
60	0.7492±0.0237	0.7201±0.0180	0.6836±0.0080
120	0.5949±0.0012	0.6025±0.0190	0.6333±0.0150
180	0.4457±0.0031	0.5203±0.0320	0.5106±0.0270
240	0.3464±0.0172	0.4407±0.0050	0.4406±0.0250

Time (min)	C/C <sub>0</sub>	
	10.0 mM H <sub>2</sub> O <sub>2</sub>	50.0 mM H <sub>2</sub> O <sub>2</sub>
0	1.0000±0.0000	1.0000±0.0000
30	0.7243±0.0220	0.7456±0.0190
60	0.6699±0.0320	0.6633±0.0080
120	0.6143±0.0220	0.6127±0.0150
180	0.5209±0.0130	0.5077±0.0270
240	0.4499±0.0330	0.4399±0.0250

Table D.10 TOC profile of alachlor degradation under different conditions

Time (min)	TOC/TOC <sub>0</sub>			
	Photocatalysis	Sonocatalysis	Sonophotocatalysis	Sonophotocatalysis with addition of K <sub>2</sub> S <sub>2</sub> O <sub>8</sub>
0	1.00	1.00	1.00	1.00
240	0.98	0.94	0.98	0.84
360	0.76	0.76	0.69	0.61
480	0.71	0.72	0.41	0.35

ศูนย์วิทยทรัพยากร  
จุฬาลงกรณ์มหาวิทยาลัย

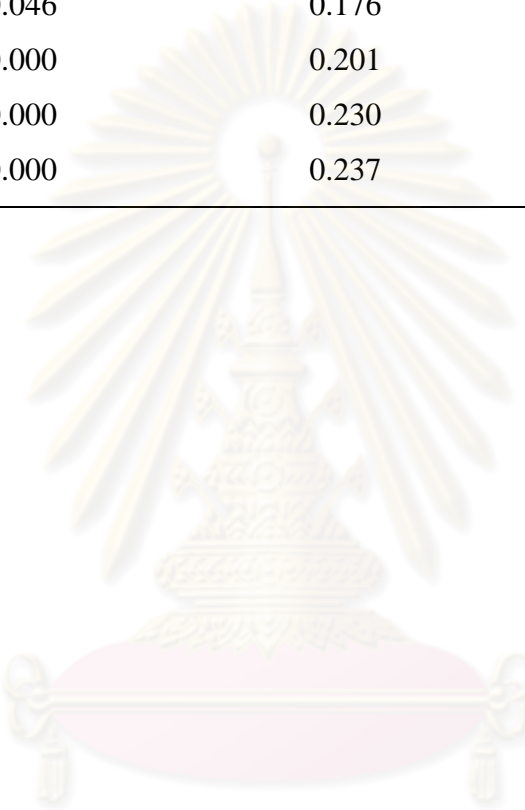
Table D.11 Photocatalytic, sonocatalytic and sonophotocatalytic oxidation of  $\text{Fe}^{2+}$  over S-doped  $\text{TiO}_2$

Time (min)	$\text{Fe}^{3+}$ concentration		
	Photocatalysis	Sonocatalysis	Sonophotocatalysis
0	0.0000	0.0000	0.0000
60	0.0695	0.1391	0.1616
120	0.2107	0.1841	0.3170
180	0.3477	0.2189	0.4541
240	0.4909	0.2536	0.5584

ศูนย์วิทยทรัพยากร  
จุฬาลงกรณ์มหาวิทยาลัย

Table D.12 Sonophotocatalytic oxidation of ion remaining

Time (min)	Concentration (mg L <sup>-1</sup> )			
	NO <sub>2</sub> <sup>-</sup>	NO <sub>3</sub> <sup>-</sup>	Cl <sup>-</sup>	SO <sub>4</sub> <sup>-</sup>
0	0.000	0.000	0.000	0.000
60	0.046	0.176	0.209	0.000
120	0.000	0.201	0.386	0.000
180	0.000	0.230	0.541	0.000
240	0.000	0.237	0.745	0.000



ศูนย์วิทยทรัพยากร  
จุฬาลงกรณ์มหาวิทยาลัย

## BIOGRAPHY

Mr. Danutawat Tipayarom was born on December 2, 1980 in Chachoengsao province, Thailand. The author received his Bachelor's Degree in Agricultural Engineering from the Faculty of Engineering, King Mongkut's Institute of Technology Ladkrabang in August, 2002. He obtained a Master's Degree in Environmental Engineering from the Asian Institute of Technology (AIT), Thailand. He worked as research associate in the environmental engineering and management fields in the School of Environment, Resources and Development at AIT for three years.

### Conferences and Publications

Tipayarom D., Wantala K. and Grisdanuruk N.(2009) Combined system of photocatalysis and sonolysis in degradation of alachlor by S-doped TiO<sub>2</sub> under visible light. International Conference on Green and Sustainable Innovation, December 2 – 4, 2009, Chiang Rai EE04. Presentation

Tipayarom D. and Grisdanuruk N. Development of Fe V Ag Ce S Codoped TiO<sub>2</sub> Photocatalyst for Alachlor Degradation under Visible Light 6th European meeting on Solar Chemistry and Photocatalysis: Environmental Applications (SPEA6), Prague, June 13-16, 2010. Poster presentation

Wantala K., Tipayarom D., Laokiat L, and Grisdanuruk (2009) Sonophotocatalytic activity of methyl orange over Fe(III)/TiO<sub>2</sub>. React Kinet Catal Lett 97:249-254.

Danutawat Tipayarom, Teruhisa Ohno and Nurak Grisdanurak Ultrasonic enhancement on alachlor degradation under visible light over S-doped TiO<sub>2</sub> revised in J. Environ. Sci. Heal. B.